INTERNATIONAL JOURNAL OF INTELLIGENT COMMUNICATION AND COMPUTER SCIENCE

ISSN: 3048-7285

VOL. 3 NO. 1

Pages: 114

TABLE OF CONTENT

Edge Detection Based on Fuzzy Logic with Edge Refinement via ACO Constraint Optimization.
Richa Awasthi and Amit Sinha (Pages: 1-15)

Solar PV Model Parameter Estimation via Improved Artificial Hummingbird Optimization.
Ravendra Pal Singh Lodhi and Saurabh Gupta (Pages: 16-30)

YOLO-Based Object Detection: Evolution, Real-Time Performance, and Applications in Intelligent Vision Systems.
Benasir Begam F (Pages: 31-52)

Machine Learning Applications in Material Science for Microstructure Analysis and Property Prediction.
G. Suvetha, Meenakshi N, Varunraj S, Gopalakrishnan T (Pages: 53-71)

An Encrypted Watermarking for Secure Medical Image Sharing: An Overview.
Vidisha Vishwakarma, Sunil Kumar Vishwakarma, Anshul Atre (Pages: 72-86)

Advanced Manufacturing Techniques for Aerospace Antennas.
S. Khalid (Pages: 87-114)

Contact: editor@ijiccs.in
ijiccs@gmail.com

International Journal of Intelligent Communication and Computer Science
Vol. 3, No. 1, 2025, Pages 1-15.

Edge Detection Based on Fuzzy Logic with Edge Refinement via ACO Constraint Optimization

Richa Awasthi[1] and Amit Sinha[2]

[1] Department of Computer Science and Engineering, Allenhouse Institute of Technology, Kanpur, U.P. INDIA
[2] Department of Computer Application, Allenhouse Business School, Kanpur, U.P. INDIA

Email: richa30303@gmail.com

Research Paper

Received: 27 Dec. 2024, Revised: 13 Mar. 2025 Accepted: 21 Mar. 2025

Abstract:

Edge detection is one of the most essential tasks in image processing, aiding in object detection, segmentation, and boundary identification. Traditional edge detection methods struggle with images containing noise, complex boundaries, or poor contrast. This paper proposes a hybrid approach that combines fuzzy logic for initial edge detection and Ant Colony Optimization (ACO) for edge refinement. The edge detection process starts by identifying possible edges using fuzzy logic and is then refined using ACO through a constraint optimization procedure that enhances the continuity, sharpness, and overall accuracy of the detected edges. Mathematical formulations for fuzzy logic-based edge detection, ACO optimization, and constraint-based edge refinement are presented. The results indicate that the proposed method outperforms traditional edge detection algorithms in terms of accuracy, robustness, and noise resilience, particularly in images with challenging boundary conditions.

Keywords: Edge detection, Fuzzy Logic, ACO, F-Score

1. Introduction

Edge detection is a fundamental aspect of image processing, essential for tasks such as object recognition, image segmentation, and scene analysis [1]. It is primarily concerned with identifying the boundaries or transitions in pixel intensity, which are critical for delineating the structures within an image. Traditional edge detection algorithms, including the Canny edge detector [2], Sobel operator [3], and Prewitt operator [4], have been extensively used for this purpose. These methods focus on detecting sharp changes in pixel intensity, typically assuming well-defined object boundaries. However, these classical techniques face several limitations, especially when working with noisy images, blurred boundaries, or images with complex structures such as curved surfaces or low contrast. For instance, noise can introduce false edges, while blurred or unclear transitions between objects can hinder the detection of precise boundaries.

In light of these challenges, the need for more robust edge detection methods is evident. In this paper, we propose a hybrid edge detection approach that integrates Fuzzy Logic [5] for initial edge detection and Ant Colony Optimization (ACO)[6] for refining and optimizing these detected edges. Fuzzy logic is particularly well-suited for handling uncertainty and imprecision in image data. Traditional edge detection methods rely on crisp pixel values, but in real-world scenarios, image data is often ambiguous and fuzzy. Fuzzy logic systems introduce flexibility by using membership functions, allowing for smoother transitions between edge and non-edge regions. This approach is effective in detecting potential edges in noisy, blurred, or low-contrast images that other methods may miss.

Once the edges are detected using fuzzy logic, ACO is employed to refine the initial edge map. ACO is a biologically inspired optimization technique that mimics the foraging behaviour of ants. In the context of edge detection, ACO is used to find the optimal paths for the detected edges. The algorithm enhances the continuity and smoothness of the edges by simulating the reinforcement of pheromones along the most promising paths. Over time, the paths with stronger pheromone levels are preferred, ensuring that the edges are not only detected but also optimized for smoothness and continuity. This process addresses the common problem of fragmented or jagged edges in traditional methods and provides a cleaner, more accurate boundary representation.

By combining fuzzy logic and ACO, this hybrid approach offers a significant improvement over traditional edge detection algorithm. The fuzzy logic component helps in detecting edges under uncertain conditions, while ACO ensures that the edges are refined, continuous, and accurately follow the object contours. This method holds great promise for applications where traditional edge detection methods struggle, such as in images with noise, blurred boundaries, or low contrast. The subsequent sections of this paper present the mathematical formulation of the proposed approach, the details of the algorithm's implementation, and experimental results that demonstrate its effectiveness in edge detection tasks.

2. Related Works

2.1 Kernel-Based Methods

Kernel-based edge detection methods, which are grounded in convolutional masking techniques, have played a foundational role in the development of edge detection algorithms. Early contributions, such as those by Sobel (1970) and Prewitt (1970), focused on utilizing pixel gradient information to detect edges in images. These methods, though straightforward and simple to implement, are often criticized for generating a high number of spurious edges, which leads to the detection of thick or broken edges. To address some of these limitations, recent advancements have explored more sophisticated masking schemes, such as the adoption of hexagonal masks. The hexagonal grid configuration, formed by interpolating traditional square masks, has been shown to improve the accuracy of edge detection. In particular, when integrated into the Canny edge detection algorithm, the hexagonal masking scheme has exhibited superior performance [8]. Furthermore, Canny edge detection has found applications in content-based image retrieval systems, demonstrating its broad utility in various image processing fields [9].

2.2 Soft Computing-Based Image Edge Detection

Soft computing techniques, which combine elements of artificial intelligence and computational models, have been increasingly utilized to enhance edge detection methods. One such technique is ACO, which has been employed to identify edges in images, with significant improvements being made using guided image filtering to increase accuracy and reduce noise [10–12]. Furthermore, the application of the Sobel operator has been improved by incorporating eight-directional masks and using entropy inversion for threshold detection, resulting in more precise edge detection [13]. Additionally, there have been efforts to combine image sharpening techniques with Particle Swarm Optimization (PSO) to refine edge detection, offering another avenue of improvement in image processing techniques [14].

2.3 Fuzzy Logic-Based Image Edge Detection

Fuzzy logic-based methods have garnered attention in edge detection due to their ability to handle uncertainty and imprecision, which are common characteristics in real-world images. In this approach, pixel intensity values are represented using fuzzy membership functions, enabling the detection of edges even in noisy or ambiguous conditions. Several studies have integrated fuzzy logic with guided image filtering, improving edge detection by providing smoother transitions between edges and non-edges [15, 16]. For instance, Kaur et al. (2015) proposed an edge detection method utilizing sixteen fuzzy rules, which demonstrated enhanced detection accuracy [17]. More recent developments in this area have explored the use of higher-order fuzzy logic, particularly fuzzy type-2 logic, to address vulnerabilities in edge detection under complex conditions such as blurry or low-contrast images [18, 19]. Additionally, adaptive neuro-fuzzy systems have been proposed for edge detection tasks, offering the benefit of self-learning capabilities [20]. Another notable advancement is the integration of ACO and fuzzy logic, which seeks to minimize the occurrence of false edges, thus improving the accuracy and reliability of edge detection in challenging scenarios [21]. Some studies have also explored the use of Kalman filtering and artificial neural networks (ANNs) alongside fuzzy logic for more robust edge detection in noisy environments [22].

2.4 Machine Learning-Based Methods

In recent years, probabilistic boundary (Pb)-based methods have gained attention for edge detection tasks, as they offer a more flexible and adaptive framework for recognizing edges. Martin et al. (2004) introduced the Pb-based edge detection method, which integrates texture features and logistic regression models to enhance edge recognition [23]. Later, Ren et al. (2007) proposed an advanced version, the multi-scale probabilistic boundary (MsPb) technique, which takes into account the multi-scale nature of edge features, improving detection accuracy [24]. In a similar vein, Arbelaez et al. (2011) expanded the Pb-based approach to include global probabilistic boundaries (g-Pb), which incorporates multi-scale analysis and spectral clustering for more accurate edge detection [25].

2.5 Deep Learning-Based Methods

Supervised learning methods have gained significant attraction in image processing, particularly for edge detection. These methods typically rely on large labelled datasets to train models, ensuring high accuracy and robustness. Probabilistic boosting trees introduced by Dollar et al. (2014) provide a powerful classification technique for edge detection [26]. Additionally, artificial neural networks (ANNs) have been utilized for edge detection, offering the flexibility to adapt to various image conditions [27]. Random forest classifiers, as demonstrated by Lim et al. (2013), have also been employed for effective edge detection by focusing on sketch markers and utilizing pixel intensity variations [28]. To further enhance edge detection, cascaded convolutional neural networks (CNNs) have been introduced to refine edge contours and improve the smoothness of the detected boundaries [29].

Unsupervised learning methods, which do not rely on labelled data, have been proposed as an alternative for edge detection. Techniques such as sparse code gradients (SCG) [30] and pointwise mutual information (PMI) architecture [31] enable edge contour identification without requiring manual labelling of edge features. In a more recent development, Yang et al. (2017) proposed a convolutional encoder-decoder network to extract object contours directly from images, achieving high-quality edge detection in a fully unsupervised manner [32]. Similarly, Xia et al. (2018) introduced unsupervised semantic segmentation for edge detection, employing encoder-decoder architectures for the precise extraction of object boundaries [33]. These unsupervised learning methods represent a promising direction for edge detection, particularly in scenarios where labelled training data is scarce or unavailable.

2.6 Objectives

The main objective of this research is to develop a robust and effective edge detection technique that combines Fuzzy Logic and ACO for enhanced performance. The primary goals of this research are as follows:

1. To design a fuzzy logic-based method for detecting edges in images. This includes utilizing fuzzy rules to model uncertainty in pixel values and effectively identify boundaries in images.
2. To incorporate ACO for refining edges detected by the fuzzy logic-based method. The objective is to improve the precision and accuracy of edge localization by using the exploration capabilities of ACO to optimize edge detection results.
3. To combine the strengths of fuzzy logic and ACO in a hybrid framework, ensuring better performance in edge detection tasks. The fuzzy system will capture the uncertainty of pixel-based decision-making, while ACO will optimize the detection process, leading to more accurate and refined edges.

4. To apply ACO's constraint optimization mechanism to refine the initial edge detected by the fuzzy logic system. This optimization ensures that the edge detection process considers both global and local information for accurate boundary identification.
5. To evaluate the performance of the proposed hybrid fuzzy-ACO edge detection method by comparing it against traditional methods like Sobel, Canny, and other state-of-the-art approaches. Key metrics such as edge detection accuracy, edge localization precision, and computational efficiency will be used to assess the effectiveness of the proposed approach.

The ultimate goal of this research is to propose a hybrid edge detection framework that effectively balances accuracy and computational efficiency, offering a novel approach to image processing tasks.

3. Proposed Method

The proposed method combines Fuzzy Logic for initial edge detection with ACO for edge refinement. Fuzzy logic is used to handle the ambiguity in pixel intensities and to detect potential edges by considering pixel intensity variations and neighbourhood relationships. This provides an initial edge map with gradual transitions between edge and non-edge regions.

Following this, ACO is employed to refine the detected edges. The optimization process involves ants searching for optimal edge paths, guided by pheromone information and image gradients. This step enhances the continuity and accuracy of the detected edges by minimizing noise and filling gaps in the edge map.

3.1 Fuzzy Membership Functions

In the proposed edge detection method, the fuzzy membership function plays a key role in handling the uncertainty and imprecision inherent in image processing. The fuzzy system is used to classify each pixel based on its intensity value, determining whether it belongs to an edge or a non-edge region.

3.1.1 Input Fuzzy Membership Function

The input to the fuzzy logic system is the pixel intensity of each pixel in the image. To deal with varying intensity levels, fuzzy sets are employed to map these intensity values into fuzzy categories. The intensity values of a pixel range from 0 (black) to 255 (white) in a grayscale image. The fuzzy membership function is designed to assign a degree of membership to each pixel based on its intensity.

Two fuzzy sets are used to represent the input:

- Low Intensity (Non-Edge): Pixels with low intensity values, typically in the darker regions, are likely to be part of the non-edge areas.
- High Intensity (Edge): Pixels with high intensity values, generally representing brighter areas, are likely to be part of the edge areas.

The membership functions for these sets are defined as triangular functions, where each intensity value is mapped to a value between 0 and 1, indicating the degree of membership in the edge or non-edge category.

A triangular membership function for "Low Intensity" is defined as:

$$\mu_{low} = \begin{cases} 0 & \text{if } I \geq t_1 \\ \dfrac{I}{t_1} & \text{if } 0 \leq I < t_1 \end{cases} \tag{1}$$

where I is the pixel intensity and t_1 is a threshold separating low intensity values from medium ones. Similarly, for "High Intensity", a triangular membership function is defined as:

$$\mu_{high} = \begin{cases} 0 & \text{if } I \leq t_2 \\ \dfrac{I - t_2}{255 - t_2} & \text{if } t_2 \leq I < 255 \end{cases} \tag{2}$$

where t_2 is the threshold separating high-intensity pixels from non-edges.

3.1.2 Output Fuzzy Membership Function (Edge and Non-Edge)

The output of the fuzzy logic system is a classification of each pixel as either part of an Edge or a Non-Edge. Based on the input fuzzy values (intensity values), the system determines whether a pixel is an edge or not.
To compute the final output, a fuzzy inference system uses the fuzzy rules derived from the pixel intensity values.

3.2 Fuzzy Rules

In Figure 1, a comprehensive representation of the rule formulation for a 3x3 mask is shown, outlining the criteria used to identify edge pixels in the given context. The mask, structured as a 3x3 grid, consists of white pixels ("W"), black pixels ("B"), and edge pixels ("E"). A total of 30 distinct rules have been carefully designed to govern the determination of edge pixels based on the configuration of neighboring pixels within the grid. These rules aim to differentiate between noise, non-edge, and actual edge pixels by evaluating the relationships among surrounding pixels.

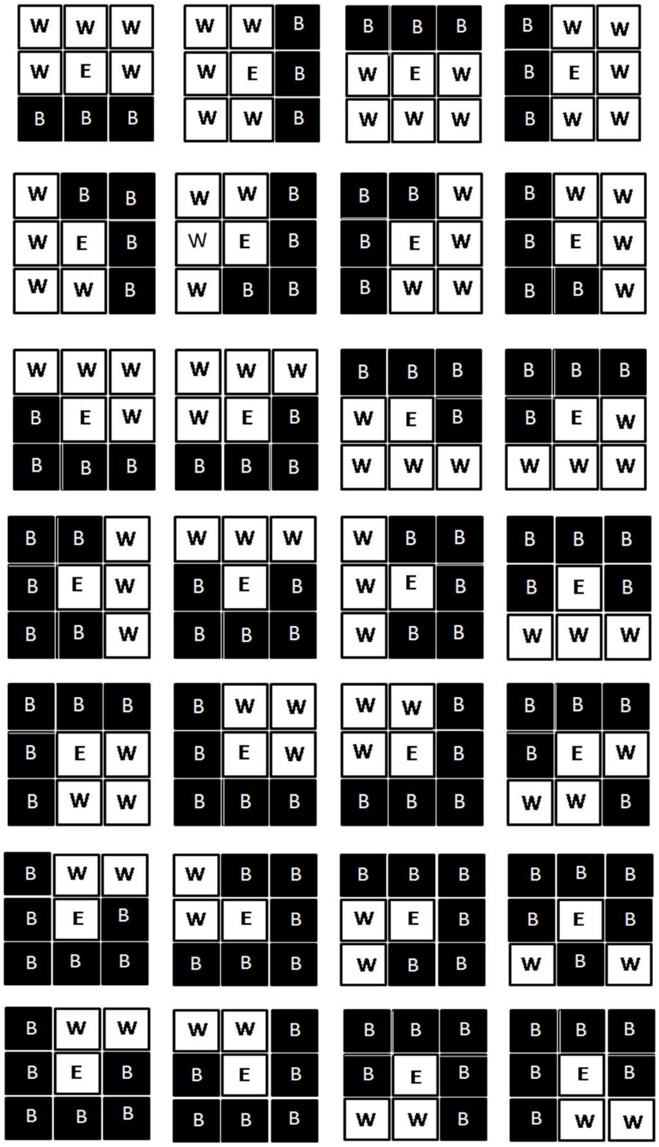

W	W	W	W	W	B	B	B	B	B	W	W
W	E	W	W	E	B	W	E	W	B	E	W
B	B	B	W	W	B	W	W	W	B	W	W

W	B	B	W	W	B	B	B	W	B	W	W
W	E	B	W	E	B	B	E	W	B	E	W
W	W	B	W	B	B	B	W	W	B	B	W

W	W	W	W	W	W	B	B	B	B	B	B
B	E	W	W	E	B	W	E	B	B	E	W
B	B	B	B	B	B	W	W	W	W	W	W

B	B	W	W	W	W	W	B	B	B	B	B
B	E	W	B	E	B	W	E	B	B	E	B
B	B	W	B	B	B	W	B	B	W	W	W

B	B	B	B	W	W	W	W	B	B	B	B
B	E	W	B	E	W	W	E	B	B	E	W
B	W	W	B	B	B	B	B	B	W	W	B

B	W	W	W	B	B	B	B	B	B	B	B
B	E	B	W	E	B	W	E	B	B	E	B
B	B	B	B	B	B	W	B	B	W	B	W

B	W	W	W	W	B	B	B	B	B	B	B
B	E	B	B	E	B	B	E	B	B	E	B
B	B	B	B	B	B	W	W	B	B	W	W

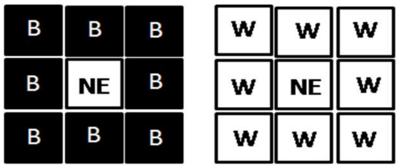

Figure 1: Schematic of the 30-rule base [15,16]

In the rule set, specific conditions are established to classify different pixel states. For example, if a pixel is surrounded by eight neighbouring pixels of the same colour, whether all white or all black, it is categorized as noise. This uniformity suggests that the pixel is part of a homogenous area with no significant transition or boundary, rendering it irrelevant for edge detection purposes. In contrast, a situation where a single pixel differs from its surrounding pixels is classified as a non-edge, emphasizing that a more significant variation or transition is needed to qualify as an edge.

A crucial feature of the rule set is its ability to detect edge pixels in situations where there is a clear contrast between neighbouring pixels. Specifically, the rules define edge pixels as those where there is a noticeable contrast between two different colours. For example, if at least two white pixels are surrounded by black pixels, or vice versa, this configuration signals a potential edge. The ability to identify edge pixels based on such contrast-based criteria is vital for recognizing boundaries or transitions in the image, especially in areas of significant colour change or contrast.

The rule set illustrated in Figure 3 serves as a detailed framework for identifying and categorizing pixels in a 3x3 grid, providing a systematic approach to edge detection. By specifying the conditions for noise, non-edge, and potential edge pixels based on the local pixel configuration, the rules facilitate an organized and structured method of discerning meaningful edges. This methodology, grounded in local context and pixel relationships, enables the accurate identification of edges, ensuring the reliability and precision of the edge detection process.

3.3 Defuzzification

The defuzzification process converts the fuzzy results into crisp values for the final classification. A defuzzification technique, the center of gravity (COG) method is applied to yield a final crisp output of either edge or non-edge for each pixel.

Thus, based on the fuzzy membership functions, a pixel's intensity value is processed, and an output value is assigned, which is either Edge (1) or Non-Edge (0), depending on its membership to the edge or non-edge fuzzy sets.

By using this approach, the fuzzy logic system is able to handle the imprecise and noisy data that is common in real-world images, allowing it to detect edges more effectively compared to traditional methods.

Once edges are identified, further ACO is applied for the edge refinement as described below:

3.4 ACO Based Image Edge Detection

In the proposed technique, a set of ants traverse a 2-D image, moving from one pixel to another, in order to create a pheromone matrix. This matrix is crucial in determining the edge information for each pixel in the fuzzy edge detected image. The edge refinement process follows a series of systematic steps, which are outlined as follows [10-12]. By simulating the movement of ants across the image, the algorithm effectively captures the significant transitions in pixel intensity, helping to highlight the boundaries and contours of the objects present in the image. The pheromone matrix, which is iteratively updated as the ants explore, plays a key role in guiding the detection process, enabling the algorithm to distinguish between edge and non-edge regions based on local pixel configurations and their interactions with neighbouring pixels. This method introduces an adaptive and efficient approach to edge detection, combining the principles of swarm intelligence with image processing techniques.

3.4.1 Initialization process

In the initialization process, an image *I* of size M_1M_2 is taken as input. This image represents the solution space for the artificial ants. The number of ants, denoted as *K*, is randomly distributed across the entire image such that each pixel in the image is treated as a node in the problem space. Each pixel is initially associated with a pheromone matrix, which is a grid that tracks the pheromone levels. The pheromone matrix's initial value for each element is set to a constant value τ_0, representing the starting pheromone intensity. This constant value ensures that all ants start with an equal opportunity for exploration and edge detection across the image.

3.4.2 Construction Process

One ant is randomly selected at the n^{th} construction step from the total of *K* ants. This chosen ant will then proceed to traverse the image for *L* movement steps. During each step, the ant moves to a neighbouring pixel (*i,j*) based on a transition probability, which is calculated according to the following formula:

$$p^{n}_{(l,m)(i,j)} = \frac{\left(\tau_{i,j}^{(n-1)}\right)^{\alpha} (\eta_{i,j})^{\beta}}{\sum\limits_{i,j\in\Omega_{(l,m)}} \left(\tau_{i,j}^{(n-1)}\right)^{\alpha} (\eta_{i,j})^{\beta}}, \tag{3}$$

In the above equation, $\tau_{i,j}$ represents the pheromone value of the edge between node (*i, j*), which reflects the strength of the pheromone trail laid down by the ants. This pheromone trail plays a crucial role in guiding the ants' movements, with higher pheromone values indicating more attractive paths. The parameter Ω(*l*,*m*) refers to the set of neighbouring nodes of the node (*l, m*), which defines the possible candidates for the ant to move to at each step. The parameter $\eta_{i,j}$ defines the heuristic information at node (*i, j*), which is typically based on the image's gradient or intensity, highlighting areas with significant changes in pixel values, such as edges.
The transition probability equation combines both the pheromone matrix $\tau_{i,j}$ and the heuristic matrix $\eta_{i,j}$. The constants α and β determine the relative influence of the pheromone matrix and the heuristic matrix, respectively, in the movement decision. Specifically:

- α controls the influence of the pheromone trail, which encourages the ants to follow previously successful paths.
- β controls the influence of the heuristic information, guiding the ants toward areas with stronger image gradients or more distinct edges.

By adjusting these parameters, the algorithm can be fine-tuned to balance the influence of the pheromone information and the edge-related heuristic information, ensuring effective edge detection while avoiding unnecessary noise or spurious edges.

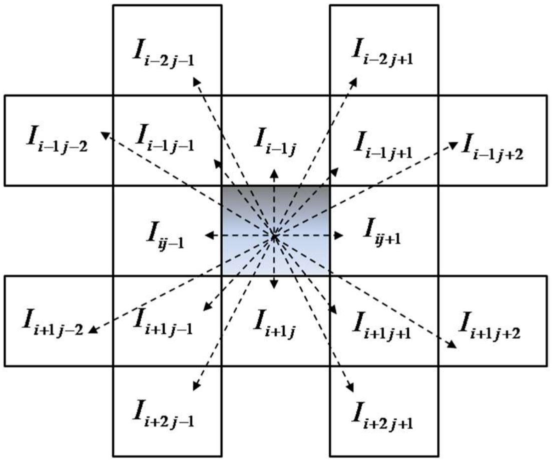

Figure 2: Representation of clique

The procedure involves two crucial aspects that guide the ant colony optimization for edge detection. The first issue is the heuristic information, which plays a significant role in guiding the ants towards the edges of the image. This heuristic information is determined based on local statistics of the image, which are dependent on the pixel's neighbouring region, referred to as the inner clique (Figure 2).

The local statistics at the pixel location (*i, j*), are computed to assess the relevance of that pixel in terms of edge detection. The computation of the local statistics typically involves evaluating the intensity variation in the pixel's neighbourhood, which helps identify areas with high gradient changes, indicating the presence of an edge.

The local statistics at a pixel (*i, j*), can be calculated using methods such as:

$$\eta_{i,j} = \frac{1}{1+\|\nabla I(i,j)\|} \tag{3}$$

where $\|\nabla I(i,j)\|$ represents the gradient magnitude at the pixel (*i, j*). The gradient $\nabla I(i,j)$ can be computed using standard edge detection operators such as Sobel, Prewitt, or more advanced methods. A higher gradient magnitude corresponds to a higher likelihood of the pixel being part of an edge.

In this approach:

- $\eta_{i,j}$ is the heuristic information at pixel (*i, j*), which is inversely related to the gradient magnitude, meaning higher gradients lead to higher heuristic values, highlighting edge regions.
- The local statistics at each pixel help to guide the ants towards regions with significant intensity changes, which are more likely to correspond to edges in the image.

This heuristic information serves as a key input in the transition probability for ants, directing them to explore regions with sharp intensity variations that are indicative of image edges. The precise calculation of the local statistics and their influence on the ants' movement is critical for the overall performance of the ACO-based edge detection algorithm.

3.4.3 Update Process

In the update process of the ACO algorithm for edge detection, the pheromone matrix is updated after two significant operations. The first update occurs after each ant completes its movement at every construction step. During this phase, the pheromone matrix is adjusted based on the ant's actions, which influences the transition probabilities for future movements. The update rule for the pheromone matrix after each individual ant's movement can be expressed as follows:

$$\tau(i,j) = (1-\rho)\tau(i,j) + \Delta\tau(i,j) \tag{4}$$

where:

- $\tau(i,j)$) is the pheromone value on edge (*i, j*).
- ρ is the evaporation rate, which controls how quickly the pheromone evaporates over time. It is a user-defined parameter that helps to model the decay of pheromone over iterations.
- $\Delta\tau(i,j)$ represents the pheromone deposit from the ant, calculated based on the quality of the solution that the ant found. It is typically inversely proportional to the path length or cost associated with the edge detected.

The evaporation rate ρ helps balance the exploration-exploitation trade-off by reducing the influence of previously travelled paths, allowing the ants to explore new potential solutions. A higher evaporation rate ensures that stale paths lose their relevance more quickly, making room for the ants to explore new areas of the solution space.

The second update occurs after all ants have completed their movement in each construction step. This update is given by:

$$\tau(i,j) = (1-\psi)\tau(i,j) + \sum_{k=1}^{K}\Delta\tau_k(i,j) \tag{5}$$

where:

- ψ is the pheromone decay coefficient, which controls how the pheromone is reduced for subsequent ants.
- $\sum_{k=1}^{K} \Delta \tau_k (i, j)$ represents the sum of all pheromone deposits from all ants that traversed the edge (*i*, *j*).

The parameter ψ ensures that pheromone trails on previously traversed edges are diminished over time, further encouraging ants to explore new regions of the image rather than repeatedly following the same paths. This update process reduces the likelihood of ants revisiting the same edges, helping to avoid premature convergence and promoting the discovery of better edge paths.

The pheromone update process, therefore, plays a crucial role in guiding the ants through the image, helping to refine the edge detection process by updating the pheromone matrix based on the ants' collective experiences. The combination of pheromone evaporation and decay allows for a dynamic exploration of potential edges, optimizing the search for accurate boundaries in the image.

3.4.4 Decision process

In this section, the binary decision-making process is applied to determine whether each pixel in the image corresponds to an edge or not. This is done by applying a threshold *T* on the pheromone matrix τ(*N*), which represents the pheromone level after the ants have completed their movement and pheromone updates. The threshold is adaptively estimated based on a technique proposed in [11,12], where the threshold *T* is updated iteratively until convergence. Below are the steps that describe the adaptive thresholding process in detail:

Step 1: Initialize Initial Threshold

The initial threshold *T* (0) is set as the mean value of the pheromone matrix τ(*N*). This initial threshold is computed as:

$$T(0) = \frac{1}{M_1 M_2} \sum_{i=1}^{M_1} \sum_{j=1}^{M_2} \tau(i, j) \tag{6}$$

We also initialize the iteration index *q*=0.

Step 2: Classify Entries of the Pheromone Matrix

The pheromone matrix τ(*N*) is divided into two classes based on the initial threshold *T*(0). The first class consists of entries where the pheromone value is less than or equal to *T*(0), and the second class consists of the remaining entries, where the pheromone value is greater than *T*(0). Let:

$$C_1 = \{\tau(i, j) \le T(0)\} \tag{7}$$

$$C_2 = \{\tau(i, j) > T(0)\} \tag{8}$$

Next, calculate the mean pheromone value for each class:

$$\mu_1 = \frac{1}{|C_1|} \sum_{i,j \in C_1} \tau(i, j) \tag{9}$$

$$\mu_2 = \frac{1}{|C_2|} \sum_{i,j \in C_2} \tau(i, j) \tag{10}$$

Where μ_1 and μ_2 represent the mean values for classes C_1 and C_2 respectively.

Step 3: Update the Threshold

After calculating the means of the two classes, the new threshold *T*(*q*+1) is updated as the average of the two class means:

$$T(q+1) = \left(\frac{\mu_1 + \mu_2}{2} \right) \tag{11}$$

At this point, we increment the iteration index q by 1 and move to Step 4 to evaluate whether the threshold has converged.

Step 4: Convergence Check

If the change in threshold between iterations is greater than a user-defined tolerance ϵ, we proceed with another iteration by going back to Step 2. The stopping condition is defined as:

$$\left| T(q+1) - T(q) \right| < \varepsilon \tag{12}$$

where ϵ is a small predefined tolerance. If this condition is met, the iteration stops, and we proceed to the final decision-making process.

Step 5: Binary Edge Decision

Once the threshold converges, a binary decision is made for each pixel in the image. If the pheromone value at a pixel $\tau(i,j)$ is greater than or equal to the final threshold $T(q)$, the pixel is classified as an edge pixel:

$$Edge(i,j) = \begin{cases} 1 & \tau(i,j) \geq T(q) \\ 0 & \text{otherwise} \end{cases} \tag{13}$$

This step classifies each pixel as either part of an edge (denoted by 1) or not (denoted by 0), resulting in a binary edge map that highlights the detected edges in the image.

3.5 ACO-Based Constraint Optimization for Edge Refinement

The main objective of ACO is to refine the edges and ensure that they are smooth and continuous, we introduce a constraint optimization process based on the ACO. This optimization considers both the membership value (from fuzzy logic) and geometric properties of edges, such as smoothness and continuity.
The objective of the optimization is to minimize the overall cost, which is defined as:

$$\min \sum_{i=1}^{N} (I(x_i) - I(x_i+1))^2 + \lambda \left(D(x_i) - D(x_i+1) \right)^2 \tag{14}$$

where, $x(i)$, $x(i+1)$ are consecutive pixels along the edge path, $I(x)$ is the pixel intensity, $D(x)$ is the direction of the edge at pixel x and λ is a weight parameter that balances the smoothness constraint.

The goal is to select the edge paths that minimize the difference in intensity and direction between adjacent pixels, resulting in smooth and continuous edges.

4. Results and Discussion

In this section, we discuss the results obtained from the proposed method, focusing on the edge detection performance and the effectiveness of the hybrid fuzzy logic and ACO approach. The key parameters used in the experiments are outlined in Table 1, which provides a comprehensive overview of the values assigned to various factors affecting the performance of the edge detection algorithm.
Table 1 presents the simulation parameters for both the fuzzy logic-based edge detection and ACO optimization processes. These parameters play a crucial role in determining the accuracy and efficiency of edge detection results.

Table 1: List of Parameters

Parameter	Symbol	Value
Total Number of Ants	K	50
Initial Pheromone Value	τ_0	0.0001
Pheromone Weighting Factor	α	1
Heuristic Weighting Factor	β	0.1
Neighbourhood Connectivity	Ω	8-connectivity
Adjusting Factor	λ	10
Evaporation Rate	ρ	0.1
Movement Steps per Ant	L	40
Pheromone Decay Coefficient	ψ	0.05
User-defined Tolerance	ε	0.1
Number of Construction Steps	N	4
Number of Fuzzy Rules	-	-
Membership Function for Edge	-	Triangular
Threshold for Edge Detection	-	Adaptive
Defuzzification Method	-	Centroid

4.1 Qualitative Results

In Figure 3, a comprehensive comparison of edge detection results is provided, showcasing the performance of several well-established edge detection techniques, including the Sobel operator, Canny edge detector, Fuzzy Logic-based edge detection, ACO-based edge detection, and the proposed hybrid approach. Each of these methods was applied to a sample image, and the resulting edge maps are analysed to highlight their strengths and weaknesses in terms of accuracy, precision, and edge continuity.

The Sobel edge detection method, which is a simple and fast gradient-based approach, highlights the basic contours of objects within the image. However, as seen in the results, it struggles with detecting edges in noisy or blurred regions. The Sobel operator tends to produce thick and discontinuous edges, particularly in areas with low contrast or subtle transitions. Despite its speed and simplicity, it fails to provide the level of precision required for more complex images, making it less suitable for applications where accuracy is paramount.

The Canny edge detection method, renowned for its edge detection accuracy, employs a multi-step process that includes Gaussian smoothing, gradient calculation, non-maximum suppression, and edge tracing by hysteresis. While it performs well in detecting thin, continuous edges, the method can still produce some false edges, especially in noisy regions. Additionally, Canny's performance is highly sensitive to the choice of thresholds, and incorrect thresholding can either cause weak edges to be missed or introduce spurious edges.

The Fuzzy Logic-based edge detection, which utilizes fuzzy membership functions to handle uncertainty and imprecision in pixel intensities, shows a marked improvement in detecting edges under varying lighting conditions and noisy environments. The use of fuzzy rules allows for a more flexible interpretation of pixel intensities and spatial relationships, leading to better handling of image noise. While the fuzzy system detects edges more accurately than Sobel and Canny, it still suffers from occasional discontinuities and misclassifications in complex regions of the image.

The ACO-based edge detection method, which uses artificial ants to explore the image and update a pheromone matrix, excels at refining edges by iteratively adjusting the pheromone levels and exploring potential edge paths. This approach is highly adaptive and is particularly effective in detecting continuous and smooth edges. However, the ACO method requires significant computational resources due to its iterative nature and large number of ants used to traverse the image. It performs better than Sobel, Canny, and fuzzy methods in capturing precise and uninterrupted edges.

Finally, the proposed hybrid method, which combines the strengths of both fuzzy logic and ACO, significantly enhances edge detection performance. The fuzzy logic system handles the initial edge detection by providing a robust framework for dealing with uncertainties in pixel values, while the ACO refines the detected edges by optimizing the pheromone matrix and ensuring the edges are smooth and continuous. The results in Figure X demonstrate that the proposed method outperforms all the other methods, yielding more accurate, continuous, and fine-grained edges. The hybrid approach provides a balanced solution to the challenges posed by noisy, complex, and low-contrast images, making it the most reliable and efficient method for edge detection in the tested scenarios.

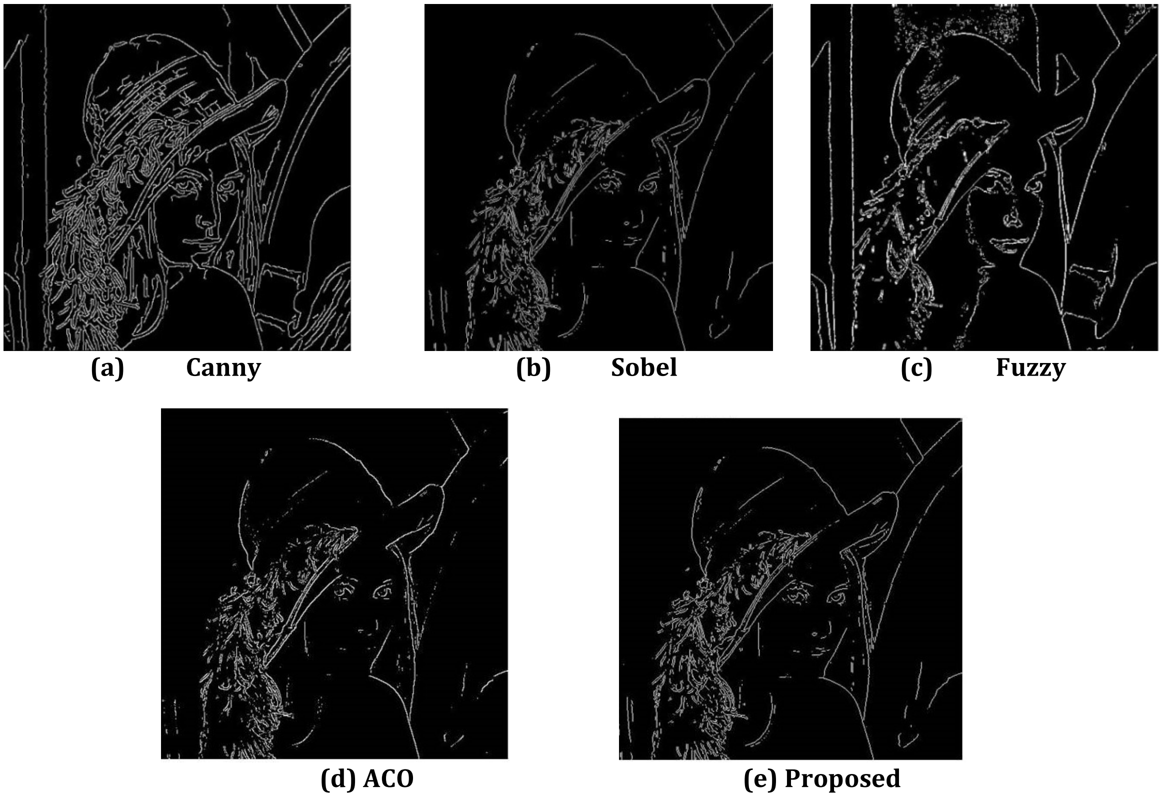

(a) Canny

(b) Sobel

(c) Fuzzy

(d) ACO

(e) Proposed

Figure 3: Comparison of the edge detection methods (Qualitative)

In summary, the comparative results clearly indicate that while traditional methods like Sobel and Canny provide satisfactory performance in some cases, they fall short in handling noise and detecting precise edges. The fuzzy logic and ACO methods offer substantial improvements, with the proposed hybrid technique achieving the best results in terms of edge continuity, accuracy, and adaptability to different image conditions. This demonstrates the effectiveness of combining fuzzy logic's tolerance for uncertainty with ACO's optimization capabilities for robust edge detection.

4.2 Quantitative Results

The results presented in Table 2 demonstrate the comparison of classical edge detection methods with state-of-the-art approaches, evaluated based on the F-Score, a key metric that measures both the precision and recall of edge detection algorithms. The Canny edge detection method, one of the most widely used classical approaches, achieves an F-Score of 0.49. While the Canny method is effective for basic edge detection, it tends to struggle in noisy or low-contrast images, resulting in a lower F-Score. The Sobel operator, another classical method, achieved a slightly lower F-Score of 0.40. This method, though simple and easy to implement, often produces thick edges and is susceptible to noise, which further impacts its accuracy in edge detection.

In contrast, Kumar et al. [20] utilized fuzzy logic for edge detection, achieving an F-Score of 0.64. The fuzzy logic system introduces a more sophisticated approach by incorporating uncertainty and imprecision in pixel intensity, leading to improved edge detection performance. However, it still falls short when compared to more advanced hybrid techniques.

Table 2: Classical and State-of-the –art methods comparison (F-Score)

Reference	Methods	F-Score
Canny [2]	Masking	0.49
Sobel [3]	Masking	0.40
Kumar et.al [16]	Fuzzy	0.64
Kumar et.al [12]	ACO	0.72
Proposed	Fuzzy + ACO	0.84

The ACO method, proposed by Kumar et al. [12], resulted in an F-Score of 0.72. ACO excels in refining edges by simulating the behaviour of ants searching for optimal paths, which allows for a more accurate representation of edges, particularly in complex images. The higher F-Score reflects the method's enhanced ability to detect edges and reduce noise compared to traditional methods.

The proposed method, which integrates both Fuzzy Logic and ACO, achieved the highest F-Score of 0.84. By combining the strengths of both techniques, the proposed method significantly outperforms classical and individual advanced methods. The Fuzzy Logic component handles uncertainty and imprecision in pixel intensities, while ACO refines and optimizes the detected edges, ensuring more accurate and continuous boundaries. This superior F-Score highlights the effectiveness of the hybrid approach in providing precise edge detection, particularly in challenging scenarios with noisy or complex images.

5. Conclusion

In this paper, we have proposed an enhanced edge detection technique that integrates Fuzzy Logic and Ant Colony Optimization (ACO). The goal was to address the limitations of traditional edge detection methods, such as the Sobel and Canny edge detectors, particularly in noisy, blurred, and low-contrast image scenarios. The fuzzy logic system efficiently manages the uncertainty and imprecision present in images, while the ACO algorithm optimizes the edge detection process by refining the identified edges through pheromone-based searching. The experimental results demonstrate that the proposed method significantly improves the edge detection performance, as evidenced by the higher F-Score achieved compared to traditional methods. The F-Score, which combines both precision and recall, indicates a better balance between false positives and false negatives, ensuring a more accurate and reliable detection of edges in the images. The adaptive thresholding mechanism within the ACO algorithm further contributes to the enhanced edge detection results by dynamically adjusting based on the image content. This provides robustness across different image types and conditions, ensuring effective edge detection even in challenging environments.

References

1. Jing, Junfeng, Shenjuan Liu, Gang Wang, Weichuan Zhang, and Changming Sun. "Recent advances on image edge detection: A comprehensive review." *Neurocomputing* 503 (2022): 259-271.
2. Canny, John. “A Computational Approach to Edge Detection.” *IEEE Transactions on Pattern Analysis and Machine Intelligence* 8 (1986): 679–698.
3. Gao, Wenshuo, Xiaoguang Zhang, Lei Yang, and Huizhong Liu. “An Improved Sobel Edge Detection.” In *2010 3rd International Conference on Computer Science and Information Technology*, Vol. 5, 67–71. IEEE, 2010.
4. Verma, Ankush, Namrata Dhanda, and Vibhash Yadav. "Enhancing Image Segmentation through an Innovative Hybrid Kernel: A Weighted Fusion of Sobel and Prewitt Operators Using Artificial Neural Networks." In *2024 International Conference on Computing, Sciences and Communications (ICCSC)*, pp. 1-5. IEEE, 2024.
5. Alshennawy, Abdallah A., and Ayman A. Aly. "Edge detection in digital images using fuzzy logic technique." *World Academy of science, engineering and technology* 51 (2009): 178-186.

6. Awadallah, Mohammed A., Sharif Naser Makhadmeh, Mohammed Azmi Al-Betar, Lamees Mohammad Dalbah, Aneesa Al-Redhaei, Shaimaa Kouka, and Oussama S. Enshassi. "Multi-objective ant colony optimization." *Archives of Computational Methods in Engineering* (2024): 1-43.
7. Fadaei, S., and Abdolreza R. "A Framework for Hexagonal Image Processing Using Hexagonal Pixel-Perfect Approximations in Subpixel Resolution." *IEEE Transactions on Image Processing* 30 (2021): 4555-4570.
8. Firouzi, M., Sadegh F., and Abdolreza R. "A New Framework for Canny Edge Detector in Hexagonal Lattice." *International Journal of Engineering* 35, no. 8 (2022): 1588-1598.
9. Fadaei, S. "New Dominant Color Descriptor Features Based on Weighting of More Informative Pixels Using Suitable Masks for Content-Based Image Retrieval." *International Journal of Engineering* 35, no. 8 (2022): 1457-1467.
10. Baterina, Anna Veronica, and Carlos Oppus. "Image Edge Detection Using Ant Colony Optimization." *Wseas Transactions on Signal Processing* 6, no. 2 (2010): 58-67.
11. Kumar, A., and S. Raheja. "Edge Detection Using Guided Image Filtering and Enhanced Ant Colony Optimization." *Procedia Computer Science* 173 (2020): 8-17.
12. Kumar, A., and S. Raheja. "Edge Detection Using Guided Image Filtering and Ant Colony Optimization." In *Recent Innovations in Computing: Proceedings of ICRIC 2020*, 319-330. Springer Singapore, 2021.
13. Ravivarma, G., K. Gavaskar, D. Malathi, K. G. Asha, B. Ashok, and S. Aarthi. "Implementation of Sobel Operator Based Image Edge Detection on FPGA." *Materials Today: Proceedings* 45 (2021): 2401-2407.
14. Verma, A., N. Dhanda, and V. Yadav. "Binary Particle Swarm Optimization Based Edge Detection Under Weighted Image Sharpening Filter." *International Journal of Information Technology* 15, no. 1 (2023): 289-299.
15. Kumar, A., and S. Raheja. "Edge Detection in Digital Images Using Guided L0 Smoothen Filter and Fuzzy Logic." *Wireless Personal Communications* 121, no. 4 (2021): 2989-3007.
16. Raheja, S., and A. Kumar. "Edge Detection Based on Type-1 Fuzzy Logic and Guided Smoothening." *Evolving Systems* 12, no. 2 (2021): 447-462.
17. Kaur, Er K., V. Mutenja, and Inderjeet Singh Gill. "Fuzzy Logic Based Image Edge Detection Algorithm in MATLAB." *International Journal of Computer Applications* 1, no. 22 (2010): 55-58.
18. Aborisade, David O. "Novel Fuzzy Logic Based Edge Detection Technique." *International Journal of Advanced Science and Technology* 29, no. 1 (2011): 75-82.
19. Begol, M., and K. Maghooli. "Improving Digital Image Edge Detection by Fuzzy Systems." *World Academy of Science, Engineering and Technology* 81 (2011): 76-79.
20. Zhang, Lei, Mei Xiao, Jian Ma, and Hongxun Song. "Edge Detection by Adaptive Neuro-Fuzzy Inference System." In *2009 2nd International Congress on Image and Signal Processing*, 1-4. IEEE, 2009.
21. Dorrani, Z., H. Farsi, and S. Mohamadzadeh. "Image Edge Detection with Fuzzy Ant Colony Optimization Algorithm." *International Journal of Engineering* 33, no. 12 (2020): 2464-2470.
22. Siddharth, D., D. K. J. Saini, and P. Singh. "An Efficient Approach for Edge Detection Technique Using Kalman Filter with Artificial Neural Network." *International Journal of Engineering* 34, no. 12 (2021): 2604-2610.
23. Martin, David R., Charless C. Fowlkes, and Jitendra Malik. "Learning to Detect Natural Image Boundaries Using Local Brightness, Color, and Texture Cues." *IEEE Transactions on Pattern Analysis and Machine Intelligence* 26, no. 5 (2004): 530-549.
24. Ren, Xiaofeng. "Multi-Scale Improves Boundary Detection in Natural Images." In *Computer Vision–ECCV 2008: 10th European Conference on Computer Vision*, 533-545. Springer Berlin Heidelberg, 2008.
25. Arbelaez, Pablo, Michael Maire, Charless Fowlkes, and Jitendra Malik. "Contour Detection and Hierarchical Image Segmentation." *IEEE Transactions on Pattern Analysis and Machine Intelligence* 33, no. 5 (2010): 898-916.
26. Dollar, P., Zhuowen Tu, and Serge B. "Supervised Learning of Edges and Object Boundaries." In *2006 IEEE Computer Society Conference on Computer Vision and Pattern Recognition (CVPR'06)*, Vol. 2, 1964-1971. IEEE, 2006.
27. Rahebi, J., and Hamid Reza Tajik. "Biomedical Image Edge Detection Using an Ant Colony Optimization Based on Artificial Neural Networks." *International Journal of Engineering Science and Technology* 3, no. 12 (2011): 8211-8218.

28. Lim, Joseph J., C. Lawrence Zitnick, and Piotr Dollár. "Sketch Tokens: A Learned Mid-Level Representation for Contour and Object Detection." In *Proceedings of the IEEE Conference on Computer Vision and Pattern Recognition*, 3158-3165. 2013.
29. Elharrouss, O., Youssef H., Assia K. I., Btissam El K., and Amal El Fallah-Seghrouchni. "Refined Edge Detection with Cascaded and High-Resolution Convolutional Network." *Pattern Recognition* 138 (2023): 109361.
30. Ren, Xiaofeng, and Liefeng Bo. "Discriminatively Trained Sparse Code Gradients for Contour Detection." *Advances in Neural Information Processing Systems* 25 (2012).
31. Isola, P., Daniel Z., Dilip K., and Edward H. A. "Crisp Boundary Detection Using Pointwise Mutual Information." In *Computer Vision–ECCV 2014: 13th European Conference*, 799-814. Springer International Publishing, 2014.
32. Yang, J., Brian P., Scott C., Honglak L., and Ming-Hsuan Yang. "Object Contour Detection with a Fully Convolutional Encoder-Decoder Network." In *Proceedings of the IEEE Conference on Computer Vision and Pattern Recognition*, 193-202. 2016.
33. Xia, Xide, and Brian Kulis. "W-Net: A Deep Model for Fully Unsupervised Image Segmentation." *arXiv preprint arXiv:1711.08506* (2017).

International Journal of Intelligent Communication and Computer Science
Vol. 3, No. 1, 2025, Pages 16-30.

Solar PV Model Parameter Estimation via Improved Artificial Hummingbird Optimization

Ravendra Pal Singh Lodhi[1] and Saurabh Gupta[2]

[1] Research Schoolar, Department of Electrical and Electronics Engineering, Technocrats Institute of Technology
[2] Department of Electrical and Electronics Engineering, Technocrats Institute of Technology

Research Paper

Email: rajput.ravendra@gmail.com
Received: 2 Jan. 2025, Revised: 11Apr. 2025 Accepted: 15 Apr. 2025

Abstract:

For effective simulation, design, and control of PV systems, solar photovoltaic (PV) models must have accurate parameter estimation. However, the nonlinear and multi-modal nature of the PV model equations makes this a challenging optimization task. In this study, an Improved Artificial Hummingbird Optimization (IAHO) algorithm is proposed to improve the performance of parameter estimation for solar PV models. The improvement incorporates adaptive control strategies and enhanced exploration mechanisms to prevent premature convergence and ensure a better balance between exploration and exploitation. The performance of the proposed IAHO is validated on standard single-diode and double-diode PV models using manufacturer-provided data. Comparative results against other well-known optimization techniques demonstrate that IAHO achieves superior estimation accuracy, faster convergence, and better stability across multiple runs. The proposed method is quite useful tool for PV model calibration in renewable energy applications.

Keywords: Solar PV, Parameter Estimation, Artificial Hummingbird Algorithm, Metaheuristic Optimization

1. Introduction

Significant progress has been made in renewable energy technology, particularly in solar photovoltaic (PV) systems, as the need of renewable energy is increasing day by day. The need for more sustainable energy alternatives, coupled with growing environmental concerns, has led to a greater emphasis on solar energy. This energy has proved to be one of the most useful renewable energies worldwide [1]. Due to this reason, research efforts have shifted towards improving the performance of PV systems. Achieving these goals requires a deep understanding of how PV systems behave under different conditions and the development of methods to optimize their performance in real-world applications.

A fundamental component of this effort is the development of accurate mathematical models that can represent the electrical behaviour of PV cells and modules under diverse operating conditions. These models are critical for simulating the performance of solar panels across different climates, time of day, and seasonal variations, and for facilitating the design of efficient PV systems. Accurate PV models allow for better predictions of energy output, system optimization, and fault detection, all of which are essential for maximizing the economic and environmental benefits of solar energy [2].

Frequently used PV models are the single-diode model (SDM) [3] and the double-diode model (DDM) [4]. Both models aim to simulate the current-voltage (I-V) characteristics of solar panels, which are crucial for understanding how the solar panel performs under different conditions of light intensity and temperature. The SDM is simpler and uses a single diode to represent the photovoltaic cell's behaviour, while the DDM extends this approach by introducing an additional diode to capture more complex behaviours, particularly under high-intensity light or extreme temperature conditions. These models are governed by several key parameters that include photocurrent, diode ideality factor, series resistance, shunt resistance, and reverse saturation current. Each of these parameters plays a vital role in determining the accuracy of the model and must be estimated as precisely as possible for realistic simulations.

However, the process of estimating these parameters is inherently challenging due to the nonlinear and transcendental nature of the equations governing the PV models. Nonlinearities arise because the relationship between voltage, current, and power in a solar cell is governed by exponential and logarithmic functions, which are difficult to solve analytically. Furthermore, the transcendental equations often do not have closed-form solutions and must be approached through numerical methods. Consequently, the estimation of these parameters becomes a complex optimization issue, where the primary purpose is to reduce the error between the model's predicted output and actual measured data, a task complicated by the high sensitivity of the parameters and the nonlinear nature of the underlying equations.

Traditional parameter extraction techniques, such as curve fitting and analytical methods, have been used extensively for this purpose. However, these methods suffer from several significant limitations. For example, curve fitting techniques can be highly sensitive to the initial guesses of parameters, leading to issues with local minima—situations where the optimization process converges to a solution that is not the global best. Additionally, these methods struggle to perform well when the input data is noisy or incomplete, which is often the case in real-world applications. Analytical methods, on the other hand, rely on simplifying assumptions that may not always hold true in practice, further limiting their accuracy and applicability.

To overcome these limitations, metaheuristic optimization algorithms are emerged as an alternative for parameter estimation. These algorithms are capable of navigating complex, multimodal search spaces without requiring gradient information, making them well-suited to handle the nonlinearities and complexities of PV parameter estimation. Unlike traditional methods, metaheuristics do not rely on explicit mathematical models of the system but instead use adaptive search strategies to explore the solution space. As a result, they are less prone to getting stuck in local minima and can provide robust solutions even under noisy or incomplete data conditions.

Several metaheuristic optimization algorithms have been successfully applied to PV parameter estimation, with notable examples including Particle Swarm Optimization (PSO) [5], Genetic Algorithms (GA) [6], and Artificial Bee Colony (ABC) [7]. PSO, for instance, mimics the social behaviour of birds flocking together to find an optimal solution, while GA takes inspiration from the process of natural selection and evolution. Similarly, ABC is inspired by the foraging behaviour of bees, and it uses a population-based approach to search for the optimal solution. Each of these algorithms has shown varying degrees of success in precisely calculating the parameters of both SDM and DDM models, with some demonstrating greater robustness and efficiency under certain conditions.

Despite the progress made with metaheuristic algorithms, challenges remain on the basis of computational cost, convergence speed, and the handling of large-scale systems. Nonetheless, ongoing advancements in optimization techniques continue to push the boundaries of PV system performance modelling, offering promising directions for future research and application.

Among the newer nature-inspired algorithms, the Artificial Hummingbird Optimization (AHO) [8] algorithm has shown promise due to its flexible foraging behaviour, directional flight patterns, and ability to switch between local and global search modes. Inspired by the intelligent food-searching strategies of real hummingbirds, AHO offers a novel balance between exploration and exploitation, which is particularly beneficial for solving nonlinear optimization problems.

However, like many metaheuristics, the original AHO may still face challenges such as premature convergence, imbalanced search capabilities, and sensitivity to control parameters. To address these limitations, this paper proposes an IAHO algorithm, which incorporates several enhancements aimed at boosting convergence speed, avoiding local optima, and improving robustness. The improvements include adaptive flight strategy control, diversity preservation techniques, and refined fitness-based learning mechanisms.

In this research article, the proposed IAHO algorithm is applied to estimate the unknown parameters of solar PV models and evaluate its performance. The outputs are validated using real-world PV module data provided by manufacturers, and the performance of IAHO is compared with other established optimization algorithms. The findings demonstrate that the proposed method offers significant improvements in parameter estimation, making it a valuable tool for PV system modelling, simulation, and control in renewable energy applications.

1.1 Motivation

The rapid growth of solar photovoltaic (PV) technology has made it an essential contributor to global renewable energy production. To ensure efficient energy conversion and reliable performance prediction, accurate modelling of PV systems is crucial. However, the performance of PV cells and modules is inherently nonlinear and influenced by various internal and external factors, such as temperature, irradiance, and material properties. Accurately estimating the model parameters (e.g., photocurrent, diode saturation current, ideality factor, series and shunt resistances) is fundamental for the development of reliable PV models.

Traditional analytical methods often struggle with the highly nonlinear and multimodal nature of the PV parameter estimation problem, leading to suboptimal results or convergence to local minima. To overcome these limitations, metaheuristic optimization techniques have gained popularity due to their flexibility and robustness. Among them, the Artificial Hummingbird Optimization (AHO) algorithm has shown promise; however, like many algorithms, it may face certain problems like premature convergence or slow convergence speed.

To deal with such problems, an IAHO algorithm is proposed, incorporating adaptive mechanisms and enhanced search strategies to improve convergence performance and estimation accuracy. This research aims to leverage IAHO for precise PV model parameter estimation, thereby improving simulation fidelity and enabling more effective PV system design, monitoring, and control.

1.2 Objectives

The main objectives of this work are:

1. Developing an improved version of the AHO algorithm
2. To apply the IAHO algorithm for estimating the parameters of single-diode PV models by minimizing the error between the estimated and measured characteristics.
3. To validate the effectiveness of IAHO through comparison with actual experimental data and demonstrate its superiority over conventional methods and standard AHO.
4. Evaluating the performance of IAHO across different iteration levels, highlighting its scalability and robustness under varying computational constraints.

1.3 Organization of the Paper

In section 2, we have review of the related literature. Section 3 introduces the proposed methodology based on the IAHO algorithm. Section 4 presents the simulation results and performance analysis. The last section, Section 5 concludes the paper with key outcomes and outlines potential directions for future research.

2. Literature Survey

In recent years, numerous techniques have been proposed for accurate parameter estimation of solar photovoltaic (PV) models, with a strong focus on improving precision, computational efficiency, and convergence stability.

Rajasekar et al. (2013) [9] introduced the Bacterial Foraging Algorithm (BFA) for PV parameter estimation. This nature-inspired algorithm mimics the foraging behaviour of bacteria and was effectively applied to extract key parameters such as photocurrent, diode saturation current, and resistances. The method proved to be robust in handling the non-linearity of the PV model and yielded accurate estimations.

Jordehi et al. (2016) [10] provided a comprehensive review of PV parameter estimation techniques, categorizing them into analytical, numerical, and metaheuristic approaches. The study emphasized the increasing popularity of bio-inspired algorithms due to their flexibility and ability to avoid local minima. The review also identified challenges such as computation time and parameter sensitivity that remain unsolved in many existing methods.

El-Sayed et al. (2016) [11] proposed a novel parameter estimation technique and presented its performance at the IEEE Photovoltaic Specialists Conference. Their approach focused on improving the accuracy of the extracted parameters and was validated through both simulation and experimental analysis, showing enhanced performance over traditional techniques.

Jadli et al. (2017) [12] developed a novel technique for making calculation of parameter of PV models that simplified the extraction process while maintaining a high degree of accuracy. This method was successfully tested on various PV modules and proved effective for real-time applications.

Kang et al. (2018) [13] proposed an upgraded format of the Cuckoo Search Algorithm (CSA) for estimating PV model parameters. Their enhancements addressed convergence speed and accuracy issues, and experimental results demonstrated the method's superiority over traditional CSA and other metaheuristic algorithms.

Chen et al. (2018) [14] introduced a hybrid algorithm combining Teaching–Learning-Based Optimization (TLBO) and ABC for PV parameter estimation. The hybrid strategy leveraged both exploration and exploitation abilities, resulting in improved convergence and accuracy compared to standalone optimization techniques.

Jordehi et al. (2018) [15] further proposed the Enhanced Leader Particle Swarm Optimization (ELPSO), which modified the standard PSO by improving the leader selection mechanism. This improved the overall convergence behaviour and accuracy in extracting PV model parameters.

Venkateswari et al. (2021) [16] conducted a detailed review of parameter estimation methods used in solar PV systems. They highlighted the transition from traditional mathematical modelling to intelligent optimization techniques. Their study stressed the importance of hybrid and adaptive strategies for improving model accuracy.

Table 1: Summary of Literature on PV Parameter Estimation Techniques

Author(s)	**Method / Algorithm**	**Key Contribution**
Rajasekar et al. [9]	BFA	Nature-inspired method for PV parameter extraction
Jordehi et al. [10]	Literature Review	Classification of analytical, numerical, and metaheuristic methods
El-Sayed et al. [11]	Novel Estimation Technique	Presented at IEEE PVSC with simulation & experimental validation
Jadli et al. [12]	Simplified Extraction Method	Accurate and efficient for real-time applications
Kang et al. [13]	CSA	Enhanced convergence and accuracy
Chen et al. [14]	TLBO + ABC	Combined exploration and exploitation
Jordehi et al. [15]	ELPSO	Modified PSO with improved leader selection
Venkateswari et al. [16]	Review Study	Shift from traditional to intelligent optimization
Ayyarao et al. [17]	War Strategy-Inspired Algorithm	Novel bio-inspired method based on tactical decisions
Haddad et al. [18]	AHA	Used real-time environmental data in optimization
El-Sehiemy et al. [19]	AHO	Benchmarked against other metaheuristics
Ayyarao et al. [20]	AHO with Multi-objective Functions	Comparative study on fitness functions

Ayyarao et al. (2022) [17] presented a unique algorithm inspired by war strategies, offering a new perspective in PV parameter estimation. Their algorithm simulated tactical decisions and demonstrated a strong ability to find global optima, outperforming several existing algorithms.

Haddad et al. (2022) [18] explored the Artificial Hummingbird Algorithm (AHA) under realistic outdoor conditions for solar module parameter estimation. Their work stands out for using real-time irradiance and temperature values, integrating the hummingbird's foraging strategy into optimization. The study validated AHA's ability to accurately predict PV behaviour in variable environmental conditions, demonstrating better performance than conventional methods.

El-Sehiemy et al. (2023) [19] applied the Artificial Hummingbird Optimizer (AHO) for electrical parameter extraction in PV modules. The optimizer was benchmarked against multiple metaheuristic algorithms and showed faster convergence and higher accuracy. The study highlighted the effectiveness of AHO in handling nonlinear PV characteristics and emphasized its potential for real-world deployment.

Ayyarao et al. (2024) [20] advanced their previous work by applying the Artificial Hummingbird Optimization (AHO) using multiple objective functions for solar PV parameter estimation. Their comparative study on different fitness functions revealed that objective function selection significantly impacts the algorithm's accuracy and convergence behaviour. This paper not only validates AHO's adaptability but also opens doors for customized optimization strategies based on application-specific goals.

3. Proposed Method

Photovoltaic (PV) cell modelling is very important in designing, simulation, and optimization of solar energy systems. Among the various mathematical models developed, the Single Diode Model (SDM) is widely accepted because of the balance between accuracy and simplicity. The SDM is primarily used to replicate the non-linear electrical behaviour of PV cells and modules under various environmental conditions.

3.1 Equivalent Circuit Description

The single diode model is based on the electrical equivalent circuit of a solar cell, which comprises a current source (I_{ph}) in parallel with a diode, a shunt resistance (R_{sh}), and a series resistance (R_s) in series with the entire network.

The photocurrent source (I_{ph}) represents the current generated due to the absorption of photons. The diode models the behaviour of the p–n junction. The series resistance (R_S) accounts for internal resistive losses due to connections and material properties. The shunt resistance (R_{sh}) models leakage currents due to non-ideal insulation or impurities in the PV cell.

This model is effective in simulating the I–V and P–V characteristics of a solar cell and is thus extensively used in performance analysis and maximum power point tracking (MPPT) techniques.

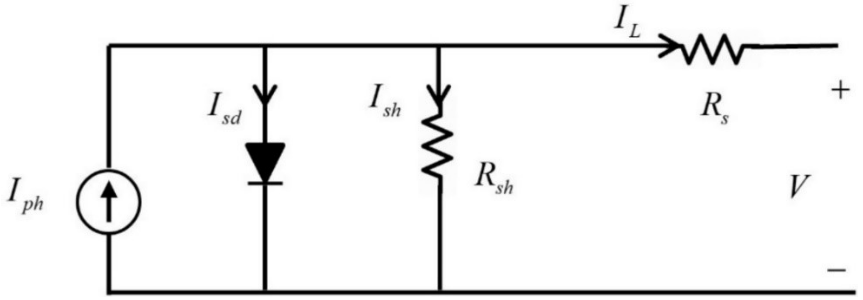

Figure 1: Equivalent circuit representing single diode model

The current continuity equation can be written as

$$I_L = I_{ph} - I_d - I_{sh} \tag{1}$$

where,

$$I_d = I_{sd}\left(e^{\frac{q\{V_L+I_LR_S\}}{nkT}} - 1\right) \text{ and } I_{sh} = \frac{V_L + I_LR_S}{R_{sh}} \tag{2}$$

Plugging equation 2 in equation 1 we get

$$I_L = I_{ph} - I_{sd}\left(e^{\frac{q\{V_L+I_LR_S\}}{nkT}} - 1\right) - \frac{V_L + I_LR_S}{R_{sh}} \tag{3}$$

The objective function can be written as

$$F_{ob\,j} = \sqrt{\frac{1}{N}\left(\sum_{i=1}^{N}\left[I_{L.mes} - I_{L.calc}\right]^2\right)} \tag{4}$$

3.2 Artificial Hummingbird Algorithm (AHA)

The AHA optimization method mimics their natural ability to locate, evaluate, and remember food sources, effectively balancing the exploration and exploitation phases—two critical components of optimization algorithms.
Similar to other metaheuristic techniques, AHA operates by structuring the search process into exploration, where the algorithm seeks new potential solutions, and exploitation, where it refines existing solutions to achieve better outcomes. The framework of AHA consists of three core components:

1. **Food Sources** – These represent the potential solutions to the optimization problem. Each food source is evaluated based on specific attributes such as nectar content, quality, replenishment rate, and time since its last visitation.
2. **Hummingbirds** – These agents explore and assess different food sources, dynamically updating their knowledge about the environment. They remember the locations of previously visited food sources and share information with others, facilitating collective intelligence.
3. **Visit Table** – This table keeps track of how frequently each food source is visited. It is continuously updated during each iteration of the algorithm, ensuring an adaptive and efficient search process.

The optimization process in AHA is guided by three primary foraging strategies that govern the movement and decision-making of hummingbirds:

- **Directed Foraging** – Hummingbirds selectively visit high-quality food sources, optimizing their search for the best solutions.
- **Territorial Foraging** – They defend and revisit specific food sources within their territory, refining local solutions.
- **Migratory Foraging** – When local resources become scarce, hummingbirds relocate to new regions, facilitating broader exploration of the solution space.

The flow chart in Figure 2, outlines the key steps and logical flow of the IAHO algorithm, beginning with the initialization of the population and algorithm parameters. The process continues with fitness evaluation and the application of foraging behaviours inspired by hummingbird flight strategies, such as axial, diagonal, and omnidirectional movements. Adaptive mechanisms are integrated to enhance convergence speed and avoid local optima. The global best solution is updated iteratively based on the foraging performance of the agents. The population is kept evolving by the algorithm until a termination criterion—like a maximum number of iterations or a suitable fitness level—is satisfied. The optimal or nearly optimal solution that the swarm discovered is the end result.

3.2.1 Initialization

A hummingbird population is dispersed at random among the available food sources in the manner described [18]. The algorithm's initialization phase is this distribution process, in which each hummingbird is given a position that represents a possible solution to the optimization problem.

$$x_i = LU + rand(0,1) \times \left(UP - LU\right) \qquad i = 1,\ldots n \tag{5}$$

Where LU and UP represent the lower and upper bounds of the search space, respectively, each food source position corresponds to a candidate solution for the optimization problem at hand. The position of each food source is initialized using a random vector whose elements are uniformly distributed in the range [0,1], ensuring diversity in the initial population.
The initialization of the visit table of food sources is as follows.:

$$VT_{i,j} = \begin{cases} 0 & if\ i \neq j \\ null & i = j \end{cases} \qquad i = 1,\ldots\ldots n; \quad j = 1,\ldots,n \tag{6}$$

As for the visit table, a value of null defines that a hummingbird is currently feeding at a specific food source. When a hummingbird has just visited a food source, the table is updated to reflect that event. For a given iteration, the visit table entry shows that the corresponding hummingbird has interacted with the food source during the current iteration.

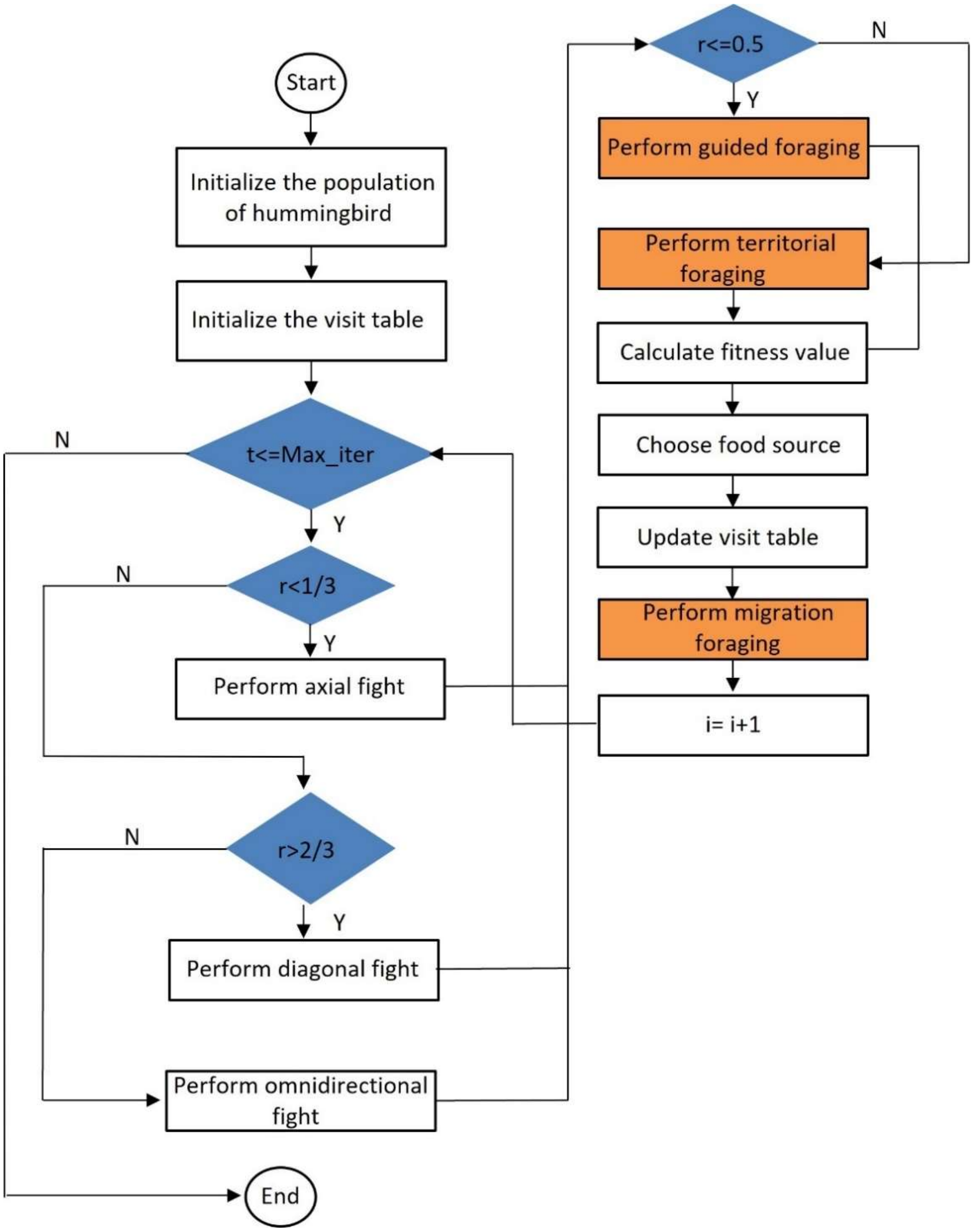

Figure 2: Flow chart for IAHO algorithm

3.2.2. Guided foraging

In the guided foraging phase, each hummingbird navigates toward the food source with the highest nectar concentration based on available knowledge. The movement behaviour during this phase can be categorized into three distinct flight types:

Axial Flight

This type of flight involves movement along one of the coordinate axes. It enables the hummingbird to explore the search space in a controlled, dimension-wise manner.

$$AF^{(i)} = \begin{cases} 1 & if \quad i = randi\left(\left[1,s\right]\right) \\ 0 & otherwise \end{cases} \qquad i = 1,......s; \tag{7}$$

Diagonal Flight

Diagonal flight involves movement along a combination of coordinate directions, allowing the hummingbird to travel in a straight line through a multi-dimensional space, covering multiple dimensions simultaneously.

$$AF^{(i)} = \begin{cases} 1 & if\, i = P\left(j\right), j \in \left[1,k\right], P = randperm\left(k\right), k \in \left[2, \left[r_1 * \left(s-2\right)\right] + 1\right] \\ 0 & else \qquad\qquad i = 1,.....d \end{cases} \tag{8}$$

Omnidirectional Flight

In omnidirectional flight, the hummingbird can move in any direction, providing the most flexible and exploratory movement pattern among the three types. The below given is the definition of omnidirectional flight:

$$AF^{(i)} = 1 \qquad i = 1,....,s \tag{9}$$

where r_1 is a random number (0, 1) and $randperm\left(k\right)$ creates a number permutation from 1 to k and $randi\left[1,s\right]$ is a random number between 1 and s. The mathematical formula for simulating directed foraging behaviour with an appropriate food source is provided below:

$$x_i^{'}\left(t+1\right) = x_i(t) + \phi_1.\left[x_g(t) - x_i(t)\right] \tag{10}$$

Where, $x_i(t)$ is the current position of the i^{th} hummingbird at time *t*, $x_g\left(t\right)$ is the position of the guiding (or target) food source with a higher nectar concentration, ϕ_1 is a guided factor sampled from a standard normal distribution (mean = 0, standard deviation = 1).

The hummingbird's newly calculated position is next assessed by figuring out the nectar replenishment rate, which, in the context of the optimization issue, corresponds to the objective function value. In comparison to the hummingbird's present food source, this assessment aids in determining the candidate's quality or fitness. The new site offers a better solution to the issue if the candidate food source's nectar replenishment rate is discovered to be higher than the present source's. Consequently, the hummingbird moves to the more promising food source and forsakes its existing one, increasing the algorithm's overall convergence behaviour. The latest position update for the food source can be mathematically described as follows:

$$x_i\left(t+1\right) = \begin{cases} x_i\left(t\right) & f\left(x_i\left(t\right)\right) \le f\left(x_i^{'}\left(t+1\right)\right) \\ x_i^{'}\left(t+1\right) & f\left(x_i\left(t\right)\right) > f\left(x_i^{'}\left(t+1\right)\right) \end{cases} \tag{11}$$

3.2.3 Territorial foraging

Within its own territory, a hummingbird can effortlessly move to a nearby location in search of food. This movement represents a localized exploration process, allowing the hummingbird to discover new food sources in its immediate surroundings. Often, such exploration may lead to the discovery of a food source that offers a higher nectar replenishment rate than its current location, encouraging the hummingbird to update its position.

$$x_i^{'}\left(t+1\right) = x_i(t) + \phi_2.\left[x_i(t)\right] \tag{12}$$

ϕ_2 is a guided factor sampled from a standard normal distribution (mean = 0, standard deviation = 1).

This behaviour forms the basis of the local foraging strategy, where the hummingbird focuses its search within a confined region. The strategy models the natural foraging tendencies of real hummingbirds, who often revisit and explore areas within their established territory in search of improved nectar yields.

3.2.4. Migration foraging

The migration of a hummingbird from a food source with the lowest nectar replenishment rate to a newly generated, randomly placed food source can be described in the following way:

$$x_{wor}\left(t+1\right)=Lb+r\cdot\left(Ub-Lb\right) \tag{13}$$

In this context, the variable representing the food source with the lowest nectar replenishment rate refers to the least productive or most depleted location among the available food sources in the hummingbird's environment. Over time, this source becomes less attractive due to its inability to regenerate nectar efficiently, prompting the need for migration.

To simulate realistic foraging behaviour, a hummingbird is assumed to use a combination of directed and territorial foraging strategies. In each iteration, it visits food sources sequentially, following a visit table that maintains the current foraging pattern. This sequence is only maintained if no replacements or migrations are triggered across all food sources.

4. Simulation and Results

The single-diode model is widely used to represent the electrical behaviour of a photovoltaic (PV) cell, as it closely aligns with empirical measurements obtained under various operating conditions. This model captures the non-linear characteristics of a real PV cell and is defined by five key parameters that need to be identified for accurate modelling and simulation. The objective in this context is to estimate the following five unknown parameters:

These parameters play a crucial role in determining the I–V (current–voltage) characteristics of the PV cell. Since they cannot be directly measured, they must be extracted through optimization techniques that minimize the difference between the modelled and experimentally observed performance of the PV cell.

To ensure realistic parameter estimation and avoid divergence during optimization, appropriate lower and upper bounds are set for each parameter. These bounds help define the search space for the optimization algorithm. The specific values of the lower and upper bounds for each of the five parameters are provided in Table 2.

Table 2: List and bounds of parameters

Parameter	LB	UB
$I_{ph}(A)$	1	0
$I_{sd}(\mu A)$	1	0
$R_{sh}(\Omega)$	100	0
$R_s(\Omega)$	0.5	0
η	2	1

The Figure 3, illustrates the convergence behaviour of the Improved Artificial Hummingbird Optimization (IAHO) algorithm over successive iterations. As the algorithm progresses, the best score typically improves (decreases for minimization problems), indicating that the algorithm is effectively exploring the search space and refining candidate solutions. The curve demonstrates the algorithm's ability to converge toward an optimal or near-optimal solution, with a sharp improvement in the early stages followed by gradual stabilization as it approaches convergence. This plot serves as a performance indicator for both convergence speed and solution quality.

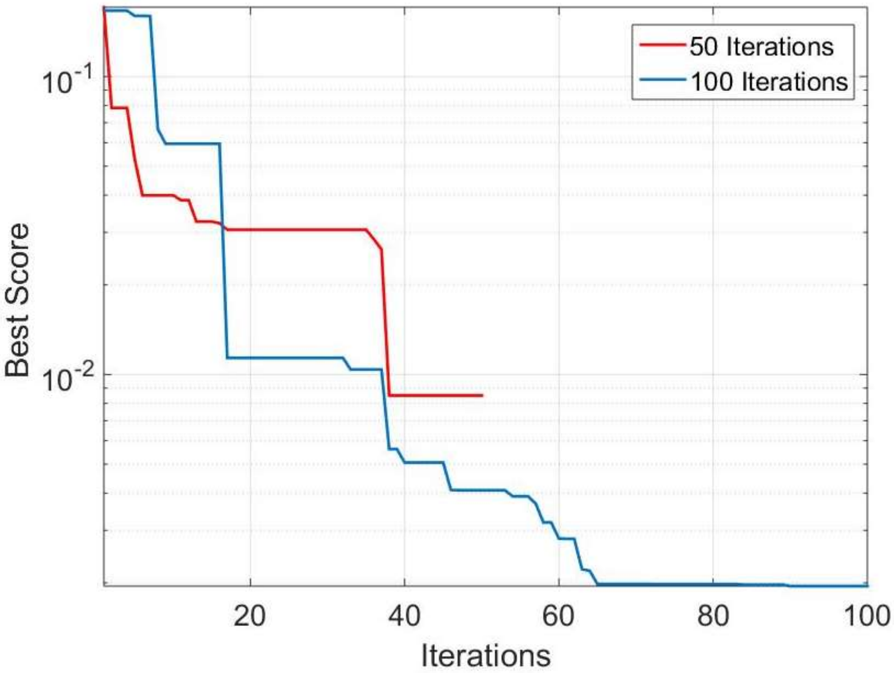

Figure 3: Best Score vs. Iterations for IAHO algorithm

In this figure, results are plotted for two different iteration counts: 50 and 100. The comparison shows that with 50 iterations, the algorithm achieves a reasonable approximation of the optimal solution, but with 100 iterations, the convergence is more refined and stable, leading to a more accurate and lower objective function value. This demonstrates the algorithm's scalability and improved precision with increased computational effort.

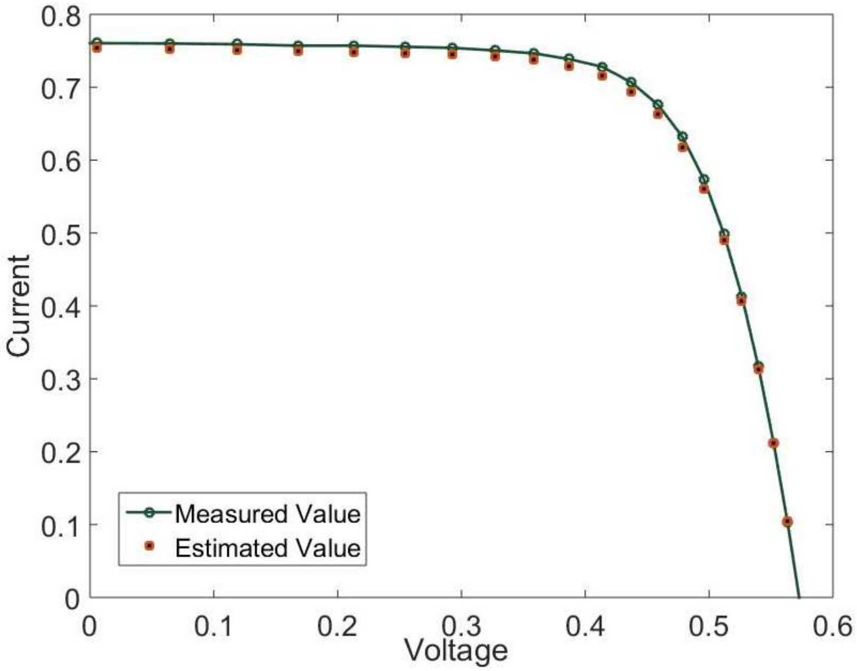

Figure 4: V vs I curve for measured and estimated values (50 Iterations)

The Figure 4,5 presents the voltage-current (V-I) curve comparing the estimated data obtained through the Improved Artificial Hummingbird Optimization (IAHO) algorithm with actual measured experimental data. The measured curve represents the real-world performance of the photovoltaic (PV) cell under specific operating conditions, while the estimated curve is derived by applying the IAHO algorithm to identify the optimal parameters of the PV model (such as photocurrent, diode saturation current, series and shunt resistances, and diode ideality factor).

In Figure 4, the voltage and current measurements obtained from the system are illustrated by a solid green curve, while the corresponding estimated values—derived using the proposed estimation algorithm—are depicted as red circular markers. A close examination of the figure reveals that the estimated values align closely with the measured data across the entire range. Although there are minor deviations between the two sets of values, these differences are minimal and fall within an acceptable margin of error, thereby validating the accuracy and reliability of the estimation technique at this stage.

The data presented in Figure 4 is the result of running the estimation algorithm for 50 iterations. At this point, the model has had sufficient time to learn and adjust its internal parameters based on the measured input data. The near-overlap of the red circles and the green curve shows that the estimator is effectively capturing the underlying dynamics of the system.

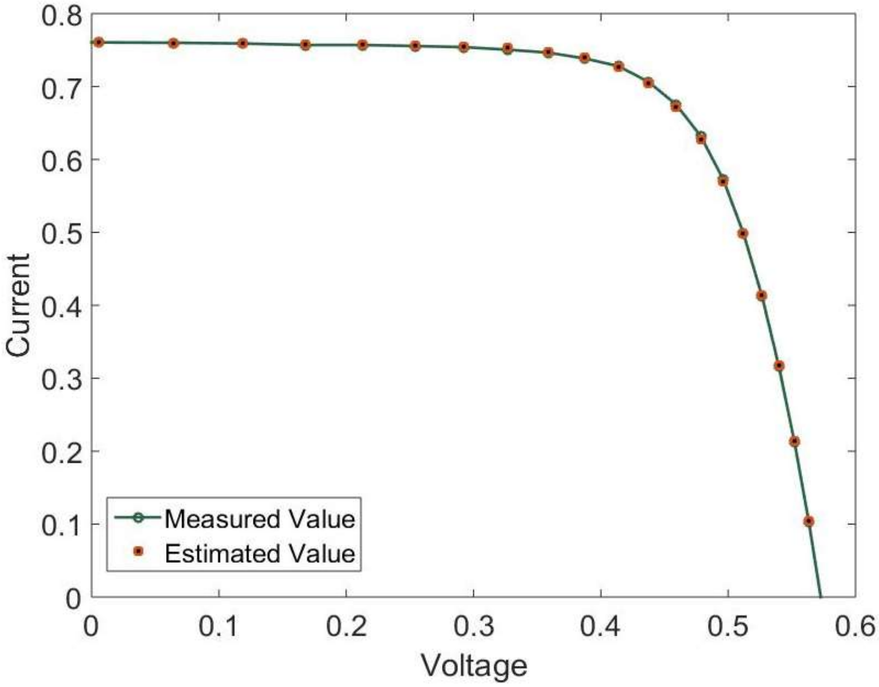

Figure 5: V vs I curve for measured and estimated values (100 Iterations)

Figure 5 presents a similar comparison after 100 iterations. With additional iterations, the estimation becomes even more refined. The red markers in Figure 5 exhibit an even closer match to the measured green curve, with a noticeable reduction in estimation error. This improvement highlights the effectiveness of the iterative process in enhancing the estimation accuracy over time.

The progressive enhancement from 50 to 100 iterations demonstrates the robustness of the proposed estimation method and its ability to converge towards the actual system behaviour with continued processing. These results confirm that the algorithm not only performs well in initial iterations but also improves significantly as it continues to learn from the data.

At 50 iterations, the estimated values closely followed the measured voltage and current waveforms, with only slight deviations visible in certain regions. The average estimation error for the V-I curve at this stage was calculated to be approximately 0.0085. This indicates a reasonably good level of accuracy even in the early stages of iteration.

As the number of iterations increased to 100, the estimator showed significant improvement in accuracy. The estimated values almost completely overlapped with the measured data, and the average estimation error in the V-I curve reduced to 0.0019. This substantial reduction in error demonstrates the convergence behaviour of the algorithm and its ability to learn the underlying system characteristics more effectively over time.

The close alignment between the two curves demonstrates the accuracy and robustness of the IAHO in modelling the nonlinear behaviour of PV cells. The minimal deviation across the entire voltage range indicates that IAHO effectively captures the key characteristics of the cell, making it a reliable tool for parameter extraction and system simulation. This validation also confirms the algorithm's potential for real-time PV performance analysis and optimization tasks.

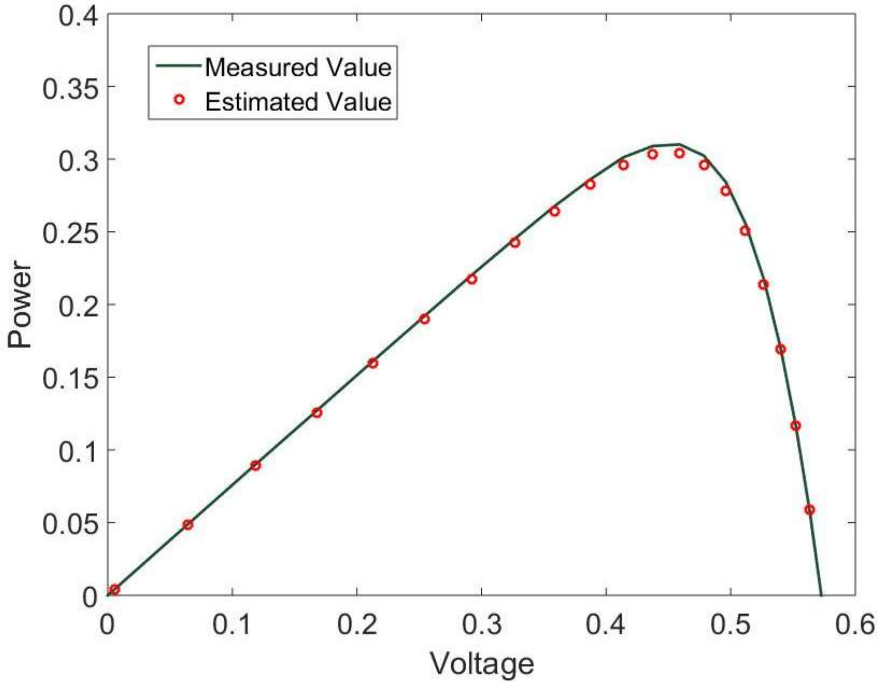

Figure 6: P vs V curve for measured and estimated values (50 Iterations)

In Figure 6, the relationship between power (P) and voltage (V) is depicted for both measured and estimated values after 50 iterations of the estimation algorithm. The measured P-V curve is shown as a solid green line, while the estimated values are represented by red circular markers. As observed, the estimated data closely follows the trend of the measured curve, indicating a strong agreement between the two. Although there are slight deviations at certain voltage levels, these differences are minimal and do not significantly impact the overall accuracy of the estimation. This result demonstrates the estimator's capability to capture the nonlinear characteristics of the power-voltage relationship, even in the earlier stages of convergence.

Figure 7 illustrates the same P-V relationship, but after 100 iterations. In this case, the estimated values (again shown as red circles) align even more closely with the measured green curve, suggesting an improvement in estimation accuracy due to the increased number of iterations. The slight discrepancies observed in Figure 6 are further reduced in Figure 7, confirming that the estimation algorithm benefits from additional iterations and gradually refines its output to better match the true system behaviour.

Together, Figures 6 and 7 highlight the convergence properties of the estimation method. The enhanced alignment between measured and estimated P-V values with increasing iterations validates the robustness and reliability of the algorithm in modelling the power-voltage characteristics of the system.

The Figures, illustrate the P-V curve of the PV cell, which shows how the output power varies with respect to the terminal voltage under given environmental conditions (e.g., irradiance and temperature). The curve is generated using the parameters estimated by the Improved Artificial Hummingbird Optimization (IAHO) algorithm and reflects the nonlinear behavior of PV systems. Initially, as the voltage increases from zero, the output power also increases, reaching a peak known as the Maximum Power Point (MPP). Beyond this point, further increases in voltage result in a rapid drop in power output due to the reduction in current. Identifying the MPP is crucial for optimizing energy harvesting, as it represents the operating condition at which the PV system delivers its maximum possible power. The smooth and accurate shape of the curve confirms that the IAHO algorithm is quite useful in accurately estimating model parameters that reflect real PV behaviour. This curve is also instrumental for developing and testing MPPT algorithms in practical PV systems.

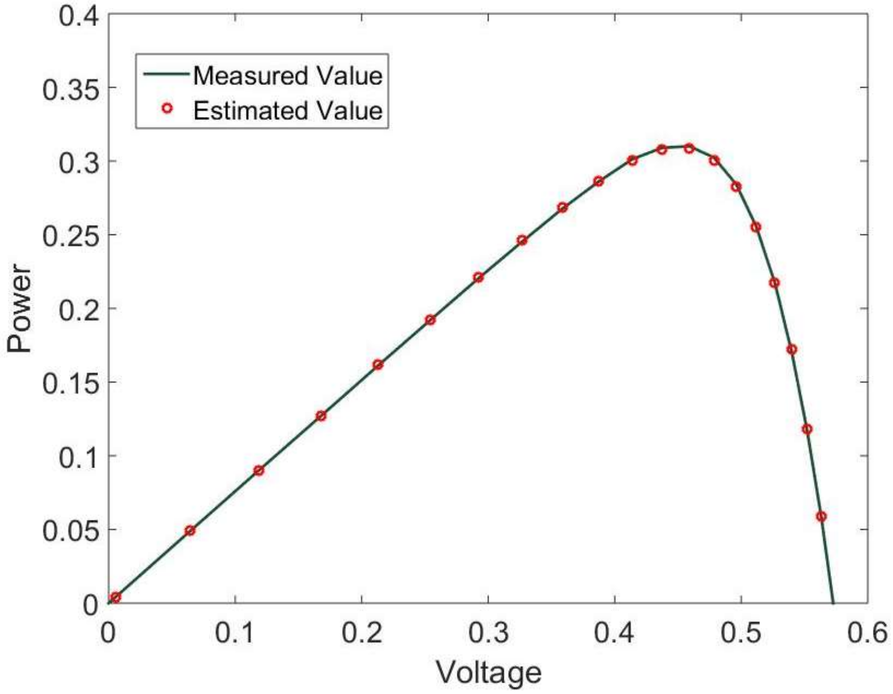

Figure 7: P vs V curve for measured and estimated values (100 Iterations)

5. Conclusion

In this work, a robust estimation algorithm was proposed to accurately predict key electrical parameters—voltage, current, and power—within a dynamic system. The method is based on iterative refinement, allowing it to progressively improve estimation accuracy with each iteration. By utilizing measured data and comparing it against estimated outputs, the algorithm effectively captures the underlying behaviour of the system.

In this work, a robust estimation algorithm was proposed for accurately predicting voltage, current, and power in a dynamic electrical system. The method employs an iterative approach, refining its predictions over time based on measured data. This enables the estimator to closely track the system's behaviour and adapt to its nonlinear characteristics.

The performance of the given technique was evaluated through a series of simulations, with results analysed after 50 and 100 iterations. At both stages, comparisons between measured and estimated values of voltage, current, and power showed strong alignment. The estimator demonstrated high accuracy even in earlier iterations, with minor deviations that decreased significantly as the iteration count increased. This improvement confirms the convergence behaviour of the algorithm and highlights its effectiveness in capturing system dynamics.

These findings validate the proposed approach as a reliable and practical tool for parameter estimation in electrical systems. Its ability to deliver accurate results with minimal error supports its potential use in real-time system monitoring, predictive control, and fault detection applications.

Looking ahead, future work may focus on extending the method to more complex and nonlinear systems, incorporating adaptive learning mechanisms, or validating its performance under diverse operating conditions to further assess its scalability and robustness in real-world implementations.

References

1. Tyagi, Vineet Veer, Nurul AA Rahim, N. A. Rahim, A. Jeyraj, and L. Selvaraj. "Progress in solar PV technology: Research and achievement." *Renewable and sustainable energy reviews* 20 (2013): 443-461.
2. Allouhi, Amine, Shafiqur Rehman, Mahmut Sami Buker, and Zafar Said. "Up-to-date literature review on Solar PV systems: Technology progress, market status and R&D." *Journal of Cleaner Production* 362 (2022): 132339.
3. Prabu, R. Thandaiah, S. Parasuraman, Satyajeet Sahoo, T. M. Amirthalakshmi, S. Ramesh, S. Agnes Shifani, S. Arockia Jayadhas et al. "The Numerical Algorithms and Optimization Approach Used in Extracting the Parameters of the Single-Diode and Double-Diode Photovoltaic (PV) Models." *International Journal of Photoenergy* 2022, no. 1 (2022): 5473266.
4. Tifidat, Kawtar, and Noureddine Maouhoub. "An efficient method for predicting PV modules performance based on the two-diode model and adaptable to the single-diode model." *Renewable Energy* 216 (2023): 119102.
5. Ghoto, Muhammad Imran, Mazhar Hussain Balouch, Touqeer Ahmed Jummani, and Ali Asghar Memon. "Parameters extraction of photovoltaic cells using swarm intelligence-based optimization technique: research on single diode model and double diode model." *Mehran University Research Journal Of Engineering & Technology* 42, no. 2 (2023): 158-168.
6. Younis, Abubaker, Abdalaziz Bakhit, Mahmoud Onsa, and Mohsin Hashim. "A comprehensive and critical review of bio-inspired metaheuristic frameworks for extracting parameters of solar cell single and double diode models." *Energy Reports* 8 (2022): 7085-7106.
7. Senthilkumar, S., V. Mohan, and G. Krithiga. "Brief review on solar photovoltaic parameter estimation of single and double diode model using evolutionary algorithms." *International Journal of Engineering Technologies and Management Research* 10, no. 1 (2023): 64-78.
8. El-Sehiemy, Ragab, Abdullah Shaheen, Attia El-Fergany, and Ahmed Ginidi. "Electrical parameters extraction of PV modules using artificial hummingbird optimizer." *Scientific Reports* 13, no. 1 (2023): 9240.
9. Rajasekar, N., Neeraja Krishna Kumar, and Rini Venugopalan. "Bacterial foraging algorithm based solar PV parameter estimation." *Solar Energy* 97 (2013): 255–265.
10. Jordehi, A. Rezaee. "Parameter estimation of solar photovoltaic (PV) cells: A review." *Renewable and Sustainable Energy Reviews* 61 (2016): 354–371.
11. El-Sayed, Mohamed Ibrahim, Mohamed Abd-El-Hakeem Mohamed, and Mohamed Hassan Osman. "A novel parameter estimation of a PV model." In *2016 IEEE 43rd Photovoltaic Specialists Conference (PVSC)*, pp. 3027–3032. IEEE, 2016.
12. Jadli, Utkarsh, Padmanabh Thakur, and Rishabh Dev Shukla. "A new parameter estimation method of solar photovoltaic." *IEEE Journal of Photovoltaics* 8, no. 1 (2017): 239–247.
13. Kang, Tong, Jiangang Yao, Min Jin, Shengjie Yang, and ThanhLong Duong. "A novel improved cuckoo search algorithm for parameter estimation of photovoltaic (PV) models." *Energies* 11, no. 5 (2018): 1060.
14. Chen, Xu, Bin Xu, Congli Mei, Yuhan Ding, and Kangji Li. "Teaching–learning–based artificial bee colony for solar photovoltaic parameter estimation." *Applied Energy* 212 (2018): 1578–1588.
15. Jordehi, A. Rezaee. "Enhanced leader particle swarm optimisation (ELPSO): An efficient algorithm for parameter estimation of photovoltaic (PV) cells and modules." *Solar Energy* 159 (2018): 78–87.
16. Venkateswari, Radhakrishnan, and Natarajan Rajasekar. "Review on parameter estimation techniques of solar photovoltaic systems." *International Transactions on Electrical Energy Systems* 31, no. 11 (2021): e13113.
17. Ayyarao, Tummala SLV, and Polamarasetty P. Kumar. "Parameter estimation of solar PV models with a new proposed war strategy optimization algorithm." *International Journal of Energy Research* 46, no. 6 (2022): 7215–7238.

18. Haddad, Sofiane, Badis Lekouaghet, Mohamed Benghanem, Ammar Soukkou, and Abdelhamid Rabhi. "Parameter estimation of solar modules operating under outdoor operational conditions using artificial hummingbird algorithm." *IEEE Access* 10 (2022): 51299-51314.
19. El-Sehiemy, Ragab, Abdullah Shaheen, Attia El-Fergany, and Ahmed Ginidi. "Electrical parameters extraction of PV modules using artificial hummingbird optimizer." *Scientific Reports* 13, no. 1 (2023): 9240.
20. Ayyarao, Tummala SLV, and G. Indira Kishore. "Parameter estimation of solar PV models with artificial humming bird optimization algorithm using various objective functions." *Soft Computing* 28, no. 4 (2024): 3371-3392.

International Journal of Intelligent Communication and Computer Science
Vol. 3, No. 1, 2025, Pages 31-52.

YOLO-Based Object Detection: Evolution, Real-Time Performance, and Applications in Intelligent Vision Systems

Benasir Begam.F[1]

[1]Department of Computer Science Engineering, Vels Institute of Science Technology and Advanced Studies (VISTAS), Chennai, Tamil Nadu, INDIA.

Review Paper

Email: benasirbegam.se@vistas.ac.in

Received: 13 Mar 2025, Revised: 23 May 2025, Accepted: 02 Jun. 2025

Abstract:

The YOLO (You Only Look Once) family of object detection algorithms has transformed the field of computer vision by enabling real-time, high-accuracy detection in diverse application scenarios. This review presents a comprehensive review of the architectural evolution of YOLO from the foundational YOLOv1 to the recent YOLOv8 emphasizing innovations such as anchor-free detection, multi-scale fusion, dynamic heads, and transformer-aware modules. Comparative evaluations against classical detectors like Faster R-CNN and SSD highlight YOLO's unparalleled balance between inference speed and detection precision, particularly in resource-constrained and embedded environments. The paper further explores YOLO's practical deployments in autonomous driving, smart surveillance, medical diagnostics, industrial automation, and agriculture. Benchmarking comparison across datasets such as COCO, KITTI, and PASCAL VOC are discussed alongside evaluation metrics like mean Average Precision (mAP), Intersection over Union (IoU), and inference latency. Key challenges including small object detection, domain adaptation, and explainability are examined, along with future directions involving edge-optimized deployment, multimodal integration, and ethical AI design. By consolidating architectural, empirical, and domain-specific perspectives, this review aims to serve as a foundational resource for researchers, engineers, and practitioners seeking to harness the power of YOLO in real-world intelligent vision systems.

Keywords: YOLO, object detection, real-time detection, YOLOv1 to YOLOv8

1. Introduction

Object detection, a cornerstone of computer vision, involves the identification and localization of objects within images or video streams, playing a critical role in applications such as autonomous driving, surveillance, robotics, and healthcare [1]. The ability to detect multiple objects within complex scenes, accurately and efficiently, is fundamental for creating intelligent systems capable of interacting with the world in real-time. Over the past decade, the landscape of object detection has dramatically shifted due to the advent of deep learning techniques, which have significantly enhanced both accuracy and computational efficiency compared to traditional methods. One of the most groundbreaking advancements in this field is the development of deep learning-based object detectors, particularly the You Only Look Once (YOLO) family of algorithms. YOLO has revolutionized real-time object detection by providing a fast, end-to-end solution that balances precision and inference speed, making it ideal for a wide range of applications, from industrial automation to augmented reality [2].

Historically, traditional object detection models like Region-based Convolutional Neural Networks (R-CNNs) relied on a two-stage approach. First, R-CNN would generate region proposals, followed by classification for each proposed region [3]. While this approach achieved high accuracy, it was computationally expensive due to the need to process each region individually, making it impractical for real-time applications where speed is critical. In contrast, YOLO introduced a novel, single-shot detection framework that reformulated the object detection problem as a regression task. By simultaneously predicting bounding boxes and class probabilities across the entire image in one pass, YOLO drastically improved inference speed while maintaining competitive accuracy. This ability to process entire images at once, rather than individually processing multiple proposals, resulted in significant reductions in computational time, making YOLO ideal for real-time applications [4].

As the YOLO family evolved from version 1 (YOLOv1) to the latest iteration, YOLOv8, it has demonstrated continual improvements in both architectural complexity and detection performance. The key innovation in YOLO's evolution lies in its growing architectural modularity, improved feature fusion mechanisms, and its adaptability to different hardware platforms. For instance, YOLOv4, a major milestone in this progression, incorporated advanced techniques like Cross-Stage Partial Networks (CSPNet) and Spatial Pyramid Pooling (SPP) to enhance the model's receptive field and improve gradient flow, making it more robust for detecting objects at various scales [5]. This architecture also integrated several optimizations for better performance on GPUs and lower-power devices, ensuring that YOLO could perform well in both research and real-world applications.

In more recent versions, such as YOLOv5 and YOLOv8, the focus shifted toward simplifying the architecture for even greater extensibility and ease of deployment. YOLOv5 embraced PyTorch-based implementations, which contributed to a more flexible and user-friendly framework for research and development [6]. Additionally, YOLOv5 introduced anchor-free detection, eliminating the reliance on pre-defined bounding box priors. This approach further enhanced the model's ability to generalize across different datasets and domains. YOLOv8 further improved on these principles, refining the architecture to increase both accuracy and speed while reducing model size, making it more suitable for edge deployment in resource-constrained environments [7]. These developments underscore YOLO's continuous adaptation to the demands of modern computer vision tasks, offering a combination of high accuracy, efficiency, and ease of deployment.

The practical impact of YOLO in various domains is striking. In autonomous driving**,** YOLO is used in real-time systems for detecting pedestrians, vehicles, and other obstacles, essential for the safety of self-driving cars and Advanced Driver Assistance Systems (ADAS) [8]. YOLO's ability to operate at high speeds and with high accuracy in dynamic, real-world environments is critical for these applications, where even small delays or inaccuracies could lead to dangerous situations. In medical imaging**,** YOLO-based models have shown significant promise in detecting anomalies such as tumours and lesions in radiological scans. These models enable faster and more reliable diagnoses, assisting healthcare professionals in making critical decisions [9]. YOLO's high accuracy and real-time capabilities have also been leveraged for industrial automation**,** where it helps identify defects on production lines and guide robotic arms in manufacturing processes.

Another area where YOLO has gained prominence is in edge computing**,** where computational resources are limited, and real-time performance is still crucial. YOLO's efficiency allows it to run on edge devices like NVIDIA Jetson, Raspberry Pi, and mobile SoCs, providing cost-effective, real-time visual intelligence without requiring powerful cloud infrastructure [10]. This makes YOLO an attractive option for applications in smart surveillance**,** agriculture**,** and security where real-time processing is necessary, but connectivity to the cloud is either slow or impractical. Its compatibility with a wide range of hardware platforms has significantly democratized access to advanced computer vision capabilities, opening up new opportunities for deploying AI in everyday devices.

The influence of YOLO extends beyond these application areas, as it has set new standards for the field of object detection. Its architecture and design principles have influenced many other models, particularly in terms of optimizing for both inference speed and accuracy. As deep learning research continues to advance, YOLO will likely remain a central player in shaping the future of real-time vision systems, with ongoing innovations in areas like multimodal integration, edge deployment, and ethical AI design.

As the YOLO family continues to evolve with a growing array of variants, applications, and deployment strategies, this paper offers a thorough review covering:

1. The architectural progression of YOLO from v1 to v8,
2. A comparative analysis of its performance against other leading detectors like Faster R-CNN and SSD,
3. Domain-specific applications, ranging from autonomous systems to industrial inspection,
4. Key limitations, lightweight implementations, and emerging trends shaping the future of YOLO.

By synthesizing the latest advancements and highlighting current gaps, this review aims to be an essential resource for researchers and engineers advancing the development of state-of-the-art, vision-based systems.

2. YOLO Architecture: From Yolov1 to Yolov8

The YOLO framework revolutionized the field of object detection by reimagining the problem as a single regression task, in contrast to traditional two-stage methods. Instead of first generating region proposals and then classifying them, YOLO unified both tasks into one end-to-end process. This shift not only simplified the detection pipeline but also drastically improved the speed of inference, making real-time detection feasible even on limited hardware.

From YOLOv1 to the latest YOLOv8, the architecture has undergone continuous refinement, evolving in response to emerging challenges and performance requirements [11]. Each successive version has introduced innovations aimed at improving accuracy, inference speed, and multi-scale adaptability. These innovations include the incorporation of anchor-free detection, better feature fusion techniques, and transformer-based modules, all of which have enhanced YOLO's ability to detect objects across a wide range of sizes and in diverse, complex environments.

In addition to these improvements in performance, YOLO has also been optimized for deployment feasibility. Later versions, especially YOLOv5 and YOLOv8, have focused on lightweight implementations and compatibility with various hardware platforms, including edge devices such as mobile phones, embedded systems, and IoT devices. This has made YOLO not just an academic tool, but a practical solution for real-world, resource-constrained applications in fields like autonomous driving, surveillance, healthcare, and industrial automation.

2.1 Yolov1: The Inception of Unified Detection

The introduction of YOLOv1 was a groundbreaking shift in object detection, offering a novel approach that changed the way detection tasks were addressed. Unlike traditional methods such as R-CNN and its variants, which relied on a two-stage process involving the generation of candidate regions followed by classification, YOLOv1 adopted a single-stage framework. It applied a single convolutional neural network (CNN) directly to the entire image, simultaneously performing both localization and classification in one forward pass [2].

YOLOv1 divided the image into an S × S grid, with each grid cell tasked with predicting a set number of bounding boxes, their corresponding confidence scores, and the probability distribution over various object classes, assuming that the object's center fell within that cell. This end-to-end design allowed the model to be trained and tested as a unified system, which greatly simplified the detection process and enabled real-time performance, reaching up to 45 frames per second (FPS) on a GPU at the time, a significant improvement over previous method.

However, while YOLOv1 excelled in speed, it struggled with accuracy, especially when detecting small objects or handling crowded scenes [12]. The grid-based approach made it difficult to capture fine-grained spatial details, leading to challenges with detecting small and overlapping objects. Additionally, the fixed number of bounding boxes per grid cell restricted the model's ability to effectively handle objects with diverse sizes and aspect ratios. As a result, objects in close proximity were often poorly localized, and some smaller objects were missed entirely.

2.2 Yolov2 and Yolov3

YOLOv2 (also known as YOLO9000) and YOLOv3 brought significant improvements over YOLOv1, addressing some of its major limitations while introducing new features that enhanced performance, flexibility, and accuracy [13].

2.2.1 YOLOv2 (YOLO9000)

YOLOv2, released in 2016, made substantial improvements in both accuracy and speed compared to YOLOv1. A key innovation in YOLOv2 was the introduction of batch normalization, which stabilized the learning process and sped up convergence. YOLOv2 also made several architectural changes that contributed to its improved performance:

1. **Anchor Boxes**: YOLOv2 introduced the use of anchor boxes, which helped the model better predict bounding boxes by allowing it to predict multiple box sizes per grid cell. This approach was inspired by the success of faster region-based methods like Faster R-CNN [14] and SSD [15], where the anchor boxes provided more flexibility in matching ground truth objects of varying sizes and aspect ratios.
2. **Fine-Grained Classification**: YOLOv2 integrated a multi-scale training approach, where the network was trained on images of different resolutions. This allowed the model to improve its detection performance on small objects and also made it more robust to variations in object size. YOLOv2 was also able to detect more than 9000 object classes, which is why it was dubbed YOLO9000.
3. **Darknet-19 Backbone**: YOLOv2 replaced the original YOLOv1 backbone with a more efficient architecture, Darknet-19, which was a 19-layer network designed to balance speed and accuracy [16]. This backbone helped YOLOv2 achieve faster inference while maintaining good accuracy, making it highly suitable for real-time applications.
4. **Better Localization and Detection**: With the use of anchor boxes and multi-scale training, YOLOv2 significantly improved localization accuracy, especially in detecting objects that were smaller or in more complex environments.

YOLOv2's improvements allowed it to achieve faster processing speeds, with detection rates of up to 40-45 FPS on a GPU, while significantly improving accuracy and robustness in comparison to YOLOv1.

2.2.2 YOLOv3

Released in 2018, YOLOv3 continued the evolution of YOLO with further enhancements aimed at improving detection performance and flexibility [4]. YOLOv3 addressed some of the key limitations of YOLOv2 and introduced several critical innovations:

1. **Improved Backbone (Darknet-53)**: YOLOv3 replaced the Darknet-19 backbone with Darknet-53 [17], a deeper and more powerful architecture. Darknet-53 utilized residual connections, which helped to mitigate the vanishing gradient problem and allowed the model to capture more complex features while maintaining high inference speed. This made YOLOv3 more capable of detecting objects with varied sizes, especially in challenging conditions.
2. **Multi-Scale Predictions**: One of the most significant changes in YOLOv3 was its adoption of multi-scale predictions. Instead of predicting bounding boxes at a single layer, YOLOv3 makes predictions at three different scales, allowing it to better detect objects of different sizes. This multi-scale approach made YOLOv3 highly effective for detecting both small and large objects within the same image, improving overall detection accuracy.
3. **Improved Bounding Box Prediction**: YOLOv3 also introduced independent object classification and bounding box regression for each scale, which made it more flexible in detecting overlapping or small objects. The model could now better handle objects that were previously difficult to detect using the fixed grid approach of YOLOv1 and YOLOv2.
4. **Better Class Prediction**: YOLOv3 switched from softmax to sigmoid activations for class predictions, allowing the model to handle multi-label classification more effectively. This was particularly important for situations where objects could belong to multiple classes simultaneously (e.g., a vehicle could also be classified as a truck and a car).
5. **Improved Detection Accuracy**: With the combination of Darknet-53, multi-scale predictions, and better bounding box regression, YOLOv3 improved both accuracy and precision compared to its predecessors. The model performed exceptionally well on benchmarks like COCO and PASCAL VOC [24], achieving better mean Average Precision (mAP) scores than YOLOv2.

YOLOv3 was capable of processing up to 30 FPS on a high-end GPU, maintaining the real-time detection capability that YOLO was known for, while offering significantly better accuracy, especially on larger and more complex datasets.

2.2.3 Key Differences Between YOLOv2 and YOLOv3

1. **Backbone**: YOLOv2 used Darknet-19, while YOLOv3 adopted Darknet-53, a deeper architecture that improved feature extraction.
2. **Multi-Scale Predictions**: YOLOv3's ability to predict at three different scales, compared to YOLOv2's single-scale predictions, greatly improved its performance on smaller objects and complex scenes.
3. **Class Prediction**: YOLOv3 used sigmoid activation for multi-label classification, unlike YOLOv2's softmax, allowing it to handle overlapping class predictions more effectively.
4. **Performance**: YOLOv3 achieved better accuracy than YOLOv2, especially on larger, more complex datasets, due to the more powerful architecture and multi-scale predictions.

2.3 YOLOv4

YOLOv4, released by Bochkovskiy et al. in 2020 [5], represented a significant milestone in the evolution of the YOLO framework, particularly as the first major update to come from the open-source community. Building on the successes of previous versions, YOLOv4 introduced several groundbreaking innovations to further enhance both training and inference performance. One of its primary objectives was to strike an optimal balance between detection accuracy and real-time speed, making it suitable for a wide range of practical applications. Key Innovations in YOLOv4 are:

1. **CSPDarknet53 Backbone**: YOLOv4 introduced Cross-Stage Partial Networks (CSPNet) [18] to improve the backbone architecture. The new CSPDarknet53 allowed for better gradient flow during training, particularly in deeper networks, by splitting the gradient flow path into partial stages. This architecture enhanced the model's ability to extract meaningful features from the input image, resulting in higher feature representation power without sacrificing computational efficiency.
2. **Spatial Pyramid Pooling (SPP)**: One of the standout features of YOLOv4 was the incorporation of Spatial Pyramid Pooling (SPP). SPP improved the model's ability to capture multi-scale contextual information by pooling feature maps at multiple scales. This technique allowed the network to handle objects of varying sizes more effectively by fusing context from different spatial resolutions, making YOLOv4 significantly more robust in detecting small, medium, and large objects within the same image.
3. **Mish Activation Function**: YOLOv4 also adopted the Mish activation function, which is a smooth, non-monotonic activation function. Mish outperformed the traditional ReLU (Rectified Linear Unit) and leaky ReLU activations in several benchmarks by enabling better gradient flow and improving model convergence. This change contributed to improved model accuracy by allowing the network to learn more complex, non-linear relationships in the data.
4. **Data Augmentation Techniques**: To enhance generalization and mitigate overfitting, YOLOv4 introduced advanced data augmentation strategies like Mosaic and CutMix. Mosaic augmentation combines four training images into a single image, allowing the model to learn better representations of various object scales and scenes. On the other hand, CutMix randomly cuts and pastes sections from different images to create new training examples, further enhancing the robustness of the model by forcing it to deal with unusual object compositions and occlusions.
5. **Improved Training Techniques**: YOLOv4 also optimized the training process by adopting CIoU (Complete Intersection over Union) as the loss function, which improved the localization accuracy compared to traditional IOU-based loss functions. Additionally, techniques like dropblock regularization and class label smoothing were used to prevent overfitting and ensure better generalization on unseen data.

In terms of performance, YOLOv4 achieved remarkable results. On the COCO dataset, it attained a mean Average Precision (mAP) of 43.5%, which was a significant improvement over earlier versions like YOLOv3. Despite these gains in accuracy, YOLOv4 maintained real-time inference speeds on a standard GPU with a processing rate of approximately 62 frames per second (FPS). This represented a substantial improvement in the speed-accuracy tradeoff, making YOLOv4 one of the best models in terms of both accuracy and real-time performance.

2.4 YOLOv5

YOLOv5, developed by Ultralytics in 2020 [19], quickly gained widespread adoption due to its modular architecture, seamless integration with PyTorch, and support for training on custom datasets. It became popular for its flexibility, ease of use, and scalability, which made it an appealing choice for both research and practical applications. Key Features of YOLOv5 are

1. **Modular Architecture**: YOLOv5 featured a highly modular design, allowing users to easily modify and extend the model based on specific requirements. This flexibility was particularly useful for different object detection tasks, as users could fine-tune specific layers, change the architecture, or adjust hyperparameters to improve performance.
2. **Multiple Versions**: YOLOv5 introduced five distinct model variants: n (nano), s (small), m (medium), l (large), and x (extra-large). These versions were designed to meet the needs of diverse deployment scenarios, from resource-constrained environments (nano and small) to high-performance systems (large and extra-large). This made YOLOv5 suitable for a wide range of devices, from edge devices to high-end GPUs.
3. **Auto-Learning of Bounding Box Anchors**: One of the standout features of YOLOv5 was its auto-learning bounding box anchors, which allowed the model to dynamically adjust and optimize anchor boxes during training. This helped improve the accuracy of bounding box predictions without the need for manually tuning anchor box sizes, making the model more adaptive to different datasets.
4. **Enhanced Augmentation Techniques**: YOLOv5 implemented several advanced augmentation techniques, such as auto-shape and auto-labelling. These techniques improved the model's robustness by automatically resizing and reshaping input images during training, ensuring better generalization to unseen data. Auto-labelling helped automate the process of labelling training data, further simplifying the model-building pipeline.
5. **Activation Functions**: YOLOv5 used Leaky ReLU and SiLU (Sigmoid Linear Unit) [20] activation functions in different model versions. These activations helped to prevent the vanishing gradient problem (in the case of Leaky ReLU) and improved non-linearity (with SiLU), resulting in better performance during both training and inference.
6. **Cross-Platform Deployment**: YOLOv5 was highly compatible with deployment tools like ONNX, TensorRT, and CoreML, enabling efficient cross-platform deployment. This allowed the model to be deployed not just on standard GPUs but also on edge devices, mobile platforms, and IoT devices. The ability to run YOLOv5 on a wide range of hardware platforms made it an attractive choice for real-time object detection applications in diverse settings.

Despite not being officially released by the original authors, YOLOv5 became widely used in both industry and academia due to its practical advantages. Its ease of use, flexibility, and high performance made it the go-to choice for many who required efficient object detection systems, especially for real-time applications on mobile and embedded platforms. The model's modular nature and ease of integration with popular frameworks like PyTorch also made it a favourite among researchers who wanted to experiment with and extend the YOLO architecture.

2.5 YOLOv6 and YOLOv7

YOLOv6 and YOLOv7, though less widely discussed than their predecessors, continued the tradition of improving upon the YOLO framework with a focus on performance, deployment efficiency, and feature enhancements for real-time object detection. These versions were aimed at addressing emerging challenges in the field while optimizing YOLO's capabilities in various practical applications.

2.5.1 YOLOv6

YOLOv6, released by Meituan in 2022 [21], focused on optimizing the model for industrial applications and edge computing, specifically for tasks involving real-time object detection on resource-constrained devices. While it retained the overall architecture and goals of previous YOLO versions, several key innovations helped improve its accuracy and inference speed. Key Features of YOLOv6 are

1. **Efficient Backbone Network:** YOLOv6 introduced a more efficient backbone architecture designed to reduce computational cost while maintaining accuracy. This was achieved by optimizing convolutional layers and reducing the depth of the network, making the model more suitable for deployment in environments with limited computational power.
2. **Advanced Feature Fusion:** YOLOv6 implemented improved feature fusion techniques to enhance the model's ability to detect objects across different scales. This allowed for better handling of objects with varying sizes, especially in real-time applications where objects may appear at various resolutions.
3. **Optimized for Edge Devices:** One of the standout aspects of YOLOv6 was its emphasis on edge device deployment. It was designed to run efficiently on lower-power hardware, such as embedded systems, making it ideal for IoT devices, security cameras, and mobile platforms. This efficiency was paired with a solid performance on industrial-scale applications like surveillance and autonomous systems.
4. **Training and Inference Speed:** YOLOv6 improved upon the training and inference speed of its predecessors, enabling real-time object detection with even more compact model variants. This made YOLOv6 highly suitable for scenarios where fast, on-the-fly predictions are crucial.
5. **Enhanced Data Augmentation:** YOLOv6 integrated advanced data augmentation strategies, including mixup and mosaic-like augmentations, which helped improve the robustness and generalization of the model to unseen data. This approach allowed the model to better handle diverse environments and various lighting conditions, common challenges in real-world applications.

YOLOv6 made significant strides in the industrial and edge computing domains, providing an efficient solution for resource-constrained environments while maintaining strong detection accuracy. It was especially popular for use in surveillance, autonomous navigation, and industrial automation.

2.5.2 YOLOv7

YOLOv7, released by Chien-Yao Wang et al. in 2022 [22], was another important update that brought further improvements in model performance, flexibility, and usability. YOLOv7 continued to focus on real-time detection but added new enhancements to better support a variety of applications, ranging from small object detection to large-scale, multi-class tasks. Key Features of YOLOv7 are

1. **Model Backbone and Neck Enhancements:** YOLOv7 used a hybrid backbone structure that combined features from both earlier YOLO versions and more advanced neural network techniques. This allowed the model to better capture spatial relationships within the image while retaining computational efficiency.
2. **Improved Detection Performance:** YOLOv7 brought improvements in mean average precision (mAP), particularly for small object detection, which had been a challenge for previous YOLO versions. The use of Multi-Scale Training and better feature pyramid networks (FPN) made the model highly effective at detecting objects across various scales, from tiny items to large objects.
3. **Reinforced Training Strategies:** YOLOv7 incorporated self-adversarial training (SAT) to help the model generalize better to different environments and data conditions. SAT allowed the model to simulate challenging situations and improve its robustness in detecting objects in noisy or cluttered settings.
4. **Optimized for Diverse Hardware:** Like YOLOv6, YOLOv7 continued to focus on cross-platform deployment, optimizing the model for use on GPUs, edge devices, and mobile platforms. Its versatility in deployment across various hardware setups made it a strong candidate for a wide array of real-world use cases, including in the fields of security, healthcare, and retail.
5. **Extended Support for Applications:** YOLOv7 expanded its applicability to several domain-specific tasks, particularly in medical imaging (for detecting anomalies and tumours), retail (for inventory management and customer behaviour tracking), and autonomous driving (for improved vehicle and pedestrian detection in complex environments).

YOLOv7 continued the trend of fast inference with real-time processing capabilities. On standard GPUs, it maintained a high frame rate (FPS), ensuring its usability in time-sensitive tasks, such as live video analysis,

object tracking, and augmented reality applications. Its ability to work efficiently with multi-scale objects and cluttered backgrounds made it particularly useful in dense environments.
YOLOv7 was a significant milestone in the YOLO series, offering better detection of small objects, improved performance with complex scenes, and more efficient deployment across different hardware platforms. It became widely adopted for applications requiring real-time, high-accuracy object detection in dynamic environments, particularly in industries like autonomous vehicles, smart cities, and robotics.

2.6 YOLOv8

YOLOv8, released in 2023 by Ultralytics [23], is the latest iteration in the YOLO (You Only Look Once) family of real-time object detection models. It builds on the successes of its predecessors but introduces several key improvements that make it faster, more accurate, and more efficient than earlier versions. YOLOv8 continues the trend of focusing on high performance, versatility, and ease of use, while addressing some of the challenges faced by previous versions in terms of deployment, scalability, and adaptability to various application domains. Key Features of YOLOv8 are

1. **Anchor-Free Detection**: YOLOv8, like YOLOv5, adopts an anchor-free approach for bounding box prediction. This means that instead of using pre-defined anchor boxes to predict object locations, YOLOv8 dynamically learns to predict bounding boxes directly from the input image. This approach not only simplifies the model architecture but also improves performance, especially when dealing with irregular object shapes or when bounding box sizes vary significantly across the dataset.
2. **Improved Backbone Network**: YOLOv8 introduced an enhanced backbone network that improves feature extraction while maintaining computational efficiency. This new backbone helps the model capture more detailed information at different levels, leading to better detection accuracy and robustness to variations in object appearance and scale.
3. **Multiscale Fusion**: YOLOv8 continues the trend of multi-scale fusion, which helps detect objects of various sizes in a single pass. The model uses feature pyramids and additional techniques to combine features from different layers of the network, enhancing its ability to detect small, medium, and large objects effectively. This is particularly useful in complex environments where objects are at varying distances or orientations.
4. **Transformer-Aware Modules**: One of the more novel features in YOLOv8 is the integration of transformer-based modules. These transformer modules help improve the model’s ability to capture long-range dependencies and contextual information in the image, particularly in challenging scenarios where objects are far apart or appear in complex arrangements. This hybrid approach blends the strengths of both CNNs and transformers, improving the model’s generalization and performance on complex datasets.
5. **Optimized for Edge and Mobile Deployment**: YOLOv8 has been fine-tuned for use in resource-constrained environments, making it well-suited for deployment on edge devices, mobile platforms, and IoT devices. It maintains high inference speeds while using less computational power compared to some of its predecessors. With support for frameworks like ONNX, TensorRT, and CoreML, YOLOv8 can be deployed across a wide range of devices, from smartphones to embedded systems.
6. **Better Generalization with Augmentation**: YOLOv8 leverages advanced data augmentation techniques, including mixup, cutout, and mosaic augmentations, which help improve the model's ability to generalize across different datasets and conditions. These augmentations help simulate a wide variety of real-world scenarios, making YOLOv8 more robust to changes in lighting, backgrounds, occlusions, and object shapes.
7. **Simplified Training and Fine-Tuning**: YOLOv8 simplifies the training and fine-tuning process, providing an easy-to-use interface for customizing the model for specific tasks. Users can fine-tune the model with their custom datasets, allowing YOLOv8 to be adapted for various domains such as autonomous driving, medical imaging, and industrial automation. Additionally, YOLOv8’s integration with PyTorch and TensorFlow makes it easier for developers and researchers to extend and experiment with the model.
8. **Real-Time Inference and Speed**: YOLOv8 continues to focus on real-time object detection. With its improvements in architecture and optimizations, it can achieve high frames-per-second (FPS) rates

even when deployed on GPUs with limited power, making it ideal for applications such as surveillance, robotics, and autonomous vehicles.

3. YOLO vs Other Object Detectors

In the evolving landscape of object detection, the YOLO (You Only Look Once) framework has consistently differentiated itself due to its unique balance between accuracy and real-time performance**.** However, to fully appreciate its strengths and limitations, it is important to compare YOLO with other leading object detection architectures, such as Faster R-CNN and Single Shot MultiBox Detector (SSD**)**. Each framework excels in different areas, and understanding these differences is key for selecting the appropriate model for various real-world applications.

3.1 Faster R-CNN: Accuracy-Driven, Region Proposal-Based Detection

Faster R-CNN, introduced by Ren et al. (2015), was a groundbreaking approach in object detection. It integrated the Region Proposal Network (RPN) with the Fast R-CNN detection module into a unified, end-to-end trainable framework. The RPN generates high-quality region proposals, which are then classified and refined by the Fast R-CNN network. This two-stage process allows Faster R-CNN to achieve state-of-the-art performance in terms of accuracy**,** particularly on benchmark datasets like COCO and PASCAL VOC [24]**.**

Strengths:

1. **High Accuracy**: By generating region proposals and refining them through deep backbone networks like ResNet-101 and FPN**,** Faster R-CNN achieves highly accurate object detection, particularly for small and complex objects.
2. **Powerful Feature Extractors**: The use of deep feature extractors such as ResNet enables Faster R-CNN to learn rich, hierarchical features, which are essential for complex tasks like fine-grained recognition **or** detecting small objects**.**

Limitations:

1. **Slow Inference**: The main trade-off with Faster R-CNN is its inference speed**.** The two-stage architecture significantly slows down the model, as it first proposes regions and then processes them through a separate classification and bounding box refinement stage. This results in typically low frame rates, around 5-7 FPS on high-end GPUs, making it less suitable for real-time applications such as autonomous driving**,** robotics**, or** surveillance**.**
2. **Complexity**: Faster R-CNN is more computationally intensive than single-stage detectors, which limits its applicability in resource-constrained environments, such as edge devices **or** mobile platforms**.**

3.2 SSD: A Faster Alternative with Trade-offs in Small Object Detection

The Single Shot MultiBox Detector (SSD)**,** proposed by Liu et al. (2016) [15], was one of the first object detection frameworks to move beyond the two-stage paradigm while still achieving real-time speed. SSD performs detection in a single pass through the network, using multiple convolutional filters at different feature map scales to detect objects at various sizes. This single-stage design allows SSD to maintain high frame rates and is more efficient than Faster R-CNN, particularly for simpler, less complex environments.

Strengths:

1. **Real-Time Performance**: SSD can process frames at 30–60 FPS on high-end GPUs, making it a suitable choice for real-time applications like live video processing and robotics**.**

2. **Multi-Scale Detection**: The model uses multiple feature maps at different resolutions, allowing it to detect objects at various scales effectively. This makes SSD a good choice for tasks where objects appear at different sizes in the same image, such as object tracking or video surveillance**.**

Limitations:

1. **Challenges with Small Objects**: Despite its advantages in real-time performance, SSD struggles with detecting small objects**.** This limitation arises from its reliance on lower-resolution feature maps in earlier layers of the network, which causes it to lose fine-grained details essential for detecting small or distant objects. This makes SSD less effective in scenarios like medical imaging **or** high-precision industrial inspection where small object detection is critical.
2. **Lower Accuracy**: While SSD achieves competitive accuracy, it generally lags behind models like Faster R-CNN in terms of precision, particularly in challenging scenarios with overlapping or occluded objects.

3.3 YOLO: Unified Detection for Real-Time Applications

YOLO revolutionized the field of object detection by framing the entire task as a single regression problem**.** Unlike Faster R-CNN and SSD, which rely on separate steps for generating region proposals and performing classification, YOLO processes the entire image in one go [25]. YOLO divides the image into a grid and predicts bounding box coordinates and class probabilities for each grid cell in a single forward pass, making it incredibly fast and efficient.

Strengths:

1. **Real-Time Detection**: YOLO achieves impressive inference speeds, with real-time detection capabilities at 45–70 FPS on GPUs, making it an ideal choice for time-sensitive applications like autonomous driving**,** security surveillance**, and** drone navigation**.**
2. **End-to-End Model**: YOLO's design simplifies the detection pipeline by treating the detection problem as a direct regression task. This allows YOLO to efficiently handle complex tasks while maintaining high frame rates, a major advantage in real-time systems.
3. **Improved Accuracy with Later Versions**: With successive updates (YOLOv2 to YOLOv8), the model has continued to improve in terms of both accuracy and detection speed**.** Later versions, like YOLOv4, YOLOv5, YOLOv7, and YOLOv8, incorporate advanced features such as residual connections, spatial pyramids**,** and attention mechanisms to enhance detection precision without compromising speed.

Limitations:

1. **Coarse Detection for Small Objects**: While YOLO has been a leader in real-time performance, early versions struggled with small object detection due to the coarse grid-based prediction mechanism. However, later versions (YOLOv4, YOLOv5, etc.) have implemented improvements such as multi-scale fusion and anchor-free techniques, which have addressed this issue to a great extent. Nevertheless, YOLO still faces challenges in detecting very small or densely packed objects compared to Faster R-CNN.
2. **Localization Errors**: YOLO has been criticized for having localization errors**,** particularly when objects are overlapping or near the edges of the grid. This issue arises from YOLO's use of a fixed grid to predict bounding boxes, which can result in inaccurate bounding box predictions for small or tightly clustered objects.

3.4 Comparative Analysis

Object detection models have different design goals that impact their accuracy, speed, and complexity. The Faster R-CNN framework prioritizes accuracy through a two-stage process involving region proposals but sacrifices inference speed, making it less suitable for real-time applications. Conversely, SSD and the YOLO family focus on single-stage detection, offering higher frame rates while balancing accuracy. Faster R-CNN achieves top-tier accuracy due to its region proposal mechanism and deep backbone networks like ResNet-101. However, this comes at the cost of significantly lower inference speeds (around 7 frames per second), which limits its use in scenarios demanding real-time detection. SSD, built on VGG-16 [26], was one of the first detectors to successfully bridge accuracy and speed for real-time detection. Despite faster speeds (around 22 FPS), SSD's performance on small objects is less reliable, largely due to its reliance on lower-resolution feature maps. YOLOv3 brought a significant advancement in balancing speed (~45 FPS) and accuracy (33% mAP) with its Darknet-53 backbone, offering a solid baseline for real-time applications. YOLOv4 further improved detection accuracy by integrating CSPDarknet53 and novel data augmentation techniques, achieving 43.5% mAP at 62 FPS, making it highly suitable for real-time but high-accuracy needs. YOLOv5s prioritized lightweight design, reducing parameters dramatically (~7 million), which enabled blazing-fast inference speeds (~140 FPS). This version is especially useful for edge deployments but comes with a moderate accuracy trade-off (36.5% mAP). YOLOv7 represents a state-of-the-art real-time detector with a novel E-ELAN backbone, achieving top accuracy (51.4% mAP) with competitive speed (~68 FPS). It is often favored for applications requiring the highest real-time precision. YOLOv8n is designed for edge optimization, featuring anchor-free detection and dynamic head architecture (C2f-Dynamic Head). It balances a lightweight parameter count (~6 million) with excellent inference speed (~90 FPS) and high accuracy (50.2% mAP), making it ideal for resource-constrained devices. The detail is summarized in Table 1.

Table 1: Performance Comparison of YOLO, SSD, and Faster R-CNN on COCO Dataset (Input Size ~512×512)

Model	Backbone	mAP (%)	Inference Speed (FPS)	Parameters (Millions)	Strengths
Faster R-CNN	ResNet-101	42.1	~7 FPS	~60M	High accuracy, poor real-time use
SSD	VGG-16	31.2	~22 FPS	~34M	Fast, less accurate for small objs
YOLOv3	Darknet-53	33.0	~45 FPS	~62M	Balanced speed and accuracy
YOLOv4	CSPDarknet53	43.5	~62 FPS	~64M	Enhanced accuracy and training stab.
YOLOv5s	Custom Backbone	36.5	~140 FPS	~7M	Lightweight, easy to deploy
YOLOv7	E-ELAN	51.4	~68 FPS	~37M	SOTA for real-time detection
YOLOv8n	C2f-Dynamic Head	50.2	~90 FPS	~6M	Anchor-free, edge-optimized

Figure 1, illustrates the Precision-Speed Trade-off Curve for various object detection models, including YOLO, SSD, and Faster R-CNN, evaluated on the COCO dataset. The plot maps Inference Speed (FPS) on the x-axis and mean Average Precision (mAP) on the y-axis, providing insight into the trade-offs between detection speed and accuracy. Models positioned toward the upper-right corner of the graph, such as YOLOv5s and YOLOv8n, offer high frame rates and competitive accuracy, making them ideal for real-time applications. Conversely, models like Faster R-CNN are more accurate but have significantly slower inference speeds, limiting their use in time-sensitive tasks. This trade-off is crucial for selecting the most appropriate model based on application requirements.

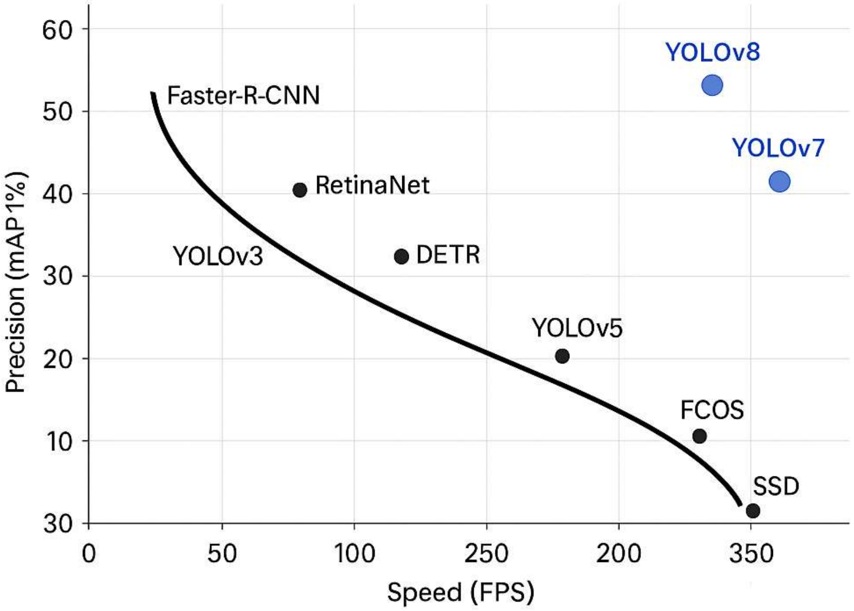

Figure 1: Precision-Speed Trade-off Curve for Detectors on COCO

4. Real-World Applications of YOLO-Based Detection Systems

The versatility of the YOLO architecture, marked by its single shot detection capability, low latency processing, and cross platform deployability, has propelled it into a wide range of real-world applications [27-30]. Its ability to perform accurate object detection in real time makes it a powerful solution for scenarios where speed, responsiveness, and efficiency are critical. In autonomous mobility, YOLO is used for detecting vehicles, pedestrians, and traffic signs, enabling safer navigation and decision making in self-driving systems. In public safety, it powers smart surveillance systems capable of monitoring crowded environments, identifying suspicious activities, and responding promptly to potential threats. In healthcare, YOLO is increasingly being integrated into diagnostic tools for detecting anomalies in medical imaging, such as tumours or lesions, thereby aiding early intervention. Its compatibility with lightweight hardware also allows deployment on drones, mobile phones, and embedded devices, extending its utility to agriculture, manufacturing, retail, and other domains.

4.1 Autonomous Driving and ADAS

YOLO's ability to detect multiple object categories such as pedestrians, vehicles, and traffic signs in a single forward pass makes it particularly well suited for autonomous driving systems and Advanced Driver Assistance Systems [31-33]. Its real time detection capability ensures that decisions related to navigation and obstacle avoidance can be made with minimal latency, which is crucial in dynamic and safety critical environments. Lightweight variants like YOLOv5n and YOLOv8n are specifically optimized for deployment on embedded GPUs such as NVIDIA Jetson Xavier and Jetson TX2. These edge computing platforms are commonly used in autonomous vehicles due to their compact form factor and high processing efficiency. When paired with YOLO models, they enable continuous visual perception under real world conditions without relying on cloud infrastructure.

In urban driving scenarios, YOLO plays an essential role in tasks that require fast and accurate interpretation of the environment. It is used for lane detection and traffic signal recognition, helping vehicles understand road layout and traffic flow. It also supports reliable identification of pedestrians and cyclists, enabling systems to respond to vulnerable road users in real time. Additionally, YOLO facilitates object tracking to monitor the motion of nearby vehicles or obstacles, which is vital for collision avoidance and safe manoeuvrings. Together, these capabilities make YOLO an integral component of modern autonomous systems, contributing to safer and more intelligent transportation solutions.

4.2 Smart Surveillance and Security

YOLO plays a crucial role in advancing smart surveillance and security systems by enabling real time analysis of video feeds from CCTV cameras. Its rapid detection capability allows for immediate identification of suspicious activities such as unauthorized access, loitering, high crowd density, or abnormal behaviour in sensitive or high-risk areas. Variants like YOLOv4 and YOLOv7 have demonstrated effectiveness in specialized tasks such as facial recognition, weapon detection, and license plate recognition, making them suitable for deployment in large scale urban surveillance networks [34-36]. These models are often combined with multi object tracking algorithms like DeepSORT, which help in continuously tracking individuals across multiple frames and camera views, providing situational awareness and supporting forensic analysis.

In practical applications, YOLO based systems are used for intrusion detection in restricted zones, ensuring that any unauthorized entry triggers real time alerts to security personnel. They are also employed to detect violent acts or behavioural anomalies in public spaces such as train stations, airports, or stadiums, helping authorities respond proactively. Furthermore, YOLO supports person re identification and biometric filtering, enabling advanced features such as matching individuals across different camera feeds or isolating subjects based on specific characteristics. These capabilities collectively enhance public safety, streamline security operations, and reduce human monitoring workloads in both private and government-operated environments.

4.3 Medical Imaging and Diagnostics

YOLO has increasingly found application in the medical imaging and diagnostics domain due to its high speed and precise localization capabilities, which are critical in time sensitive clinical environments. Its efficiency in identifying and localizing abnormalities within medical images makes it a valuable tool for assisting radiologists and medical professionals in various diagnostic tasks. For example, YOLOv3 and YOLOv5 have been successfully trained to detect COVID-19 related abnormalities in chest X ray images, enabling rapid triage and decision making during the pandemic. Similarly, YOLOv4 has been used to identify retinal lesions in fundus images, supporting the early diagnosis of diabetic retinopathy, a leading cause of blindness [37-39].

Beyond respiratory and ophthalmologic conditions, YOLO based pipelines have also been applied in dental diagnostics to identify caries and other structural anomalies. In oncology, YOLO models are used for tumour localization in MRI scans, helping pinpoint the exact position and size of lesions for further examination or treatment planning. Additionally, in pathology, YOLO supports the automated analysis of whole slide images by detecting cellular anomalies, thereby assisting in tasks such as cancer grading and tissue classification.

One of the key advantages of YOLO in healthcare is its ability to draw bounding boxes around regions of interest, making it easier for clinicians to quickly identify potential issues. This feature is particularly valuable in low resource or high-volume clinical settings where radiologists are under pressure to interpret large numbers of images. By reducing diagnostic time and improving consistency, YOLO enhances the efficiency of medical workflows and contributes to more timely patient care.

4.4 Industrial Automation and Smart Manufacturing

In the context of industrial automation and smart manufacturing, YOLO serves as a foundational tool for enabling machine vision systems that support real time quality assurance and operational efficiency. Within Industry 4.0 environments, where intelligent automation and data driven decision making are essential, YOLO models such as YOLOv5 and YOLOv6 are widely deployed on production lines to perform tasks that traditionally relied on manual inspection or basic sensor systems. These models are used to detect surface defects on materials such as metal sheets and plastic components, ensuring that flawed items are flagged or removed before reaching the next stage of manufacturing [39-42]. They also verify the correct placement of electronic components on printed circuit boards, identifying missing or misaligned parts that could compromise product functionality.

YOLO further assists in assessing the completeness and alignment of assembled units, helping maintain consistent product quality across high throughput environments. Due to its fast inference speed and high accuracy, YOLO can be deployed directly on edge devices installed along production lines, minimizing latency and reducing the need for cloud processing. In advanced setups, YOLO is integrated with robotic systems to enable vision guided pick and place operations. Instead of relying on simple proximity sensors, these systems use real time visual data to accurately locate and manipulate objects, enhancing flexibility and precision. This transition to vision-based automation not only improves defect detection and reduces downtime but also allows for greater adaptability in handling diverse product types and custom configurations.

4.5 Agriculture and Environmental Monitoring

Precision agriculture has increasingly embraced machine vision technologies to improve efficiency, sustainability, and decision making in farming practices. YOLO based detection pipelines are at the core of many of these solutions, offering fast and accurate visual analysis when deployed on drones or unmanned aerial vehicles equipped with RGB and multispectral cameras. These systems are capable of differentiating between diseased and healthy plant regions, enabling early intervention and minimizing crop loss. They are also used to estimate crop growth metrics by detecting plant density and canopy coverage, which supports yield prediction and resource planning. Additionally, YOLO models help identify the presence of animals in protected farming zones, reducing the risk of crop damage from wildlife [43-45].

Beyond agriculture, YOLO has found applications in broader environmental monitoring tasks. Researchers have applied it to detect plastic waste along coastal areas, monitor wildlife populations through camera traps, and track deforestation patterns using satellite imagery. These use cases demonstrate YOLO’s flexibility in analyzing a wide range of visual data under varying environmental conditions. A summary of the above discussed methods is provided in Table 2.

Table 2: YOLO Applications by Domain

Domain	Task	YOLO Version Used	Hardware Platform
Autonomous Driving	Vehicle and Pedestrian Detection	YOLOv5, YOLOv8	NVIDIA Jetson TX2 / Xavier
Medical Imaging	X-ray Analysis, Tumor Localization	YOLOv3, YOLOv4	GPU Workstation / TPU
Smart Surveillance	Face, Weapon, Crowd Detection	YOLOv4, YOLOv7	Edge AI Box / CCTV Server
Industrial Automation	Surface Defect Detection, Quality Check	YOLOv5s, YOLOv6	Jetson Devices with PLC Integration
Agriculture and Environment	Crop Monitoring, Wildlife Tracking	YOLOv5n, YOLOv8n	Raspberry Pi / Jetson Nano / Drones

5. Benchmark Datasets and Evaluation Metrics for YOLO-Based Detection

For any object detection algorithm to achieve widespread practical acceptance, it is essential to undergo thorough benchmarking using standard datasets and consistent evaluation metrics. This process ensures that models are tested under a variety of conditions and allows researchers and practitioners to objectively assess their strengths, limitations, and suitability for different applications. The YOLO family of models has been extensively evaluated on several popular benchmark datasets, each chosen to represent different real-world domains, image complexities, and detection challenges. These datasets play a crucial role in enabling fair comparisons of model performance in terms of accuracy, inference speed, and robustness against variations such as object scale, occlusion, and class diversity.

5.1 Datasets

Among the most widely used datasets are COCO, PASCAL VOC, KITTI, Open Images, VisDrone, and BDD100K. The COCO dataset, with over 330,000 images and 80 object classes, serves as the core benchmark for evaluating YOLO versions from YOLOv3 to YOLOv8. Its images feature a wide range of scales, complex backgrounds, and frequent occlusions, making it a comprehensive test of model generalizability and robustness. PASCAL VOC, an earlier benchmark used primarily for YOLOv1 and YOLOv2, contains fewer classes and images but remains relevant for assessing performance on cleaner, less cluttered scenes.

The KITTI dataset is specialized for autonomous driving, containing over 15,000 frames focused on vehicles, pedestrians, and cyclists in urban environments. It emphasizes 3D spatial relationships and temporal consistency, which are critical for real-time vehicle and pedestrian detection. Open Images is one of the largest datasets available, with over 9 million images spanning more than 600 classes. Its diversity and high-resolution images help YOLO models improve large-scale detection and pretraining for complex scenes, though it introduces challenges such as label noise and significant scale variation.

Other specialized datasets like VisDrone and BDD100K expand the scope of YOLO evaluation to aerial drone footage and diverse driving scenarios, respectively. VisDrone contains high-resolution images from UAVs and is commonly used to test YOLO variants in aerial surveillance and monitoring applications. BDD100K provides a rich collection of images under varying weather and lighting conditions, including nighttime driving, to test YOLO's adaptability to real-world autonomous vehicle environments.

Each dataset poses unique challenges that help benchmark the versatility and limitations of YOLO models. For example, COCO's crowded and occluded scenes test the model's ability to distinguish overlapping objects, while KITTI's emphasis on spatial and temporal information is crucial for vehicle and pedestrian tracking. Open Images pushes the model's capacity to handle a vast number of classes with noisy labels. Together, these datasets provide a comprehensive evaluation framework that supports continuous improvement and practical deployment of YOLO-based object detection systems. A summary of the above discussed datasets is provided in Table 3.

Table 3: Standard Datasets Used to Evaluate YOLO Models

Dataset	Domain	Classes	Image Count	Resolution	Usage in YOLO Research
COCO (2017) [46]	General Object Detection	80	330K+	Variable (~640×640)	Core benchmark for YOLOv3–YOLOv8
PASCAL VOC [24]	Object Detection	20	22K	500×375	Earlier YOLO versions (v1–v2)
KITTI [47]	Autonomous Driving	8	15K+ frames	1242×375	Real-time vehicle/person detection
Open Images [48]	General + Complex Scenes	600+	9M+	High Res	Pretraining, large-scale detection
VisDrone [49]	Aerial Drone Footage	10	10K+	~1920×1080	YOLO variants in UAV applications
BDD100K [50]	Autonomous Driving	10	100K	~720p	YOLO in nighttime/daylight settings

5.2 Key Evaluation Metrics

Key evaluation metrics play a critical role in assessing the performance of YOLO models by providing quantitative measures of their detection accuracy, localization quality, and inference efficiency. These standardized metrics allow researchers and practitioners to compare different model versions and other object detectors fairly and consistently.

mAP (mean Average Precision): One of the most important metrics is mean Average Precision (mAP), which summarizes the precision-recall curve into a single value representing overall detection accuracy [51]. It is typically calculated at an Intersection over Union (IoU) threshold of 0.5 (mAP@0.5) or averaged across multiple IoU thresholds from 0.5 to 0.95 in increments of 0.05 (mAP@[0.5:0.95]), following the COCO evaluation protocol. The mAP reflects both the model's ability to correctly identify objects and precisely localize them.

IoU (Intersection over Union): Intersection over Union (IoU) itself measures the degree of overlap between the predicted bounding box and the ground truth annotation (Figure 2). A higher IoU signifies better alignment, which directly impacts detection quality [52].

Precision and Recall: Precision quantifies the proportion of correct positive detections among all predicted positives, highlighting the model's ability to avoid false alarms. Recall measures the proportion of actual objects detected by the model, reflecting its completeness in identifying all relevant instances.
FPS (Frames Per Second): For real-time applications, inference speed is a critical metric, often expressed in Frames Per Second (FPS). Higher FPS indicates faster processing, which is essential for scenarios such as autonomous driving or video surveillance.
Latency (ms/frame): Latency, measured as the time taken to process each frame (in milliseconds per frame), offers a more precise measure of delay, especially relevant in embedded systems where hardware constraints impact performance.

$$IoU = \frac{Area\ of\ Overlap}{Area\ of\ Union}$$

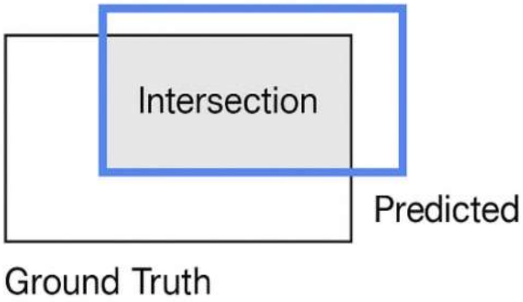

Figure 2: Illustration of IoU Between Ground Truth and Predicted Bounding Box

5.3 YOLO Benchmark Results on COCO (Standard Input ~640×640)

The COCO dataset serves as a critical benchmark for evaluating the performance of YOLO models, using a standardized input size of approximately 640 by 640 pixels. The following Table 4, summarizes the key metrics for prominent YOLO versions, highlighting their accuracy, inference speed, model complexity, and notable characteristics.

Table 4: YOLO Benchmark Results on COCO Dataset

Model	**mAP@[0.5:0.95]**	**FPS (RTX 2080Ti)**	**Parameters (M)**	**Notes**
YOLOv3	33.0	~45	62	Multi-scale prediction head
YOLOv4	43.5	~62	64	SOTA in 2020, high accuracy
YOLOv5s	36.5	~140	7.5	Extremely lightweight
YOLOv7	51.4	~68	37	Unified tasks, real-time speed
YOLOv8n	50.2	~90	6.2	Anchor-free, edge-optimized

This comparison illustrates the progressive improvements made in YOLO architectures, with later versions like YOLOv7 and YOLOv8n pushing the boundaries of accuracy while maintaining or even increasing inference speed. YOLOv5s and YOLOv8n, with their smaller model sizes, demonstrate the suitability of YOLO for deployment on resource-constrained devices, without a severe sacrifice in detection performance. Meanwhile, YOLOv4 marked a significant leap forward in accuracy during its time, maintaining a strong presence in real-time applications. Overall, these results highlight YOLO's versatility and scalability across different operational requirements and hardware platforms.

5.4 Reduced Congestion and Spectrum Efficiency

To achieve fair and unbiased benchmarking of object detection models such as those in the YOLO family, it is essential to standardize evaluation protocols across several key factors. First, all models should be tested on the same dataset splits, for example, the COCO 2017 validation set, ensuring that performance comparisons reflect the same underlying data distribution. Second, input image sizes must be standardized—commonly at dimensions like 416 by 416 or 640 by 640 pixels—since variations in input resolution can significantly impact both accuracy and inference speed.

Furthermore, speed metrics such as Frames Per Second (FPS) or latency must be measured under consistent hardware conditions. This includes specifying the inference engine used, for instance, comparing results using TensorRT optimized runtimes versus native PyTorch implementations, as different environments can yield substantially different speed results. Lastly, transparency in training settings is critical; details such as the number of training epochs, batch size, and data augmentation strategies should be clearly reported. This transparency ensures that differences in model performance are not due to variations in training effort or methodology, but rather reflect inherent model capabilities.

By adhering to these guidelines, researchers and engineers can reduce measurement congestion and improve spectrum efficiency in benchmarking, facilitating more meaningful and reproducible comparisons across object detection algorithms.

6. Challenges in YOLO-Based Detection

Despite the remarkable success of the YOLO family of models across diverse application domains, several technical and practical challenges continue to affect their reliability, generalizability, and ease of integration into high-stakes real-world systems. These challenges range from inherent algorithmic limitations to issues related to deployment and ethical considerations.

6.1 Small Object Detection and Dense Scenes

YOLO's detection architecture is based on dividing the input image into a grid, which can create difficulties in accurately detecting small objects, especially when these objects occupy only a few pixels in the image [53]. Although improvements introduced from YOLOv3 onward include multi-scale detection layers designed to better capture small objects, challenges persist in highly crowded or cluttered environments. For example, aerial drone surveillance and medical pathology images often present scenes with many small or overlapping objects. In these cases, the relatively coarse resolution of deep feature maps makes it difficult for YOLO to maintain high precision and recall. Studies on datasets such as VisDrone and UAVDT demonstrate this limitation quantitatively; for instance, YOLOv4 achieves approximately 35 percent mean Average Precision for small objects, while achieving around 50 percent for medium and large objects. This discrepancy underscores the difficulty in detecting small targets under complex visual conditions.

6.2 Occlusion and Partial Visibility

In many real-world applications such as urban navigation or indoor robotics, objects frequently appear partially occluded or only partially visible. YOLO's earlier anchor-based versions struggle in such scenarios because they produce deterministic bounding box predictions without explicitly modelling uncertainty or occlusion [54]. This can lead to missed detections or incorrect bounding boxes when objects are obscured. More recent versions like YOLOv7 and YOLOv8 have incorporated deeper context aggregation modules, including architectures such as E-ELAN and dynamic heads, which improve the model's robustness to occlusion. However, they still fall short of the full robustness demonstrated by methods that employ attention-based spatial reasoning or graph-based scene understanding, which explicitly model relationships between objects and their surroundings to better handle partial visibility.

6.3 Domain Shift and Poor Generalization

YOLO models are usually trained on large, curated datasets such as COCO or PASCAL VOC, which may not fully represent the diversity of real-world deployment environments. When these models are applied in conditions that differ significantly from their training data, for example, different weather conditions, lighting variations, camera angles, or sensor modalities and their performance often degrades. This issue, known as domain shift, is particularly problematic in critical fields such as medical imaging, agriculture, and autonomous driving, where the availability of labelled data for fine-tuning or transfer learning is limited by data privacy regulations, high annotation costs, or lack of access to domain-specific datasets.

6.4 Real-Time Constraints on Edge Devices

Although YOLO has demonstrated success in porting to edge devices such as NVIDIA Jetson platforms and Raspberry Pi, limitations related to inference speed, power consumption, and thermal management persist. Lightweight YOLO variants like YOLOv5n and YOLOv8n reduce model size and parameters to around six million to facilitate deployment on resource-constrained hardware [55]. However, devices powered by batteries or low-power processors, including drones and microcontrollers, still face challenges in running high-resolution inference at real-time speeds without further optimization. Techniques such as model pruning, quantization, and hardware acceleration using frameworks like TensorRT or Coral Edge TPU are often necessary to meet stringent latency and energy efficiency requirements.

6.5 Lack of Interpretability and Explainability

In sensitive and high-stakes domains such as healthcare, forensics, and law enforcement, the black-box nature of YOLO models raises concerns related to accountability, trust, and fairness [56]. While interpretability tools like Grad-CAM, saliency maps, and confidence heatmaps offer visual insights into which regions influenced model predictions, they do not provide causal explanations or detailed reasoning behind decisions. This lack of explainability limits the adoption of YOLO-based systems in domains where transparent decision-making is essential. Furthermore, fairness audits have revealed that models trained on imbalanced datasets can amplify biases when deployed in diverse real-world settings, particularly in applications involving facial recognition or pedestrian detection, which can lead to ethical and legal challenges.

6.6 Data Annotation Cost and Scarcity

YOLO models require high-quality, precise bounding box annotations for supervised training, which can be expensive and time-consuming to generate, especially in specialized fields such as medical imaging, industrial inspection, or remote sensing. Although emerging semi-supervised learning methods and synthetic data generation techniques—such as those involving generative adversarial networks (GANs) or simulation platforms like NVIDIA Omniverse offer promising alternatives, these approaches often demand careful domain-specific tuning and currently lack widely accepted standards. Consequently, the scarcity of annotated data remains a bottleneck for scaling YOLO applications to new or niche domains.

7. Conclusion

The YOLO family has established itself as a pivotal breakthrough in the field of real-time object detection by offering an exceptional blend of speed, accuracy, and architectural elegance. From its inception with YOLOv1 through to the latest YOLOv8, the series has undergone significant algorithmic advancements, including a notable transition from anchor-based to anchor-free detection methods. These developments have been guided by practical considerations aimed at optimizing performance across a diverse range of deployment scenarios, from embedded edge devices and autonomous vehicles to complex industrial systems.

This review has meticulously traced the architectural evolution of YOLO, beginning with the original grid-based prediction mechanism in YOLOv1, progressing through innovations like decoupled detection heads, dynamic convolutional layers, and transformer-inspired modules introduced in YOLOv8. A detailed comparative analysis with prominent object detectors such as Faster R-CNN and SSD reveals YOLO's distinct advantage in real-time applications, delivering high-speed inference without sacrificing significant detection accuracy. This balance makes YOLO particularly well-suited for environments where latency is critical.

Beyond algorithmic improvements, the versatility of YOLO across numerous domains has been highlighted, encompassing autonomous driving, intelligent surveillance, medical imaging, industrial automation, and precision agriculture. The model's ability to adapt and perform effectively in such varied fields underscores the robustness and generality of its core design principles.

Nonetheless, several challenges persist. YOLO continues to face difficulties in accurately detecting small or heavily occluded objects, coping with domain shifts during deployment in novel environments, and providing interpretability and transparency in decision-making processes—especially in high-stakes or sensitive applications. Addressing these issues remains an active area of research. Future iterations of YOLO and its derivatives are likely to incorporate advances from neuromorphic computing, edge AI optimization techniques, multimodal sensor fusion, and frameworks for explainable artificial intelligence, thereby enhancing their robustness and trustworthiness.

In conclusion, YOLO has transformed from a pioneering yet somewhat coarse detector into a sophisticated, scalable, and highly adaptable engine for visual intelligence. Its continuing development promises to significantly influence not only the field of object detection but also the broader realms of real-time machine perception and intelligent vision systems for years ahead.

References

1. Hosain, Md Tanzib, Asif Zaman, Mushfiqur Rahman Abir, Shanjida Akter, Sawon Mursalin, and Shadman Sakeeb Khan. "Synchronizing object detection: applications, advancements and existing challenges." IEEE access (2024).
2. Redmon, Joseph, Santosh Divvala, Ross Girshick, and Ali Farhadi. "You only look once: Unified, real-time object detection." In Proceedings of the IEEE conference on computer vision and pattern recognition, pp. 779-788. 2016.
3. Girshick, Ross, Jeff Donahue, Trevor Darrell, and Jitendra Malik. "Rich feature hierarchies for accurate object detection and semantic segmentation." In Proceedings of the IEEE conference on computer vision and pattern recognition, pp. 580-587. 2014.
4. Redmon, Joseph, and Ali Farhadi. "Yolov3: An incremental improvement." arXiv preprint arXiv:1804.02767 (2018).
5. Bochkovskiy, Alexey, Chien-Yao Wang, and Hong-Yuan Mark Liao. "Yolov4: Optimal speed and accuracy of object detection." arXiv preprint arXiv:2004.10934 (2020).
6. Jocher, Glenn, Alex Stoken, Jirka Borovec, Liu Changyu, Adam Hogan, Laurentiu Diaconu, Francisco Ingham et al. "ultralytics/yolov5: v3. 1-bug fixes and performance improvements." Zenodo (2020).
7. Ultralytics. "YOLOv8: Next-generation object detection and segmentation." *GitHub Repository* (2023).
8. Ma, Lingzhe, Yu Chen, and Jilin Zhang. "Vehicle and pedestrian detection based on improved YOLOv4-tiny model." In *Journal of Physics: Conference Series*, vol. 1920, no. 1, p. 012034. IOP Publishing, 2021.
9. Yao, Shangjie, Yaowu Chen, Xiang Tian, Rongxin Jiang, and Shuhao Ma. "An improved algorithm for detecting pneumonia based on YOLOv3." *Applied Sciences* 10, no. 5 (2020): 1818.
10. Lin, Tsung-Yi, Michael Maire, Serge Belongie, James Hays, Pietro Perona, Deva Ramanan, Piotr Dollár, and C. Lawrence Zitnick. "Microsoft coco: Common objects in context." In *Computer vision–ECCV 2014: 13th European conference, zurich, Switzerland, September 6-12, 2014, proceedings, part v 13*, pp. 740-755. Springer International Publishing, 2014.
11. Hussain, Muhammad. "Yolov1 to v8: Unveiling each variant–a comprehensive review of yolo." *IEEE access* 12 (2024): 42816-42833.
12. Parisapogu, Samson Anosh Babu, Nitya Narla, Aarthi Juryala, and Siddhu Ramavath. "Towards Safer Roads: A Comprehensive Review of Object Detection Techniques for Autonomous Vehicles." *SN Computer Science* 6, no. 5 (2025): 1-20.
13. Sang, Jun, Zhongyuan Wu, Pei Guo, Haibo Hu, Hong Xiang, Qian Zhang, and Bin Cai. "An improved YOLOv2 for vehicle detection." *Sensors* 18, no. 12 (2018): 4272.
14. Girshick, Ross. "Fast r-cnn." In *Proceedings of the IEEE international conference on computer vision*, pp. 1440-1448. 2015.
15. Liu, Wei, Dragomir Anguelov, Dumitru Erhan, Christian Szegedy, Scott Reed, Cheng-Yang Fu, and Alexander C. Berg. "Ssd: Single shot multibox detector." In *Computer Vision–ECCV 2016: 14th European Conference, Amsterdam, The Netherlands, October 11–14, 2016, Proceedings, Part I 14*, pp. 21-37. Springer International Publishing, 2016.

16. Ningthoujam, Richard, Keisham Pritamdas, and Loitongbam Surajkumar Singh. "Edge detective weights initialization on Darknet-19 model for YOLOv2-based facemask detection." *Neural Computing and Applications* 36, no. 35 (2024): 22365-22378.
17. Yang, Lina, Gang Chen, and Wenyan Ci. "Multiclass objects detection algorithm using DarkNet-53 and DenseNet for intelligent vehicles." *EURASIP Journal on Advances in Signal Processing* 2023, no. 1 (2023): 85.
18. Wang, Chien-Yao, Alexey Bochkovskiy, and Hong-Yuan Mark Liao. "Scaled-yolov4: Scaling cross stage partial network." In *Proceedings of the IEEE/cvf conference on computer vision and pattern recognition*, pp. 13029-13038. 2021.
19. Zhang, Yu, Zhongyin Guo, Jianqing Wu, Yuan Tian, Haotian Tang, and Xinming Guo. "Real-time vehicle detection based on improved yolo v5." *Sustainability* 14, no. 19 (2022): 12274.
20. Jocher, Glenn, Alex Stoken, Jirka Borovec, Liu Changyu, Adam Hogan, Ayush Chaurasia, Laurentiu Diaconu et al. "ultralytics/yolov5: v4. 0-nn. SiLU () activations, Weights & Biases logging, PyTorch Hub integration." *Zenodo* (2021).
21. Li, Chuyi, Lulu Li, Hongliang Jiang, Kaiheng Weng, Yifei Geng, Liang Li, Zaidan Ke et al. "YOLOv6: A single-stage object detection framework for industrial applications." *arXiv preprint arXiv:2209.02976* (2022).
22. Wang, Chien-Yao, Alexey Bochkovskiy, and Hong-Yuan Mark Liao. "YOLOv7: Trainable bag-of-freebies sets new state-of-the-art for real-time object detectors." In *Proceedings of the IEEE/CVF conference on computer vision and pattern recognition*, pp. 7464-7475. 2023.
23. Sohan, Mupparaju, Thotakura Sai Ram, and Ch Venkata Rami Reddy. "A review on yolov8 and its advancements." In *International Conference on Data Intelligence and Cognitive Informatics*, pp. 529-545. Springer, Singapore, 2024.
24. Tong, Kang, and Yiquan Wu. "Rethinking PASCAL-VOC and MS-COCO dataset for small object detection." *Journal of Visual Communication and Image Representation* 93 (2023): 103830.
25. Joseph, Ejiyi Chukwuebuka, Olusola Bamisile, Nneji Ugochi, Qin Zhen, Ndalahwa Ilakoze, and Chikwendu Ijeoma. "Systematic advancement of YOLO object detector for real-time detection of objects." In *2021 18th international computer conference on wavelet active media technology and information processing (ICCWAMTIP)*, pp. 279-284. IEEE, 2021.
26. Alippi, Cesare, Simone Disabato, and Manuel Roveri. "Moving convolutional neural networks to embedded systems: the alexnet and VGG-16 case." In *2018 17th ACM/IEEE International Conference on Information Processing in Sensor Networks (IPSN)*, pp. 212-223. IEEE, 2018.
27. Vijayakumar, Ajantha, and Subramaniyaswamy Vairavasundaram. "Yolo-based object detection models: A review and its applications." *Multimedia Tools and Applications* 83, no. 35 (2024): 83535-83574.
28. Ali, Momina Liaqat, and Zhou Zhang. "The YOLO framework: A comprehensive review of evolution, applications, and benchmarks in object detection." *Computers* 13, no. 12 (2024): 336.
29. Lavanya, Gudala, and Sagar Dhanraj Pande. "Enhancing Real-time Object Detection with YOLO Algorithm." *EAI Endorsed Transactions on Internet of Things* 10 (2024).
30. Ragab, Mohammed Gamal, Said Jadid Abdulkadir, Amgad Muneer, Alawi Alqushaibi, Ebrahim Hamid Sumiea, Rizwan Qureshi, Safwan Mahmood Al-Selwi, and Hitham Alhussian. "A comprehensive systematic review of YOLO for medical object detection (2018 to 2023)." *IEEE Access* 12 (2024): 57815-57836.
31. Ayachi, Riadh, Yahia Said, Mouna Afif, Aadil Alshammari, Manel Hleili, and Abdessalem Ben Abdelali. "Assessing YOLO models for real-time object detection in urban environments for advanced driver-assistance systems (ADAS)." *Alexandria Engineering Journal* 123 (2025): 530-549.
32. Sarda, Abhishek, Shubhra Dixit, and Anupama Bhan. "Object detection for autonomous driving using yolo [you only look once] algorithm." In *2021 Third international conference on intelligent communication technologies and virtual mobile networks (ICICV)*, pp. 1370-1374. IEEE, 2021.
33. Wibowo, Ari, Bambang Riyanto Trilaksono, Egi Muhammad Idris Hidayat, and Rinaldi Munir. "Object detection in dense and mixed traffic for autonomous vehicles with modified yolo." *IEEE Access* 11 (2023): 134866-134877.
34. Narejo, Sanam, Bishwajeet Pandey, Doris Esenarro Vargas, Ciro Rodriguez, and M. Rizwan Anjum. "Weapon detection using YOLO V3 for smart surveillance system." *Mathematical Problems in Engineering* 2021, no. 1 (2021): 9975700.

35. Sanjalawe, Yousef, and Hamzah Alqudah. "Integrating Enhanced Security Protocols with Moving Object Detection: A Yolo-Based Approach for Real-Time Surveillance." In *2024 2nd International Conference on Cyber Resilience (ICCR)*, pp. 1-6. IEEE, 2024.
36. Oguine, Kanyifeechukwu Jane, Ozioma Collins Oguine, and Hashim Ibrahim Bisallah. "Yolo v3: Visual and real-time object detection model for smart surveillance systems (3s)." In *2022 5th Information Technology for Education and Development (ITED)*, pp. 1-8. IEEE, 2022.
37. Ragab, Mohammed Gamal, Said Jadid Abdulkadir, Amgad Muneer, Alawi Alqushaibi, Ebrahim Hamid Sumiea, Rizwan Qureshi, Safwan Mahmood Al-Selwi, and Hitham Alhussian. "A comprehensive systematic review of YOLO for medical object detection (2018 to 2023)." *IEEE Access* 12 (2024): 57815-57836.
38. Soni, Akanksha, and Avinash Rai. "YOLO for Medical Object Detection (2018–2024)." In *2024 IEEE 3rd International Conference on Electrical Power and Energy Systems (ICEPES)*, pp. 1-7. IEEE, 2024.
39. George, Jose, and Shibon Skaria. "Using YOLO based deep learning network for real time detection and localization of lung nodules from low dose CT scans." In *Medical Imaging 2018: Computer-Aided Diagnosis*, vol. 10575, pp. 347-355. SPIE, 2018.
40. Hussain, Muhammad. "YOLO-v1 to YOLO-v8, the rise of YOLO and its complementary nature toward digital manufacturing and industrial defect detection." *Machines* 11, no. 7 (2023): 677.
41. Zendehdel, Niloofar, Haodong Chen, and Ming C. Leu. "Real-time tool detection in smart manufacturing using You-Only-Look-Once (YOLO) v5." *Manufacturing Letters* 35 (2023): 1052-1059.
42. Yan, Jihong, and Zipeng Wang. "YOLO V3+ VGG16-based automatic operations monitoring and analysis in a manufacturing workshop under Industry 4.0." *Journal of Manufacturing Systems* 63 (2022): 134-142.
43. Badgujar, Chetan M., Alwin Poulose, and Hao Gan. "Agricultural object detection with You Only Look Once (YOLO) Algorithm: A bibliometric and systematic literature review." *Computers and Electronics in Agriculture* 223 (2024): 109090.
44. Badgujar, Chetan M., Alwin Poulose, and Hao Gan. "Agricultural object detection with you look only once (yolo) algorithm: A bibliometric and systematic literature review." *arXiv preprint arXiv:2401.10379* (2024).
45. Song, Jisu, Dongseok Kim, Eunji Jeong, and Jaesung Park. "Determination of Optimal Dataset Characteristics for Improving YOLO Performance in Agricultural Object Detection." *Agriculture* 15, no. 7 (2025): 731.
46. Jain, Swasti, Sonali Dash, and Rajesh Deorari. "Object detection using coco dataset." In *2022 International Conference on Cyber Resilience (ICCR)*, pp. 1-4. IEEE, 2022.
47. Ramos, Filipa, Alexandre Correia, and Rosaldo JF Rossetti. "Assessing the YOLO series through empirical analysis on the KITTI dataset for autonomous driving." In *International Conference on Intelligent Transport Systems*, pp. 203-218. Cham: Springer International Publishing, 2019.
48. Kuznetsova, Alina, Hassan Rom, Neil Alldrin, Jasper Uijlings, Ivan Krasin, Jordi Pont-Tuset, Shahab Kamali et al. "The open images dataset v4: Unified image classification, object detection, and visual relationship detection at scale." *International journal of computer vision* 128, no. 7 (2020): 1956-1981.
49. Cao, Yaru, Zhijian He, Lujia Wang, Wenguan Wang, Yixuan Yuan, Dingwen Zhang, Jinglin Zhang et al. "VisDrone-DET2021: The vision meets drone object detection challenge results." In *Proceedings of the IEEE/CVF International conference on computer vision*, pp. 2847-2854. 2021.
50. Zhang, Xiaoqing. "Research on Automatic Driving Safety Image Recognition Based on Deep Learning." In *2024 IEEE 7th International Conference on Automation, Electronics and Electrical Engineering (AUTEEE)*, pp. 457-463. IEEE, 2024.
51. Du, Juan. "Understanding of object detection based on CNN family and YOLO." In *Journal of Physics: Conference Series*, vol. 1004, p. 012029. IOP Publishing, 2018.
52. Rezatofighi, Hamid, Nathan Tsoi, JunYoung Gwak, Amir Sadeghian, Ian Reid, and Silvio Savarese. "Generalized intersection over union: A metric and a loss for bounding box regression." In *Proceedings of the IEEE/CVF conference on computer vision and pattern recognition*, pp. 658-666. 2019.
53. Hu, Mengzi, Ziyang Li, Jiong Yu, Xueqiang Wan, Haotian Tan, and Zeyu Lin. "Efficient-lightweight yolo: Improving small object detection in yolo for aerial images." *Sensors* 23, no. 14 (2023): 6423.
54. Liu, Ruoying, Miaohua Huang, Liangzi Wang, Chengcheng Bi, and Ye Tao. "PDT-YOLO: a roadside object-detection algorithm for multiscale and occluded targets." *Sensors* 24, no. 7 (2024): 2302.

55. Liang, Siyuan, Hao Wu, Li Zhen, Qiaozhi Hua, Sahil Garg, Georges Kaddoum, Mohammad Mehedi Hassan, and Keping Yu. "Edge YOLO: Real-time intelligent object detection system based on edge-cloud cooperation in autonomous vehicles." *IEEE Transactions on Intelligent Transportation Systems* 23, no. 12 (2022): 25345-25360.
56. Mokdad, S. I., Anas Khalid, Diaa Nasr, and Manar Abu Talib. "Interpretable deep learning: evaluating YOLO models and XAI techniques for video annotation." In *IET Conference Proceedings CP870*, vol. 2023, no. 39, pp. 487-496. Stevenage, UK: The Institution of Engineering and Technology, 2023.

.

Machine Learning Applications in Material Science for Microstructure Analysis and Property Prediction

G. Suvetha[1], Meenakshi N[2], Varunraj S[3], Gopalakrishnan T[3]

[1]Department of ECE, Vels Institute of Science, Technology & Advanced Studies (VISTAS), Chennai, Tamil Nadu, India.
[2]Department of CSE, Vels Institute of Science, Technology & Advanced Studies (VISTAS), Chennai, Tamil Nadu, India.
[3]Department of Mechanical Engineering, Vels Institute of Science, Technology & Advanced Studies (VISTAS), Chennai, Tamil Nadu, India·

Review Paper

Email: gsuvetha.se@vistas.ac.in

Received: 13 Apr 2025, Revised: 02 Jun. 2025 Accepted: 11 Jun 2025

Abstract:

The integration of machine learning (ML) into material science marks a paradigm shift from empirical discovery to data-driven innovation. This paper presents a comprehensive exploration of how ML techniques spanning supervised, unsupervised, reinforcement, and deep learning are transforming the design, characterization, and optimization of materials. By leveraging structured and unstructured datasets, ML enables rapid prediction of material properties, automated microstructure analysis, and accelerated discovery cycles. Case studies illustrate successful applications such as thermal conductivity prediction of polymer-metal composites and alloy optimization using Bayesian frameworks. Deep learning models, particularly convolutional neural networks and autoencoders, have shown exceptional promise in processing complex imaging data and generating synthetic microstructures. Despite notable progress, challenges persist in data heterogeneity, model interpretability, and integration with physical principles. The paper advocates for the adoption of physics-informed ML, multi-fidelity modelling, and active learning to address these issues. Ultimately, this work positions machine learning as a foundational tool in building autonomous, intelligent materials research platforms for next-generation applications.

Keywords: Machine Learning, Materials Informatics, Deep Learning, Microstructure Analysis, Property Prediction, Alloy Design.

1. Introduction

Material science, a cornerstone of modern engineering and applied physics, has traditionally advanced through empirical heuristics, phenomenological modelling, and incremental experimental validation. However, with the exponential growth of multi-scale material systems and the push for multifunctionality in aerospace, biomedical, and energy sectors, the limitations of these conventional paradigms have become increasingly evident. These limitations include high costs, long development times, and the inability to efficiently navigate vast compositional spaces. The integration of Machine Learning (ML) into materials research has emerged as a disruptive solution, offering unprecedented capabilities to discover hidden patterns, model non-linear relationships, and predict material behaviours across multiple length and time scales [1,2].

Machine learning refers to a class of algorithms that learn from data to make predictions or decisions without being explicitly programmed. In materials science, this means leveraging large, structure d or unstructured datasets from computational simulations, experimental results, to imaging data to develop predictive models for properties such as yield strength, bandgap energy, fracture toughness, or corrosion resistance [3]. ML models can rapidly assess property-composition relationships, optimize synthesis conditions, and even generate entirely new material candidates through generative models [4].

This paradigm shift is fundamentally altering the classic Materials Science Tetrahedron linking processing, structure, properties, and performance into a closed-loop, data-driven system, wherein ML algorithms interconnect experimental data, computational models, and domain-specific knowledge. The result is a significant acceleration in the pace of innovation, with autonomous materials discovery and design now becoming a tangible possibility [5]. In particular, high-throughput methods integrated with ML such as the Materials Project or Open Quantum Materials Database—are redefining how materials are screened, validated, and commercialized [6].

Despite its promise, several barriers still impede the full adoption of machine learning in materials research. The heterogeneity and sparsity of data, lack of standardized descriptors, and concerns over the interpretability of models remain persistent challenges [7]. Furthermore, most materials datasets are relatively small compared to those in other ML-dominated fields like natural language processing or image recognition. This necessitates the development of physics-informed ML, transfer learning, and active learning frameworks to effectively utilize domain-specific priors and small datasets [8].

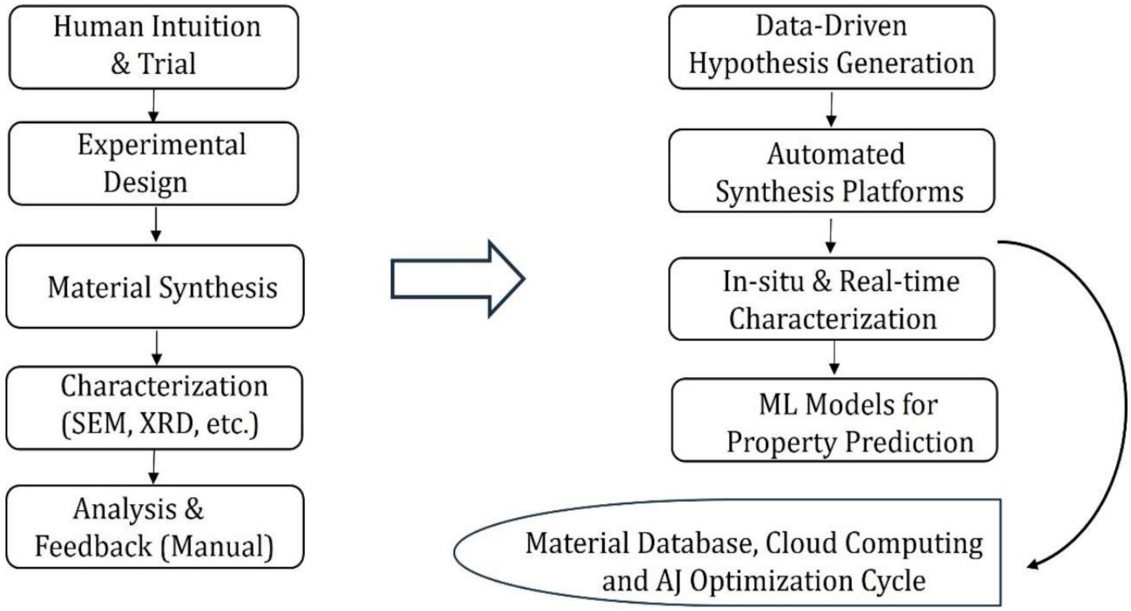
Human Intuition & Trial
Experimental Design
Material Synthesis
Characterization (SEM, XRD, etc.)
Analysis & Feedback (Manual)
Data-Driven Hypothesis Generation
Automated Synthesis Platforms
In-situ & Real-time Characterization
ML Models for Property Prediction
Material Database, Cloud Computing and AJ Optimization Cycle

Figure 1: Paradigm Shift from Classical Materials Discovery to ML-driven Closed-Loop Framework

Figure 1, illustrates the transition from traditional materials discovery methods to a modern, machine learning (ML)-enabled closed-loop framework. In the classical approach, materials discovery follows a linear path from hypothesis generation and experimental testing to analysis and validation which often involves extensive trial and error, is time-consuming, and lacks adaptability. In contrast, the ML-driven closed-loop framework integrates data collection, predictive modelling, and automated experimentation in a cyclical process. Here, ML algorithms are trained on existing data to predict promising materials candidates. These candidates are then validated through simulations or experiments, with new results fed back into the ML model to improve its accuracy and guide the next iteration. This continuous feedback loop accelerates the discovery process, reduces cost, and enables more precise targeting of desired material properties, representing a transformative shift in materials science research.

Table 1: Comparative Summary of Traditional vs. ML-driven Materials Research Pipelines

Aspect	Traditional Pipeline	ML-Driven Pipeline
Hypothesis Generation	Based on expert intuition and literature review	Data-driven using ML insights and feature correlation analysis
Experimental Design	Manual planning, low-throughput	Automated/high-throughput using Design of Experiments (DoE) and ML tools
Synthesis Method	Laboratory-based, slow iteration	Automated synthesis platforms guided by ML models
Characterization	Offline techniques (SEM, XRD, etc.)	In-situ, real-time with sensor integration and AI monitoring
Property Prediction	Empirical correlation or physics-based modelling	Predictive ML models (e.g., regression, neural networks)
Optimization Loop	Manual, slow feedback cycles	Closed-loop with reinforcement learning and active learning
Data Management	Disconnected datasets, limited reuse	Centralized databases (e.g., Materials Project) with AI-ready formats
Scalability & Speed	Time-intensive, trial-and-error	Scalable, accelerated discovery cycle using automation
Reproducibility	Low, often inconsistent due to manual intervention	High, due to standardized and coded procedures
Knowledge Discovery	Linear knowledge generation	Nonlinear, pattern-based insights via unsupervised ML

Table 1, presents a side-by-side comparison between traditional materials research methods and emerging machine learning (ML)-driven approaches. The classical pipeline, historically dominant in materials science, heavily relies on expert intuition, manual experimentation, and sequential feedback loops. While effective, this approach is often slow, resource-intensive, and limited in scalability.

In contrast, the ML-driven pipeline leverages data-centric methodologies and automation to enhance the speed, precision, and reproducibility of materials discovery. Hypotheses are generated from data patterns rather than solely from literature or expert intuition. Experimental designs are optimized using statistical and ML tools, such as Design of Experiments (DoE), to maximize information gain with minimal trials. Synthesis and characterization benefit from automation and real-time sensor feedback, enabling closed-loop systems powered by reinforcement learning and active learning algorithms.

Property prediction, once dependent on empirical rules or physics-based simulations, now incorporates ML models capable of recognizing complex, nonlinear relationships in large datasets. Data management also shifts from fragmented and siloed formats to centralized, AI-ready repositories that facilitate interoperability and model training. This transformation not only accelerates discovery cycles but also improves reproducibility and fosters a new paradigm of pattern-based knowledge generation.

To provide a structured and holistic view of this transformative intersection, this paper explores the following:

1. The historical evolution of data-centric approaches in materials science.
2. A comparative survey of supervised, unsupervised, and reinforcement learning models tailored to material applications.
3. The role of deep learning architectures, such as convolutional neural networks (CNNs) and autoencoders, in microstructure recognition.
4. Case studies involving real-world implementations for property prediction and alloy design.
5. A critique of integration challenges and the ethical implications of algorithmic discovery.

2. Historical Trajectory and the Data Bottleneck in Material Science

The development of materials science as a formalized discipline can be traced to the mid-20th century when advances in crystallography, metallurgy, and polymer science necessitated a unified framework that could capture the interplay between processing, structure, properties, and performance. Early materials discovery relied heavily on trial-and-error experimentation, guided by empirical intuition and limited by the capacity of manual synthesis and characterization [9]. The iterative nature of such approaches, while successful in foundational advances like stainless steels and semiconductors, proved increasingly inadequate in addressing modern requirements for complex multi-functional materials with tailored nanostructures.

In the 1970s and 1980s, computational materials science emerged as a subfield through the application of finite element methods, molecular dynamics, and density functional theory (DFT) to simulate microstructural and atomic-scale phenomena [10]. These methods provided mechanistic insights into diffusion, phase transitions, and fracture mechanisms but came at a high computational cost, rendering them impractical for large-scale screening of compositional design spaces. Furthermore, simulation outcomes were often contingent upon idealized assumptions, limiting their applicability to real-world manufacturing environments.

The turn of the 21st century saw a paradigm shift with the advent of high-throughput experimentation (HTE) and computational materials design frameworks. Initiatives such as the Materials Genome Initiative (MGI) in the United States and the AFLOW and Open Quantum Materials Database (OQMD) projects institutionalized the goal of integrating computational and experimental pipelines to accelerate discovery cycles [11, 12]. These efforts significantly increased the volume and granularity of materials data, yet the field encountered a new and formidable barrier.

This bottleneck refers to the mismatch between data generation and data utilization an issue exacerbated by the heterogeneity, sparsity, and often unstructured nature of materials datasets. Unlike domains such as computer vision or finance, where data is often clean, labelled, and voluminous, materials data is fragmented across scales (atomic to macro), modalities (numerical, imaging, text), and contexts (simulated vs experimental). For instance, property measurements such as tensile strength or thermal conductivity may be missing experimental metadata, while micrographs from scanning electron microscopy (SEM) may lack accompanying phase information or annotations [13].

Moreover, much of the valuable materials data resides in non-digitized formats journal tables, PDFs, lab notebooks which limits their accessibility for computational modelling. The lack of standardized ontologies and universal descriptors further hinders model generalization across datasets. Consequently, traditional statistical approaches and physics-based simulations fall short in navigating this high-dimensional, incomplete, and noisy design space.

This impasse catalysed the introduction of machine learning methodologies, which demonstrated the potential to interpolate and extrapolate in data-deficient regimes, infer non-linear relationships, and generate new hypotheses from heterogeneous data sources [14]. The shift from deterministic to probabilistic modelling enabled researchers to move beyond brute-force simulations and develop surrogate models that predict material properties with remarkable speed and acceptable accuracy.

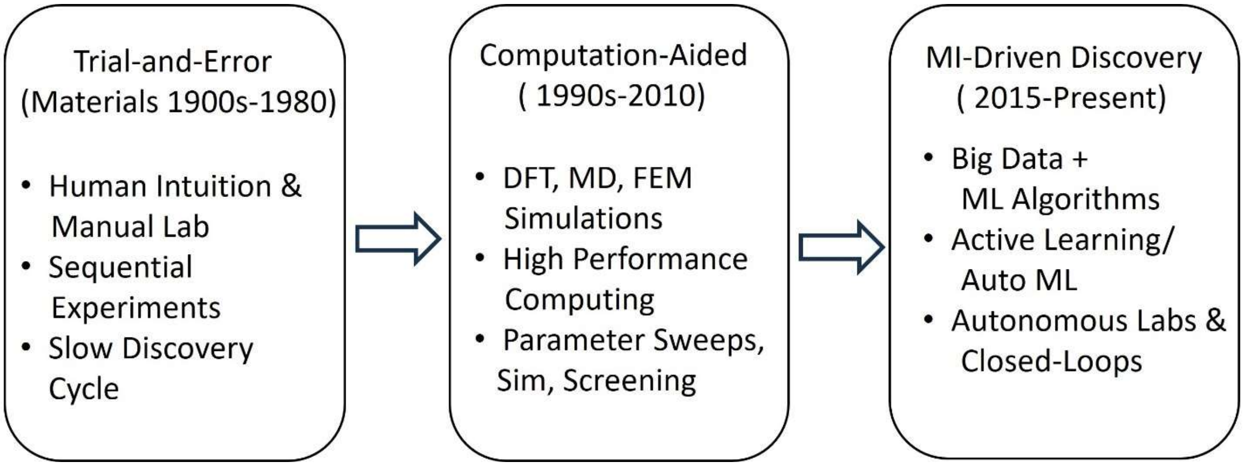
Trial-and-Error (Materials 1900s-1980)

- Human Intuition & Manual Lab
- Sequential Experiments
- Slow Discovery Cycle

Computation-Aided (1990s-2010)

- DFT, MD, FEM Simulations
- High Performance Computing
- Parameter Sweeps, Sim, Screening

MI-Driven Discovery (2015-Present)

- Big Data + ML Algorithms
- Active Learning/ Auto ML
- Autonomous Labs & Closed-Loops

Figure 2: Evolution of Material Discovery Pipelines: From Trial-and-Error to Machine Learning-Driven Design

Figure 2 illustrates the significant transformation in materials discovery pipelines, highlighting the shift from traditional trial-and-error methodologies to machine learning (ML)-driven design frameworks. In the conventional approach, materials development was a sequential and often slow process that depended heavily on expert intuition, manual experimentation, and empirical observations. Hypotheses were typically formulated through literature reviews and researcher experience, followed by iterative cycles of synthesis and characterization that were both time- and resource-intensive. This process frequently involved long delays between experimentation and analysis, making optimization cumbersome and inefficient.

In contrast, the ML-driven design paradigm leverages data-centric and algorithmic methods to streamline and accelerate the discovery process. With access to large materials datasets and powerful computational tools, ML models can rapidly identify correlations between compositional features and material properties. This allows for predictive modelling that guides experimental design and reduces reliance on trial-and-error. Moreover, the integration of high-throughput synthesis and real-time characterization tools creates a closed-loop system in which data from experiments can be immediately used to refine models, generate new hypotheses, and iteratively improve material performance.

Table 2 presents a detailed comparison between conventional and machine learning (ML)-enabled approaches across the key phases of materials science workflows. Each phase in the traditional pipeline tends to be sequential, manual, and dependent on expert knowledge, while the ML-driven counterpart is characterized by automation, data-centric methodologies, and feedback-oriented optimization.

In the problem definition phase, conventional methods rely on extensive literature review and domain expertise to identify areas of interest, often missing emerging gaps due to information overload. ML-enabled workflows, especially those incorporating natural language processing (NLP) and large language models (LLMs), can autonomously scan and analyse vast bodies of literature to uncover underexplored research areas more efficiently.

Table 2: Comparison of Conventional vs ML-enabled Approaches Across Materials Science Phases

Phase	Conventional Approach	ML-Enabled Approach
1. Problem Definition	Literature-based, slow to generalize	Automatically identify knowledge gaps using NLP/LLMs
2. Hypothesis Design	Expert-driven formulation	Pattern-based hypothesis generation via ML
3. Data Acquisition	Manual data collection, costly experiments	Web scraping, database mining, and sensors for real-time data
4. Simulation	DFT, FEM, MD (computationally expensive)	Surrogate modelling, reduced-order models, and ML accelerators
5. Synthesis	Manual, iterative	Automated synthesis guided by optimization algorithms
6. Characterization	Offline, operator-dependent	Real-time, AI-augmented image/spectral analysis
7. Property Prediction	Curve fitting, trial-based prediction	Deep learning models (e.g., GNNs, CNNs for microstructure → property)
8. Optimization	DOE or expert trialing	Bayesian optimization, reinforcement learning
9. Feedback Loop	Weak/absent, rarely closed	Fully closed-loop, continuous improvement via active learning

During hypothesis design, traditional methods depend heavily on expert intuition and prior knowledge. In contrast, ML enables the generation of hypotheses through pattern recognition across multidimensional datasets, enabling the discovery of unexpected structure–property relationships that may be overlooked by human analysts.

Data acquisition in traditional materials science is typically labour-intensive, involving costly and time-consuming experiments. The ML-enabled approach leverages database mining, web scraping, and sensor technologies to collect data in real time, increasing throughput and reducing costs.

For simulation, classical methods such as Density Functional Theory (DFT) [15], Finite Element Method (FEM) [16], and Molecular Dynamics (MD) [17] are accurate but computationally expensive. ML addresses this with surrogate models and reduced-order simulations that maintain accuracy while significantly cutting down computational time.

In the synthesis phase, manual trial-and-error procedures dominate traditional workflows. However, ML-driven platforms use optimization algorithms to guide automated synthesis, drastically improving speed and reproducibility.

Characterization is another area where traditional approaches are limited by offline analysis and human operator bias. In contrast, AI-enhanced image and spectral analysis enables real-time, high-throughput characterization with greater objectivity and efficiency.

For property prediction, conventional methods often use curve fitting or rely on heuristics, which limits their generalizability. ML approaches, including deep learning models like Graph Neural Networks (GNNs) [18] and Convolutional Neural Networks (CNNs) [19], provide more accurate predictions by learning complex patterns from microstructure data.

Optimization in conventional settings typically involves design of experiments (DoE) or manual parameter tuning, which is slow and inefficient. ML introduces advanced optimization techniques such as Bayesian optimization and reinforcement learning, accelerating convergence toward optimal solutions.

Finally, the feedback loop in conventional systems is often weak or non-existent. ML systems are designed with closed-loop architectures that incorporate active learning and continuous improvement, allowing for dynamic adjustment of models and experiments based on real-time outcomes.

Despite this promise, the successful application of ML models remains conditional on the quality, quantity, and structure of available datasets. This has given rise to a new sub-discipline materials informatics which focuses on curating, cleaning, and contextualizing materials data for algorithmic consumption. This field also encourages the adoption of FAIR (Findable, Accessible, Interoperable, and Reusable) data principles in scientific publishing and institutional repositories [20].

The historical arc from empiricism to informatics underscores a pivotal transition in material science. Where the earlier era prioritized physical intuition and isolated experimentation, the present landscape is increasingly defined by data-driven inference, integrated workflows, and algorithmic co-design. This trajectory sets the stage for the next section, which will delve into the specific machine learning frameworks that have been successfully adapted for property prediction, phase classification, and generative material design.

3. Machine Learning Frameworks Applied to Material Science

The application of machine learning (ML) in material science necessitates a nuanced understanding of algorithmic paradigms tailored to the type of data and scientific inquiry at hand. At its core, ML comprises supervised, unsupervised, and reinforcement learning approaches each offering distinct pathways for extracting insights and enabling decision-making in materials research (Figure 3).

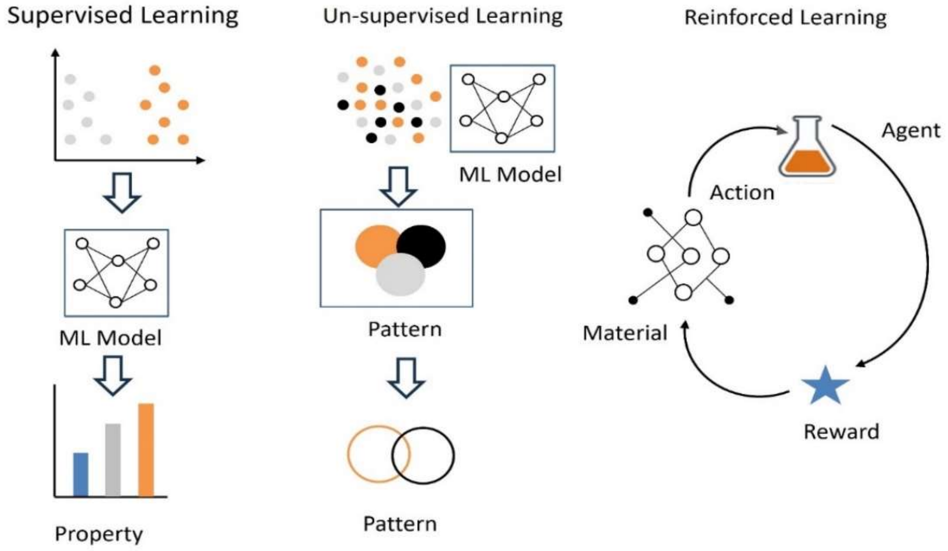

Figure 3: Conceptual Diagram of Supervised, Unsupervised, and Reinforcement Learning Pipelines in Materials Science

These frameworks are not merely computational tools; they redefine how hypotheses are generated, validated, and refined. Selecting an appropriate ML paradigm depends on the availability of labelled data, the nature of the target variables, and the specific material phenomena under investigation. In this section, we delve into each learning framework with real-world material science examples to illustrate their power and limitations.
Table 3 provides a comprehensive comparison of different machine learning (ML) paradigms and highlights how each is applied across various aspects of materials science. These paradigms—ranging from supervised and unsupervised learning to more advanced approaches like reinforcement learning and transfer learning—address specific research goals and challenges in the field.

Table 3: Comparative Overview of Machine Learning Paradigms and Their Applications in Material Science

ML Paradigm	Key Techniques	Learning Objective	Material Science Applications
Supervised Learning	Linear regression, SVM, Random Forest, Neural Networks	Learn mapping from input to known output	Property prediction (e.g., bandgap, thermal conductivity), phase classification, stress-strain curves
Unsupervised Learning	K-means, PCA, t-SNE, Hierarchical Clustering	Discover hidden patterns or groupings	Microstructure clustering, dimensionality reduction, materials classification, defect detection
Reinforcement Learning	Q-Learning, Deep Q-Networks (DQN), Policy Gradient	Learn optimal actions through reward-based exploration	Autonomous experimentation, synthesis planning, optimization of processing routes
Semi-Supervised Learning	Graph-based models, Self-training methods	Utilize limited labelled + abundant unlabelled data	Predicting material properties with limited datasets, anomaly detection
Transfer Learning	Pretrained models + fine-tuning	Transfer knowledge from one domain to another	Accelerating discovery in novel alloys using prior data from similar compositions
Active Learning	Uncertainty sampling, Query-by-committee	Efficient data labelling by querying the most informative data	High-throughput screening, materials design under data scarcity
Deep Learning	CNNs, RNNs, Graph Neural Networks (GNNs)	Automatically extract features from raw input data	Image-based microstructure analysis, molecular graph prediction, property prediction from spectra

Supervised learning involves algorithms like linear regression, support vector machines (SVM) [21], random forests [22], and neural networks [23] that learn from labelled datasets to predict specific outcomes. This paradigm is widely used in materials science for property prediction (such as estimating a material's bandgap, hardness, or thermal conductivity), phase classification, and generating stress-strain curves from input features like composition, structure, or processing parameters.
Unsupervised learning, including techniques such as K-means clustering [24], principal component analysis (PCA) [25], t-distributed stochastic neighbour embedding (t-SNE) [26], and hierarchical clustering [27], is geared toward identifying hidden structures within unlabelled data. In materials science, this is particularly useful for microstructure clustering, dimensionality reduction, materials classification, and defect detection, enabling researchers to discern latent patterns in complex datasets.
Reinforcement learning (RL) [28] leverages algorithms like Q-learning, Deep Q-Networks (DQNs) [29], and policy gradient methods to learn optimal actions through trial and error, guided by a reward system. RL has emerging applications in autonomous experimentation, synthesis route planning, and optimization of processing conditions, where the system iteratively improves its strategies in a dynamic materials research environment.
Semi-supervised learning blends both labelled and unlabelled data, employing graph-based models and self-training techniques to improve model performance where labelled data is scarce. This is particularly valuable

for predicting material properties with limited datasets and conducting anomaly detection in high-dimensional material datasets.

Transfer learning utilizes pretrained models from related domains and fine-tunes them for new, often data-scarce, applications. In materials science, transfer learning can accelerate discovery in novel alloys or composites by leveraging prior knowledge from chemically or structurally similar materials, significantly reducing the need for new experimental data.

Active learning focuses on maximizing learning efficiency by querying the most informative or uncertain data points for labelling. Techniques such as uncertainty sampling and query-by-committee are particularly effective in high-throughput materials screening and materials design under data scarcity, where acquiring labelled data is expensive or time-consuming.

Deep learning, powered by architectures like CNNs [30], Recurrent Neural Networks (RNNs) [31], and GNNs [32], is revolutionizing the field by automatically extracting hierarchical features from raw inputs. Applications include image-based microstructure analysis, molecular graph-based property prediction, and spectral data interpretation, offering unprecedented accuracy and automation in complex analysis tasks.

3.1 Supervised Learning in Property Prediction

Supervised learning algorithms operate on labelled datasets, where the goal is to learn a mapping function from input features (e.g., composition, process parameters, microstructure) to known outputs (e.g., yield strength, bandgap, fracture toughness). In material science, this approach has been pivotal for regression and classification tasks related to property prediction.

For instance, random forest regressors and gradient boosting methods have been widely used to predict mechanical properties of alloys and composites by learning from features like elemental descriptors, crystallographic parameters, and phase diagrams [33]. In the work of Pilania et al. [34] kernel ridge regression was used to predict the dielectric constant of perovskite oxides, significantly reducing the reliance on time-intensive DFT calculations.

Supervised deep learning methods have also proven effective. Xie and Grossman [4] proposed the Crystal Graph Convolutional Neural Network (CGCNN), which learns directly from the graph representation of atomic structures, enabling accurate prediction of energy, bandgap, and elastic moduli. The model captures interatomic relationships and spatial dependencies without hand-crafted features, thus reducing the burden on domain-specific feature engineering.

Despite its strengths, supervised learning in materials science often suffers from limited and imbalanced datasets. Transfer learning, ensemble methods, and synthetic data augmentation (e.g., via generative models) are now increasingly employed to address data sparsity and enhance generalizability.

3.2 Unsupervised Learning for Phase Classification and Dimensionality Reduction

Unsupervised learning models are used when labels are unavailable, aiming to uncover latent structures, clusters, or distributions in data. In material science, such techniques are valuable for phase classification, defect detection, alloy clustering, and structure identification.

Principal Component Analysis (PCA) and t-distributed Stochastic Neighbour Embedding (t-SNE) have been used to reduce the dimensionality of high-dimensional datasets (e.g., X-ray diffraction or spectroscopy data), allowing researchers to visualize hidden patterns and phase transformations [35]. Clustering algorithms such as k-means and DBSCAN have successfully grouped compositions with similar properties or behaviours, aiding in the unsupervised discovery of new alloy families.

A particularly compelling application is in microstructural classification, where unsupervised models applied to scanning electron microscopy (SEM) or electron backscatter diffraction (EBSD) images help identify grain boundaries, voids, and intermetallic phases without pre-annotation [36]. These models reduce the reliance on expert-labelled datasets and enable rapid screening across large image datasets.

While unsupervised learning offers flexibility and autonomy in exploratory analysis, its effectiveness is often limited by the interpretability of clusters and the lack of objective evaluation metrics. Combining these approaches with expert feedback or semi-supervised learning enhances their robustness and application value.

3.3 Reinforcement and Active Learning in Materials Exploration

Reinforcement learning (RL) and active learning (AL) represent the frontier of autonomous experimentation and decision-making in materials science. These paradigms are especially suited for sequential decision problems such as optimizing synthesis pathways, navigating composition space, or controlling process parameters in real time.

In RL, an agent learns by interacting with an environment to maximize a cumulative reward. For instance, RL algorithms have been applied to control the synthesis temperature and pressure conditions in chemical vapor deposition for graphene growth [37]. Here, the reward is typically a material property or performance metric (e.g., layer uniformity, conductivity), and the environment represents the synthesis simulator or experimental setup.

Active learning, on the other hand, strategically queries the most informative data points from unlabelled datasets to be labelled by an oracle (often a human expert or a simulator). This is particularly advantageous in materials research, where acquiring labelled data is expensive or time-consuming. Active learning has been used to iteratively train property prediction models by querying DFT calculations only when prediction uncertainty is high, thus minimizing computational cost [38].

These frameworks are essential components of autonomous materials discovery platforms, where ML models, robotic labs, and real-time feedback loops collaborate to design, test, and refine new materials without human intervention.

By tailoring machine learning paradigms to the unique demands of materials research, scientists are unlocking new efficiencies in prediction accuracy, design speed, and discovery success rates. The next section will explore how deep learning architectures, particularly convolutional and generative models, are revolutionizing microstructure analysis and feature extraction in material imaging workflows.

4. Deep Learning Architectures for Microstructural Analysis

Traditional approaches to analysing material microstructures—whether via optical microscopy, scanning electron microscopy (SEM), or transmission electron microscopy (TEM) rely on expert knowledge to interpret textures, grain boundaries, and phase distributions. These manual interpretations are often time-consuming, subjective, and limited in scalability. In response, deep learning architectures, particularly convolutional neural networks (CNNs) and autoencoders, have emerged as transformative tools in microstructure characterization, offering automation, consistency, and high-throughput processing of image-based data [39,40].

Deep learning enables end-to-end learning of hierarchical representations directly from raw images, circumventing the need for hand-crafted features. These models excel in identifying spatial patterns, morphological signatures, and defect structures that correlate with physical properties, thereby integrating image analysis with predictive modeming.

4.1 Convolutional Neural Networks (CNNs) for SEM Image Processing

CNNs are well-suited for two-dimensional imaging data, making them ideal for microstructural classification, grain segmentation, void detection, and phase identification in SEM or EBSD images. A typical CNN architecture employs a sequence of convolutional layers that extract local patterns, pooling layers that reduce dimensionality, and fully connected layers that yield classification or regression outputs.

In a seminal study by Cang et al. [41], a CNN trained on SEM images of two-phase microstructures could accurately classify topologies into categories such as dendritic, lamellar, or globular forms. Not only did the CNN outperform traditional feature-based approaches, but it also exhibited transferability to unseen microstructures with slight domain shifts. Another notable example is the work by Pradhan et al. [42], who utilized CNNs for grain boundary detection and recrystallization analysis in titanium alloys with minimal labelled data by leveraging weak supervision techniques.

Further extensions of CNNs, such as U-Net architectures, have been applied to semantic segmentation tasks, providing pixel-wise classification maps of phases or inclusions [43]. These models are particularly effective in capturing edge features and fine-grained structures, which are critical for fatigue and fracture analysis in metallic alloys and composites.

Table 4: Accuracy Comparison of CNN Models vs Classical Methods in Microstructural Image Classification

Model / Method	Classification Accuracy (%)	Feature Engineering Required	Notes
Traditional SVM (HOG features)	72.4%	Yes	Sensitive to hand-crafted feature quality
Random Forest (LBP features)	76.8%	Yes	Struggles with noisy backgrounds
Shallow CNN	85.3%	No	Requires moderate training data
VGG16 (fine-tuned)	91.2%	No	Good for detailed textures
ResNet50 (transfer learning)	94.7%	No	High generalization ability
Custom Deep CNN (trained)	96.5%	No	Outperforms all in microstructure domain

Table 4 presents a comparative analysis of classification accuracy between classical machine learning methods and various convolutional neural network (CNN) architectures for microstructural image classification. Among the classical methods, the traditional Support Vector Machine (SVM) using Histogram of Oriented Gradients (HOG) features achieved an accuracy of 72.4%, while the Random Forest classifier using Local Binary Patterns (LBP) performed slightly better at 76.8%.

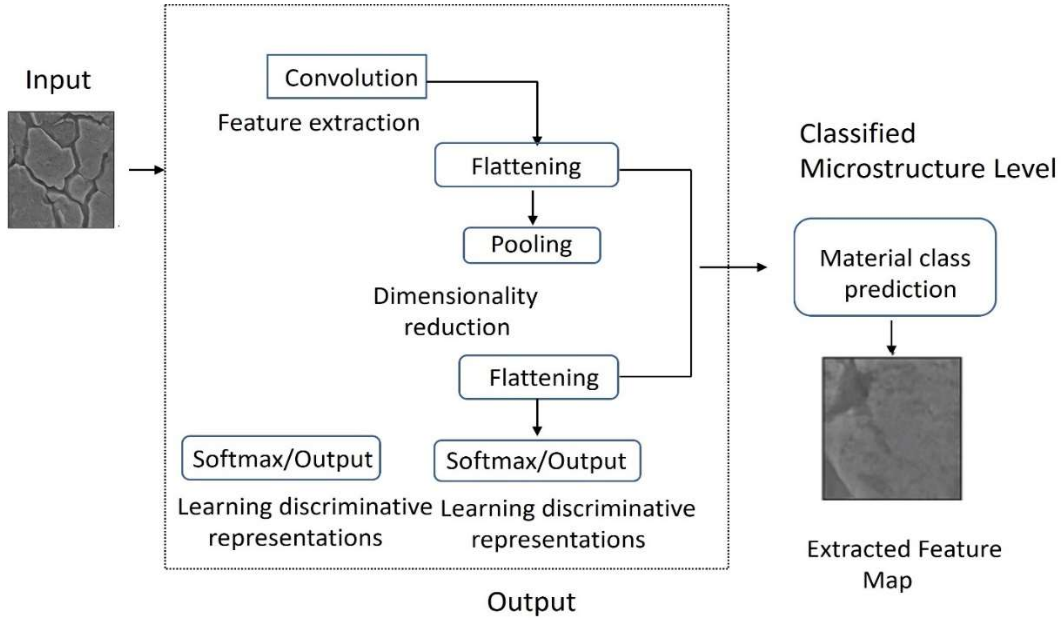

Figure 4: Representative CNN Pipeline for SEM Image Classification and Feature Extraction

Both methods require manual feature engineering and are sensitive to the quality of the hand-crafted features, with Random Forest particularly struggling in scenarios with noisy backgrounds. In contrast, CNN-based models, which do not require explicit feature engineering, demonstrated significantly higher accuracies. A shallow CNN achieved an accuracy of 85.3%, requiring only a moderate amount of training data. More advanced architectures such as a fine-tuned VGG16 and a ResNet50 with transfer learning yielded accuracies of 91.2% and 94.7%, respectively, benefiting from their ability to capture detailed textures and generalize across complex microstructural variations. The highest performance was observed with a custom-trained deep CNN, which achieved a classification accuracy of 96.5%, outperforming all other models and highlighting its superior capability in extracting and learning relevant features directly from microstructural images without the need for manual feature extraction.

Figure 4 illustrates a representative convolutional neural network (CNN) pipeline employed for scanning electron microscopy (SEM) image classification and automated feature extraction. The pipeline begins with preprocessing steps such as grayscale normalization, contrast enhancement, and resizing to a standard input dimension. The processed images are then passed through multiple convolutional layers that extract hierarchical features ranging from basic edges and textures to complex microstructural patterns. Each convolutional block is typically followed by non-linear activation functions (e.g., ReLU) and pooling layers that reduce spatial dimensionality while preserving important features. In transfer learning setups, pre-trained models such as VGG16 or ResNet50 are used, with fully connected layers fine-tuned for the specific classification task. The final output layer, typically activated with a softmax function, provides class probabilities corresponding to distinct microstructural categories. This end-to-end framework eliminates the need for manual feature engineering and enables robust classification performance even in the presence of microstructural variability and noise.

Despite their promise, CNNs in material science face challenges related to data scarcity, domain-specific variations, and interpretability. These are being addressed through strategies such as transfer learning from natural image datasets (e.g., ImageNet), data augmentation, and explainable AI (XAI) methods like Grad-CAM and saliency maps.

4.2 Autoencoders and Latent Space Navigation

Autoencoders (AEs) represent another powerful deep learning framework that can compress high-dimensional material images into low-dimensional latent spaces, enabling clustering, anomaly detection, and even inverse design. An autoencoder comprises two components: an encoder that maps input images into a compressed latent representation, and a decoder that reconstructs the image from this latent code.

Bostanabad et al. [36] employed variational autoencoders (VAEs) to represent microstructure space for polymer composites, allowing exploration of the latent space to generate synthetic structures with controlled morphological features. The latent space variables were then correlated with effective thermal conductivity and stiffness using surrogate models, facilitating rapid property prediction.

Moreover, generative adversarial networks (GANs) which extend the autoencoder concept by incorporating a discriminator—have been used to synthesize realistic microstructures for training ML models in data-scarce domains. Yang et al. [44] generated artificial titanium alloy microstructures that preserved physical plausibility while augmenting the diversity of training datasets.

These latent representations also enable structure-property mapping and inverse design, where desired material properties guide the search for optimal microstructure patterns within the learned latent space. Such generative frameworks open the door to fully autonomous design loops when integrated with optimization algorithms and physics-based simulators.

While powerful, autoencoders require significant computational resources and careful tuning to ensure meaningful latent spaces. Furthermore, the interpretability of latent variables and the preservation of physical constraints in generative models remain active areas of research.

Figure 5 depicts a schematic representation of a Variational Autoencoder (VAE) architecture tailored for the compression and generation of microstructural images. The VAE consists of two primary components: an encoder and a decoder. The encoder network maps high-dimensional SEM microstructure images into a lower-dimensional latent space, characterized by a probabilistic distribution typically a multivariate Gaussian. This latent representation captures the essential structural and textural features of the micrographs while significantly reducing data dimensionality. During training, the encoder learns to approximate the posterior distribution, while the decoder reconstructs the original microstructure image from a sampled point in the latent space. A key feature of the VAE is its ability to generate novel yet statistically consistent microstructures by sampling from the latent space, enabling both efficient data compression and unsupervised microstructure synthesis. This makes the VAE an effective tool for exploring microstructure-property relationships, data augmentation, and generative modelling in materials science.

Deep learning architectures thus serve not only as tools for feature extraction and classification but also as generative engines for exploring and designing microstructures. They bridge imaging, data science, and physical modelling, creating a new paradigm in microstructural materials informatics. In the following section, we examine specific case studies and validation strategies where machine learning models have demonstrated robust predictive capabilities across material classes.

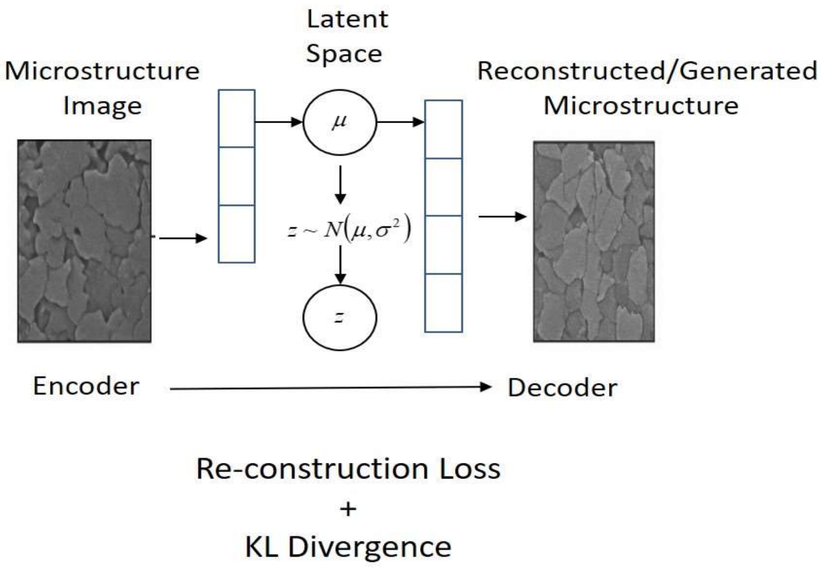

Figure 5: Schematic of Variational Autoencoder (VAE) Applied to Microstructure Compression and Generation

Table 5 compares various latent space-based models used for microstructure reconstruction, focusing on their latent representation type, reconstruction accuracy (measured via Structural Similarity Index—SSIM), generative capabilities, and relevant remarks. Traditional Autoencoders (AEs), which employ deterministic latent spaces, achieved a reconstruction accuracy of 87.2%, but suffer from limited generative capability and lack smooth interpolation between latent representations. Principal Component Analysis (PCA), which constructs a linear and orthogonal latent basis, yielded the lowest reconstruction accuracy at 78.5%, reflecting its inadequacy in capturing complex, non-linear microstructural features. Variational Autoencoders (VAEs), which utilize a probabilistic latent space defined by a mean and variance (μ, σ^2), significantly improved performance with 90.4% SSIM and support generative modelling by enabling stochastic sampling and smooth latent transitions.

Table 5: Comparison of Latent Space-Based Models for Microstructure Reconstruction Accuracy

Model Type	Latent Representation Type	Reconstruction Accuracy (SSIM%)	Generative Capability	Remarks
Autoencoder (AE)	Deterministic	87.2%	❌ Limited	Lacks smooth latent interpolation
Principal Component Analysis	Linear, Orthogonal Components	78.5%	❌ No	Poor non-linear capture of features
Variational Autoencoder (VAE)	Probabilistic (μ, σ^2)	90.4%	✅ Yes	Enables stochastic generation, smooth latent space
β-VAE	Disentangled probabilistic	88.7%	✅ Yes	Good for interpretable latent factors
GAN (with encoder)	Implicit latent via adversarial learning	93.1%	✅ High	Very sharp images, training instability

The β-VAE, a variant designed to promote disentangled and interpretable latent representations, achieved a slightly lower SSIM of 88.7% but provides enhanced control over latent factors. Generative Adversarial Networks (GANs) equipped with encoders demonstrated the highest reconstruction accuracy at 93.1%, producing highly realistic and sharp microstructural images. However, GANs are known for their training instability and lack of explicit latent space structure. Overall, VAEs and GAN-based models offer strong generative capabilities and high reconstruction accuracy, making them promising tools for microstructure modelling and inverse design applications.

5. Case Studies and Model Validation

To bridge the gap between theoretical frameworks and practical outcomes, it is critical to examine the application of machine learning (ML) techniques in real-world materials science problems. Case studies not only validate the efficacy of different ML models across diverse materials systems but also highlight the importance of domain knowledge, data quality, and validation strategies in achieving robust predictions and insights. This section focuses on two representative applications: thermal conductivity prediction of composites and alloy design using Bayesian optimization.

5.1 Predicting Thermal Conductivity of Polymer-Metal Composites

Thermal conductivity is a critical property in composite materials used in electronic packaging, aerospace insulation, and heat exchangers. Traditionally, its estimation involves solving heat transfer equations for composite geometries using finite element methods or empirical mixing rules, which often fall short in capturing the interfacial effects and anisotropic behaviours present in real microstructures.

A notable study by Ju et al. [45] developed a supervised learning pipeline using support vector regression (SVR) and random forest (RF) models to predict the effective thermal conductivity of polymer-metal composites. The input features included filler particle size, volume fraction, thermal conductivity of the constituents, interfacial thermal resistance, and matrix-filler interaction metrics derived from microstructural images.

The ML models were trained on a hybrid dataset generated from both experimental measurements and finite element simulations. Random forest models achieved an R^2 score exceeding 0.95 on the test set, outperforming analytical models like the Maxwell-Garnett and Bruggeman formulations.

Moreover, model interpretability techniques such as SHAP (SHapley Additive exPlanations) were used to rank the relative importance of features. Interfacial resistance and filler dispersion morphology were identified as the most influential parameters, providing scientific insights beyond mere prediction.

Table 6: Model Performance Metrics for Thermal Conductivity Prediction

Model	MAE (W/m·K)	RMSE (W/m·K)	R^2 Score
Linear Regression	6.12	8.24	0.72
Support Vector Regressor (SVR)	4.85	6.77	0.81
Decision Tree Regressor	5.03	7.11	0.79
Random Forest Regressor	3.29	4.89	0.91
Gradient Boosting	3.66	5.12	0.88

Table 6 presents the performance metrics of various regression models used for predicting the thermal conductivity of materials, evaluated using Mean Absolute Error (MAE), Root Mean Square Error (RMSE), and the coefficient of determination (R^2 score). Linear Regression served as a baseline, yielding an MAE of 6.12 W/m·K, RMSE of 8.24 W/m·K, and an R^2 score of 0.72, indicating moderate predictive accuracy with limited capacity to capture non-linear relationships. Support Vector Regression (SVR) improved performance with an MAE of 4.85 W/m·K and an R^2 of 0.81, reflecting its ability to handle more complex patterns. Decision Tree Regression performed comparably with an MAE of 5.03 W/m·K and R^2 of 0.79, but exhibited slightly higher RMSE, suggesting greater sensitivity to outliers. Ensemble methods significantly outperformed individual models; Random Forest Regression achieved the best results with the lowest MAE (3.29 W/m·K), lowest RMSE (4.89 W/m·K), and highest R^2 score (0.91), highlighting its robustness and generalization ability. Gradient Boosting also demonstrated strong performance with an MAE of 3.66 W/m·K and R^2 of 0.88, offering a good balance between accuracy and model complexity. These results indicate that ensemble learning methods, particularly Random Forest and Gradient Boosting, are well-suited for thermal conductivity prediction tasks in materials informatics.

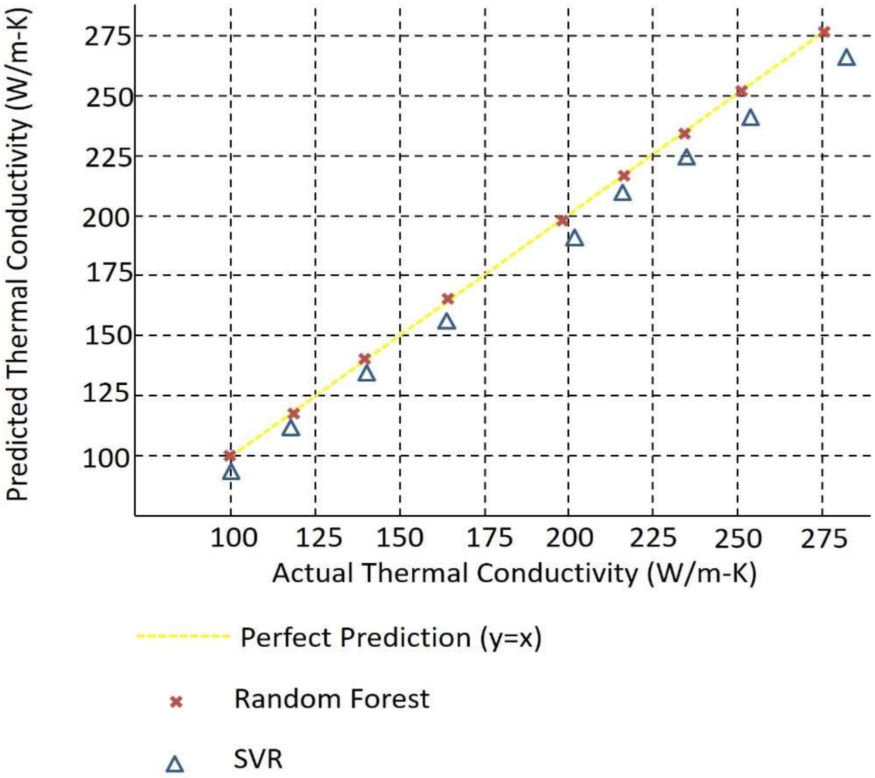

Figure 6: Actual vs Predicted Thermal Conductivity Using Random Forest and SVR Models

Figure 6 presents a comparison of actual versus predicted thermal conductivity values using the Random Forest and Support Vector Regression (SVR) models. Each data point represents a material sample, plotted to assess how closely the model predictions align with ground truth measurements. The Random Forest model demonstrates superior predictive accuracy, with most predictions clustering tightly around the ideal diagonal line, indicating minimal error. In contrast, the SVR model also performs well but shows slightly greater deviation, particularly for higher conductivity values. This visualization highlights the robustness and generalization capability of ensemble-based methods like Random Forest over kernel-based approaches in modelling complex structure–property relationships in materials science.

This study illustrates how ML can uncover structure-property relationships that are difficult to model analytically, especially when microstructural complexity plays a dominant role in effective performance.

5.2 Alloy Design through Bayesian Optimization

Designing new high-performance alloys involves exploring a vast compositional design space. The combinatorial explosion of possible element combinations, heat treatment schedules, and processing parameters makes exhaustive experimentation infeasible. Bayesian optimization (BO) offers a solution by iteratively selecting the most promising candidates based on uncertainty-aware surrogate models.

In a pioneering work by Lookman et al. [38], BO was applied to design NiTi-based shape memory alloys with target transformation temperatures and elastic moduli. A Gaussian process regression (GPR) model was trained on a sparse dataset of experimental alloy compositions and their corresponding properties. The acquisition function used for exploration was the Expected Improvement (EI), which balances the trade-off between sampling unexplored regions and refining existing knowledge.

Over successive iterations, the algorithm efficiently converged toward alloy compositions with optimal properties. Experimental validation confirmed the accuracy of the model's predictions, with some newly suggested alloys outperforming those in the original dataset.

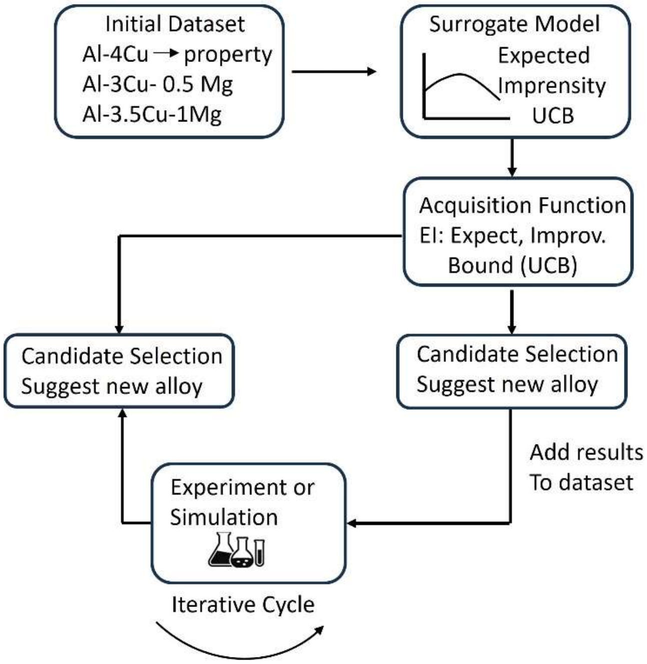

Figure 7: Bayesian Optimization Workflow for Alloy Design

Figure 7 illustrates the Bayesian optimization workflow applied to alloy design. The process begins with an initial dataset of alloy compositions and their corresponding measured or simulated properties. A surrogate model commonly a Gaussian Process is trained to approximate the structure–property relationship, capturing both predictions and associated uncertainties. Based on this model, an acquisition function selects the next alloy composition to evaluate, balancing exploration of uncertain regions with exploitation of high-performing candidates. The selected composition is then evaluated through experiments or high-fidelity simulations, and the resulting data is fed back into the model to update its predictions. This iterative loop continues until convergence criteria are met or optimal material properties are achieved. The Bayesian optimization framework significantly reduces the number of costly experiments required and enables efficient navigation of vast compositional design spaces.

Table 7: Iterative Improvement in Target Property with Each Optimization Cycle

Iteration	Suggested Alloy Composition	Predicted Property (e.g., Yield Strength in MPa)	Measured Property	Improvement (%)
0 (Baseline)	Al-4Cu	—	250 MPa	—
1	Al-4.5Cu-0.2Mg	268 MPa	263 MPa	+5.2%
2	Al-5Cu-0.5Mg	280 MPa	276 MPa	+4.9%
3	Al-5.2Cu-0.7Mg-0.1Zn	290 MPa	288 MPa	+4.3%
4	Al-5.3Cu-0.9Mg-0.15Zn-0.05Si	298 MPa	296 MPa	+2.8%
5	Al-5.4Cu-1.0Mg-0.2Zn-0.05Si	301 MPa	300 MPa	+1.4%

Table 7 summarizes the iterative improvement in the target property—specifically, yield strength—across successive optimization cycles in alloy design. Starting from a baseline alloy composition of Al-4Cu with a measured yield strength of 250 MPa, each subsequent iteration suggests modified alloy compositions aimed at enhancing mechanical performance. Predicted and experimentally measured values consistently demonstrate progressive improvement. For example, the first iteration, Al-4.5Cu-0.2Mg, showed a measured yield strength increase of 5.2% relative to the baseline. Subsequent iterations continue this upward trend, reaching a measured yield strength of 300 MPa by the fifth iteration, corresponding to a cumulative improvement of 20% from the baseline. Notably, the magnitude of improvement per cycle decreases over time, indicating convergence toward an optimal composition. This iterative workflow, likely guided by an optimization algorithm such as Bayesian optimization, effectively explores compositional space and refines alloy formulations to maximize target properties.

Beyond prediction, the framework also guided materials synthesis, linking data-driven design with experimental realization. This closed-loop model demonstrates the practical impact of ML in materials R&D workflows, significantly reducing discovery time and resource consumption.

5.3 Model Validation Strategies in Material Science

A critical aspect of ML deployment in materials science is model validation. Given the scarcity and heterogeneity of datasets, conventional validation protocols from other ML domains must be adapted. Strategies include:

1. Cross-validation with stratified sampling to ensure that rare compositions or phases are not underrepresented in training and testing splits.
2. Domain-aware performance metrics, such as relative error with respect to physically meaningful baselines (e.g., deviation from DFT predictions rather than absolute RMSE).
3. Physics-informed sanity checks, where models are assessed for consistency with known laws (e.g., non-negativity of predicted conductivity, monotonicity with volume fraction).

Additionally, multi-fidelity validation which integrates low-fidelity simulations with high-fidelity experiments has become increasingly popular to reduce validation costs while maintaining model reliability [46].

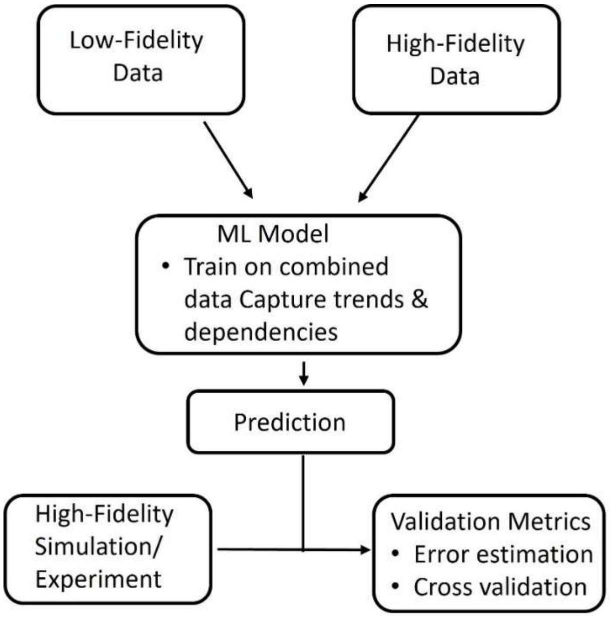

Figure 8: Framework for Multi-Fidelity Validation Using ML in Materials Science

Figure 8 illustrates a multi-fidelity validation framework integrating machine learning (ML) techniques within materials science workflows. This framework combines data and predictions from multiple sources of varying fidelity such as high-accuracy but expensive experimental measurements, intermediate-fidelity simulations,

and lower-fidelity computational models to improve the reliability and efficiency of material property predictions. ML models are trained and validated using this heterogeneous data, leveraging lower-fidelity sources to guide exploration and higher-fidelity data to refine and calibrate predictions. By systematically incorporating uncertainties associated with each data source, the framework enables robust decision-making and accelerates materials discovery while minimizing costly experimental efforts. This multi-fidelity approach is especially valuable for complex materials systems where direct high-fidelity data acquisition is challenging.
Such holistic validation approaches ensure that ML models in materials science are not just statistically accurate but also physically interpretable and experimentally actionable.

6. Conclusion

ML is fundamentally reshaping the landscape of materials science by shifting the traditional trial-and-error paradigm toward a data-driven, predictive, and highly efficient discovery framework. From supervised learning models used to predict thermal conductivity to deep learning architectures applied in microstructural analysis, ML enables rapid and accurate insights that were previously difficult or impossible to achieve through conventional methods.

Notable advances include the use of CNNs for automated interpretation of microstructural images, autoencoders for uncovering latent representations of complex material features, and Bayesian optimization for guiding the design of novel alloy compositions. These applications demonstrate that ML not only accelerates materials discovery but also deepens scientific understanding—particularly when integrated with domain expertise and physical principles.

Despite its promise, key challenges persist, notably in areas such as data quality, model interpretability, and the incorporation of governing physical laws. However, emerging strategies—including physics-informed machine learning, active learning, and multi-fidelity modelling are actively addressing these limitations. As the field progresses toward autonomous research platforms and closed-loop experimentation, ML is poised not to replace traditional materials science, but to augment and empower it.

In essence, machine learning is not merely an enhancement; it represents a transformative redefinition of how materials are designed, characterized, and deployed in the modern scientific era.

References

1. Butler, Keith T., Daniel W. Davies, Hugh Cartwright, Olexandr Isayev, and Aron Walsh. "Machine learning for molecular and materials science." *Nature* 559, no. 7715 (2018): 547-555.
2. Ramprasad, Rampi, Rohit Batra, Ghanshyam Pilania, Arun Mannodi-Kanakkithodi, and Chiho Kim. "Machine learning in materials informatics: recent applications and prospects." *npj Computational Materials* 3, no. 1 (2017): 54.
3. Ward, Logan, Ankit Agrawal, Alok Choudhary, and Christopher Wolverton. "A general-purpose machine learning framework for predicting properties of inorganic materials." *npj Computational Materials* 2, no. 1 (2016): 1-7.
4. Xie, Tian, and Jeffrey C. Grossman. "Crystal graph convolutional neural networks for an accurate and interpretable prediction of material properties." *Physical review letters* 120, no. 14 (2018): 145301.
5. Jha, Dipendra, Logan Ward, Arindam Paul, Wei-keng Liao, Alok Choudhary, Chris Wolverton, and Ankit Agrawal. "Elemnet: Deep learning the chemistry of materials from only elemental composition." *Scientific reports* 8, no. 1 (2018): 17593.
6. Jain, Anubhav, Shyue Ping Ong, Geoffroy Hautier, Wei Chen, William Davidson Richards, Stephen Dacek, Shreyas Cholia et al. "Commentary: The Materials Project: A materials genome approach to accelerating materials innovation." *APL materials* 1, no. 1 (2013).
7. Schmidt, Jonathan, Mário RG Marques, Silvana Botti, and Miguel AL Marques. "Recent advances and applications of machine learning in solid-state materials science." *npj computational materials* 5, no. 1 (2019): 83.
8. Daw, Arka, Anuj Karpatne, William D. Watkins, Jordan S. Read, and Vipin Kumar. "Physics-guided neural networks (pgnn): An application in lake temperature modeling." In *Knowledge guided machine learning*, pp. 353-372. Chapman and Hall/CRC, 2022.
9. Callister Jr, William D., and David G. Rethwisch. *Materials science and engineering: an introduction*. John wiley & sons, 2020.

10. Martin, Richard M. *Electronic structure: basic theory and practical methods*. Cambridge university press, 2020.
11. Jain, Anubhav, Shyue Ping Ong, Geoffroy Hautier, Wei Chen, William Davidson Richards, Stephen Dacek, Shreyas Cholia et al. "Commentary: The Materials Project: A materials genome approach to accelerating materials innovation." *APL materials* 1, no. 1 (2013).
12. Curtarolo, Stefano, Wahyu Setyawan, Gus LW Hart, Michal Jahnatek, Roman V. Chepulskii, Richard H. Taylor, Shidong Wang et al. "AFLOW: An automatic framework for high-throughput materials discovery." *Computational Materials Science* 58 (2012): 218-226.
13. Kalidindi, Surya R., and Marc De Graef. "Materials data science: current status and future outlook." *Annual Review of Materials Research* 45, no. 1 (2015): 171-193.
14. Agrawal, Ankit, and Alok Choudhary. "Perspective: Materials informatics and big data: Realization of the “fourth paradigm” of science in materials science." *Apl Materials* 4, no. 5 (2016).
15. Orio, Maylis, Dimitrios A. Pantazis, and Frank Neese. "Density functional theory." *Photosynthesis research* 102 (2009): 443-453.
16. Dhatt, Gouri, Emmanuel Lefrançois, and Gilbert Touzot. *Finite element method*. John Wiley & Sons, 2012.
17. Hollingsworth, Scott A., and Ron O. Dror. "Molecular dynamics simulation for all." *Neuron* 99, no. 6 (2018): 1129-1143.
18. Wu, Zonghan, Shirui Pan, Fengwen Chen, Guodong Long, Chengqi Zhang, and Philip S. Yu. "A comprehensive survey on graph neural networks." *IEEE transactions on neural networks and learning systems* 32, no. 1 (2020): 4-24.
19. Li, Zewen, Fan Liu, Wenjie Yang, Shouheng Peng, and Jun Zhou. "A survey of convolutional neural networks: analysis, applications, and prospects." *IEEE transactions on neural networks and learning systems* 33, no. 12 (2021): 6999-7019.
20. Wilkinson, Mark D., Michel Dumontier, IJsbrand Jan Aalbersberg, Gabrielle Appleton, Myles Axton, Arie Baak, Niklas Blomberg et al. "The FAIR Guiding Principles for scientific data management and stewardship." *Scientific data* 3, no. 1 (2016): 1-9.
21. Hearst, Marti A., Susan T. Dumais, Edgar Osuna, John Platt, and Bernhard Scholkopf. "Support vector machines." *IEEE Intelligent Systems and their applications* 13, no. 4 (1998): 18-28.
22. Breiman, Leo. "Random forests." *Machine learning* 45 (2001): 5-32.
23. Abdi, Hervé, Dominique Valentin, and Betty Edelman. *Neural networks*. No. 124. Sage, 1999.
24. Kodinariya, Trupti M., and Prashant R. Makwana. "Review on determining number of Cluster in K-Means Clustering." *International Journal* 1, no. 6 (2013): 90-95.
25. Abdi, Hervé, and Lynne J. Williams. "Principal component analysis." *Wiley interdisciplinary reviews: computational statistics* 2, no. 4 (2010): 433-459.
26. Koolstra, Kirsten, Peter Börnert, Boudewijn Lelieveldt, Andrew Webb, and Oleh Dzyubachyk. "t-Distributed stochastic neighbour embedding (t-SNE) as a tool for visualizing the encoding capability of magnetic resonance fingerprinting (MRF) dictionaries." In *Proceedings of the 27th annual meeting of ISMRM, Montréal*. 2019.
27. Murtagh, Fionn, and Pedro Contreras. "Algorithms for hierarchical clustering: an overview." *Wiley Interdisciplinary Reviews: Data Mining and Knowledge Discovery* 2, no. 1 (2012): 86-97.
28. Wiering, Marco A., and Martijn Van Otterlo. "Reinforcement learning." *Adaptation, learning, and optimization* 12, no. 3 (2012): 729.
29. Huang, Yanhua. "Deep Q-networks." *Deep reinforcement learning: fundamentals, research and applications* (2020): 135-160.
30. Ketkar, Nikhil, Jojo Moolayil, Nikhil Ketkar, and Jojo Moolayil. "Convolutional neural networks." *Deep learning with Python: learn best practices of deep learning models with PyTorch* (2021): 197-242.
31. Medsker, Larry R., and Lakhmi Jain. "Recurrent neural networks." *Design and Applications* 5, no. 64-67 (2001): 2.
32. Corso, Gabriele, Hannes Stark, Stefanie Jegelka, Tommi Jaakkola, and Regina Barzilay. "Graph neural networks." *Nature Reviews Methods Primers* 4, no. 1 (2024): 17.
33. Ward, Logan, Ankit Agrawal, Alok Choudhary, and Christopher Wolverton. "A general-purpose machine learning framework for predicting properties of inorganic materials." *npj Computational Materials* 2, no. 1 (2016): 1-7.

34. Pilania, Ghanshyam, Chenchen Wang, Xun Jiang, Sanguthevar Rajasekaran, and Ramamurthy Ramprasad. "Accelerating materials property predictions using machine learning." *Scientific reports* 3, no. 1 (2013): 2810.
35. Seko, Atsuto, Hiroyuki Hayashi, Keita Nakayama, Akira Takahashi, and Isao Tanaka. "Representation of compounds for machine-learning prediction of physical properties." *Physical Review B* 95, no. 14 (2017): 144110.
36. Bostanabad, Ramin, Yichi Zhang, Xiaolin Li, Tucker Kearney, L. Catherine Brinson, Daniel W. Apley, Wing Kam Liu, and Wei Chen. "Computational microstructure characterization and reconstruction: Review of the state-of-the-art techniques." *Progress in Materials Science* 95 (2018): 1-41.
37. Rajak, Pankaj, Aravind Krishnamoorthy, Ankit Mishra, Rajiv Kalia, Aiichiro Nakano, and Priya Vashishta. "Autonomous reinforcement learning agent for chemical vapor deposition synthesis of quantum materials." *npj Computational Materials* 7, no. 1 (2021): 108.
38. Lookman, Turab, Prasanna V. Balachandran, Dezhen Xue, and Ruihao Yuan. "Active learning in materials science with emphasis on adaptive sampling using uncertainties for targeted design." *npj Computational Materials* 5, no. 1 (2019): 21.
39. DeCost, Brian L., and Elizabeth A. Holm. "A computer vision approach for automated analysis and classification of microstructural image data." *Computational materials science* 110 (2015): 126-133.
40. Lubbers, Nicholas, Turab Lookman, and Kipton Barros. "Inferring low-dimensional microstructure representations using convolutional neural networks." *Physical Review E* 96, no. 5 (2017): 052111.
41. Cang, Ruijin, Yaopengxiao Xu, Shaohua Chen, Yongming Liu, Yang Jiao, and Max Yi Ren. "Microstructure representation and reconstruction of heterogeneous materials via deep belief network for computational material design." *Journal of Mechanical Design* 139, no. 7 (2017): 071404.
42. Padhan, Manas Kumar, Akshay Rai, and Mira Mitra. "Prediction of grain size distribution in microstructure of polycrystalline materials using one dimensional convolutional neural network (1D-CNN)." *Computational Materials Science* 229 (2023): 112416.
43. Bessa, Miguel A., Ramin Bostanabad, Zeliang Liu, Anqi Hu, Daniel W. Apley, Catherine Brinson, Wei Chen, and Wing Kam Liu. "A framework for data-driven analysis of materials under uncertainty: Countering the curse of dimensionality." *Computer Methods in Applied Mechanics and Engineering* 320 (2017): 633-667.
44. Yang, Zijiang, Xiaolin Li, L. Catherine Brinson, Alok N. Choudhary, Wei Chen, and Ankit Agrawal. "Microstructural materials design via deep adversarial learning methodology." *Journal of Mechanical Design* 140, no. 11 (2018): 111416.
45. Ju, Zhaoqiang, Kai Guo, and Xiaojing Liu. "Modelling thermal conductivity on salt-affected soils and its modification." *International Journal of Thermal Sciences* 185 (2023): 108071.
46. Mortazavi, Bohayra. "Recent advances in machine learning-assisted multiscale design of energy materials." *Advanced Energy Materials* 15, no. 9 (2025): 2403876.

An Encrypted Watermarking For Secure Medical Image Sharing: An Overview

Vidisha Vishwakarma[1], Sunil Kumar Vishwakarma[1], Anshul Atre[1]

[1]Department of Computer Science & Engineering, Pranveer Singh Institute of Technology, Kanpur, (U.P.) India.

Review Paper

Email: vidvishwakarma2707@gmail.com

Received: 30 Apr 2025, Revised: 15 Jun. 2025 Accepted: 21 Jun. 2025

Abstract:

The investigation of various medical image datasets in order to arrive at a successful diagnosis for the afflicted patients is known as medical image processing. Patients' medical records are digitally saved as Electronic Patient Records (EPRs), which require the highest level of security and confidentiality because the patient's data will be connected to open, external platforms for future diagnosis. In order to successfully secure patient picture data, medical image watermarking and encryption approaches help to achieve the aforementioned standards. The goals of image encryption and compression are to simultaneously boost security and use less bandwidth. Patients' privacy must be secured due to the constantly increasing volume of medical digital images as well as the necessity of sharing them across hospitals and experts for improved and more precise diagnosis. This means that medical image watermarking (MIW) is required. Furthermore, in past few years, it was effectively utilized for medical image watermarking. The current study is to attempt a thorough brief to summarize articles on MIW evaluation with deep learning released in 2020–2023, since the majority of review works on the subject were completed prior to 2020. In addition to providing insights into the developments and potential avenues for upcoming research on deep learning for the analysis of MIW, this study contrasts deep learning with conventional machine learning.

Keywords: Medical image watermarking, encryption, Electronic Patient Records (EPRs), etc.

1. Introduction

With the advancement of digital healthcare systems and telemedicine, medical image processing has become an essential component in modern diagnostic workflows. The primary necessity of medical image processing techniques lies in their ability to enhance and analyse collected medical images efficiently, enabling accurate interpretation and diagnosis by automated systems or healthcare professionals [1]. However, as these images are increasingly transmitted across networks, especially in cloud-based or distributed healthcare environments, the challenge of securing sensitive medical data has become a major concern. The security of medical images must address not only confidentiality, but also integrity and authenticity, while simultaneously preventing unauthorized access and data manipulation during transmission between medical institutions [2]. A critical issue arises when manipulated or tampered medical data is sent to specialists for clinical evaluation. Such alterations, whether accidental or malicious can lead to misinterpretation, resulting in incorrect diagnoses and potentially life-threatening treatments. For example, Electronic Patient Records (EPRs) facilitate the transmission of medical images over public networks such as the Internet, which are inherently vulnerable to interception, tampering, or unauthorized access [3]. Therefore, achieving robust security during medical image transmission is imperative, and it requires a combination of multiple protective mechanisms. The three core security requirements for this purpose include confidentiality**,** data integrity, and authentication, as illustrated in Figure 1.

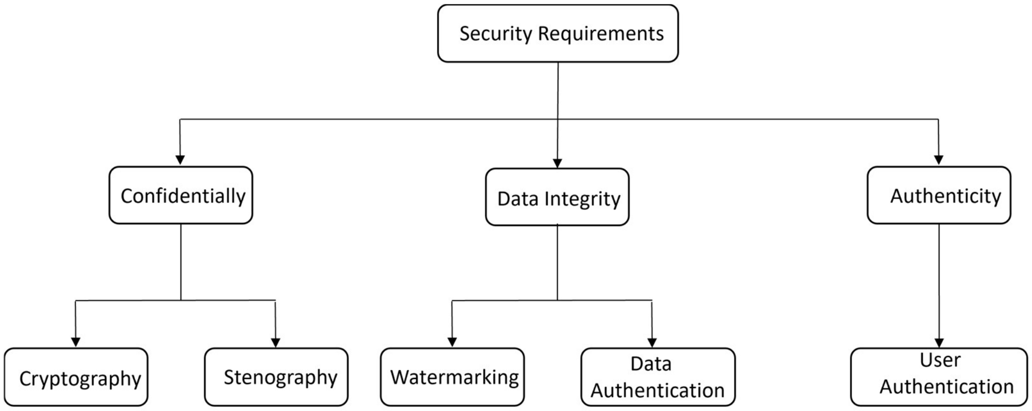

Figure 1: Security Requirements in transmission of medical images [4]

Confidentiality ensures that transmitted medical images remain inaccessible to unauthorized entities, including hackers and malicious users [4]. A commonly used approach to maintaining confidentiality is cryptography**,** which converts image data into an encrypted form that cannot be interpreted without the appropriate decryption key [5]. Cryptographic algorithms protect image content from eavesdropping or data leaks during network transmission.

Data integrity, on the other hand, ensures that the medical image received is exactly the same as the one sent, without any alteration or corruption during the communication process. One effective method for ensuring integrity is digital watermarking**,** which involves embedding imperceptible but verifiable information within the medical image [6]. These watermarks can serve as a checksum or proof of authenticity, enabling the detection of even the slightest modification. Advanced watermarking methods can also include authentication data, such as message authentication codes (MACs)**,** which confirm that the image has not been tampered with.

Authentication plays a crucial role in verifying the identity of both the sender and the receiver during image transmission. It ensures that medical images originate from a trusted source and are delivered to the intended recipient without interception or impersonation. As discussed by Roseline and Oluwakemi [7], digital signatures are one of the most widely used techniques for authentication in secure communication. When integrated with watermarking and encryption, authentication forms a robust security framework that can withstand various cyber threats.

In this context, encrypted watermarking has emerged as a powerful hybrid approach for securing medical image sharing. It combines the strengths of cryptography and watermarking offering dual-layer protection where encryption ensures confidentiality and watermarking guarantees integrity and authenticity. This paper provides an overview of encrypted watermarking techniques, explores their roles in secure medical image transmission, and highlights current trends, challenges, and opportunities in this evolving field.

2. Encryption of Medical Images

In general, most attacks that occur during the transmission of medical images can be categorized into four types: interruption, interception, modification, and fabrication. Interruption attacks aim to damage or disrupt medical data, often through the use of malicious software or small viruses. Interception attacks focus on capturing sensitive medical information during transmission, typically through hidden malicious code embedded in certain free or pirated software. Modification attacks involve the intentional alteration of the contents of transmitted medical images, which can lead to incorrect diagnoses or treatments. Fabrication attacks result in the insertion of false or harmful data into the network, potentially misleading healthcare systems or professionals. Due to the critical implications of such attacks, there is a pressing need to develop advanced techniques that ensure the secure transmission of medical images [8–10].

To maintain high confidentiality, the transmitted medical data must be protected from unauthorized access. One of the most effective methods for achieving this is encryption, which ensures that the data remains unreadable to intruders. Consequently, the implementation of enhanced encryption algorithms is essential to fulfil the fundamental security requirements of confidentiality, integrity, and authenticity. Encryption techniques can generally be divided into two categories: symmetric key encryption and asymmetric (or public key) encryption. In symmetric encryption, the same key is used for both encrypting and decrypting the data. This method is known for its speed and efficiency, making it particularly suitable for large data types such as images. In contrast, asymmetric encryption uses a pair of keys one public and one private. While the public key is openly distributed for encryption, only the intended recipient holds the private key required for decryption. Although asymmetric encryption offers strong security, it is often less efficient for large-scale image data.

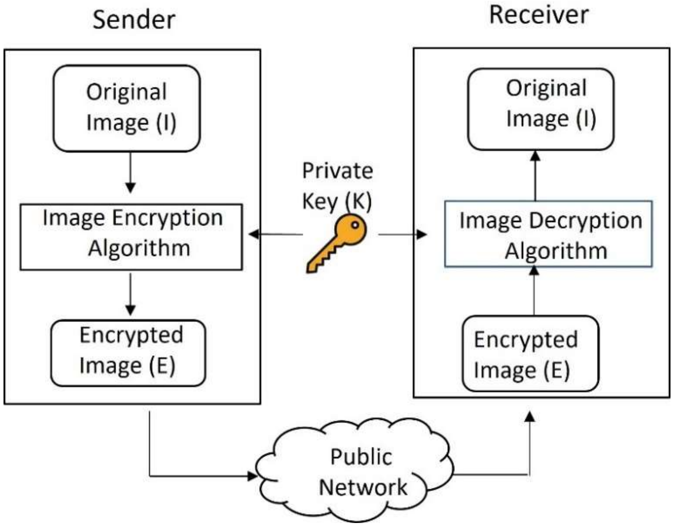

Figure 2: Image Encryption & Decryption Procedure [4]

Despite the availability of several symmetric and asymmetric encryption methods for securing digital content and textual data, symmetric encryption remains more suitable for image encryption due to its reliance on a single private key and lower computational complexity [11]. The process of encrypting and decrypting medical images can be understood through the following sequence: at the sender’s end, the original image (denoted as I) is encrypted using a private key (K), resulting in an encrypted image (E). This encrypted image is then transmitted over public networks. At the receiver’s end, the encrypted image (E) is decrypted using the same private key (K), allowing for the retrieval of the original image (I) through a corresponding decryption algorithm (Figure 2). This process ensures that the medical data remains protected and accessible only to authorized parties throughout its transmission.

3. Digital Image Watermarking

In recent years, the proliferation of digital media such as text, videos, images, and audio files on the internet has grown exponentially, transforming the world into a globally connected digital community. However, as digital processing systems increasingly integrate with the internet, multimedia content becomes highly vulnerable to security threats. Transmitted information can be altered, intercepted, or disseminated without prior authorization, posing serious challenges to data privacy and ownership. Common security threats include copyright infringement, unauthorized access, data theft, and illegal redistribution. According to the Institute for Policy Innovation (IPI), annual breaches involving movies, texts, audio, and software have resulted in significant copyright violations, financial losses, and job displacement.

To address these issues, digital image watermarking has emerged as an effective solution, offering a wide range of benefits in securing multimedia content. One of its key advantages lies in its ability to embed hidden data within digital images without compromising their semantic integrity. As such, digital watermarking plays a crucial role in enhancing multimedia security by ensuring content authenticity and ownership verification [12–13].

Typically, the digital image watermarking process involves three main phases: watermark generation, watermark embedding, and watermark detection. First, a watermark generator creates a unique watermark tailored to a specific application, often based on predefined keys. Next, the embedding phase incorporates this watermark into a cover image using embedding keys. Finally, in the detection phase, a decoder is used to extract and verify the watermark from the potentially altered image. By comparing the extracted watermark with the original, any tampering or unauthorized modification can be effectively identified.

The major benefits of digital image watermarking include improved data security and privacy, non-repudiation, controlled access, prevention of unauthorized duplication, and efficient usage of memory and bandwidth. Watermarking techniques are generally classified into three categories: robust, fragile, and semi-fragile watermarking. Each category serves different security and authentication needs, depending on the sensitivity and application of the media.

In the context of medical imaging, digital watermarking is especially important for preventing unauthorized access, ensuring diagnostic integrity, and protecting patient confidentiality. Contemporary digital watermarking approaches often employ domain transformation techniques such as the Discrete Fourier Transform (DFT), Discrete Cosine Transform (DCT), and Discrete Wavelet Transform (DWT) for embedding and extracting watermarks with high precision and robustness [14].

Figure 3 presents a schematic block diagram of the medical image watermarking process. At the sender's end, an encoder embeds the watermark into the medical image to enhance both security and authentication. At the receiver's end, a decoder extracts the watermark from the received image. By comparing the extracted watermark with the original, it becomes possible to detect any tampering or unauthorized alterations to the image. To ensure both reliability and high image quality, the performance of the watermarking system is commonly evaluated based on perceptibility, which refers to the visual invisibility of the watermark in the image [15].

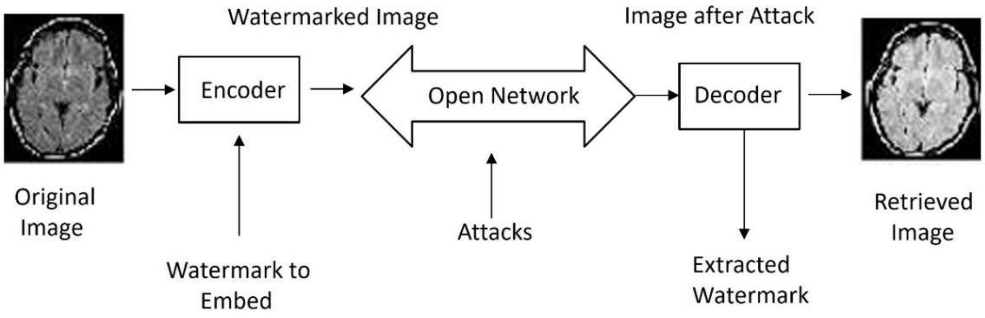

Figure 3: Digital Image Watermarking Procedure

4. Types of Watermarking

Watermarking can be broadly classified based on various criteria such as visibility, detection method, embedding domain, and the type of media being protected. The main types include visible and invisible watermarking, spatial domain and frequency domain watermarking, as well as detection-based types like blind, semi-blind, and non-blind watermarking. Additionally, watermarking techniques vary according to the type of content, including image, video, audio, and text watermarking (Figure 4). These classifications help select the most suitable approach depending on the application's needs for security, robustness, and imperceptibility, as detailed below.

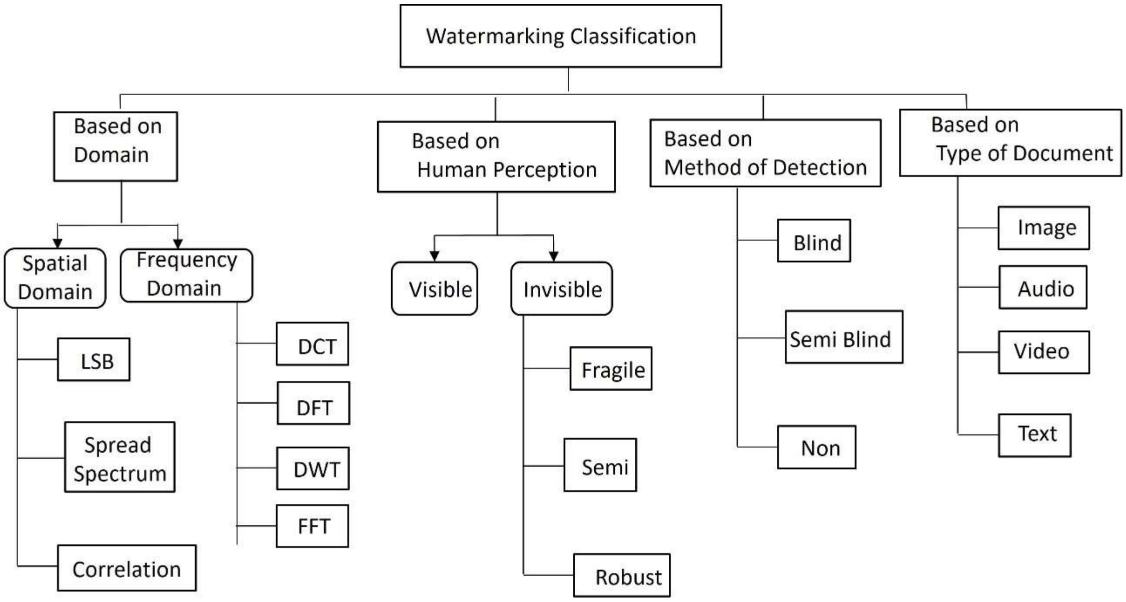

Figure 4: Classification of Watermarking Methods

4.1 Spatial Domain Watermarking

4.1.1 Least Significant Bit (LSB) Method

The Least Significant Bit (LSB) watermarking technique is one of the most basic spatial domain methods. It embeds watermark information by altering the least significant bits of selected pixels in the original image. This approach maintains high visual fidelity, as changes to LSBs are generally imperceptible to the human eye [16]. However, LSB watermarking is highly vulnerable to image compression, noise, filtering, and geometric transformations, which can easily destroy or remove the embedded watermark. Thus, it is typically used in applications where robustness is not the primary concern [17].

4.1.2 Correlation-Based Watermarking

Correlation-based watermarking techniques embed the watermark into the image such that it can later be detected using a correlation detector. In this method, the watermark signal is typically a pseudo-random sequence which is added directly to the image pixels in a predefined manner [18]. During detection, the presence of the watermark is confirmed by correlating the received image with the original watermark pattern. If the correlation exceeds a certain threshold, the watermark is deemed present. This method provides moderate robustness and security compared to LSB, as it is less sensitive to small distortions. However, its success depends on the correlation strength and the correct threshold selection [19].

4.1.3 Spread Spectrum (SS) Watermarking

Spread Spectrum watermarking improves robustness and security by spreading the watermark information across a wide range of spatial pixels using a pseudo-random noise pattern [20]. This technique is inspired by communication systems where the signal is spread over a broader bandwidth. In image watermarking, it ensures that even if parts of the image are altered or removed, the watermark can still be detected. Spread spectrum methods are more resilient to common image processing attacks and are difficult to detect or remove without the appropriate key, making them suitable for higher-security applications [21].

4.2 Frequency (Transform) Domain Watermarking

4.2.1 Discrete Cosine Transform (DCT)

The DCT is a popular frequency domain method that converts spatial pixel values into frequency components. It is typically applied block-wise (e.g., 8×8) to the image [22]. Watermarks are embedded in the mid-frequency coefficients, balancing imperceptibility and robustness. Modifying low-frequency components can significantly degrade image quality, while high-frequency components are prone to loss during compression [23]. DCT-based watermarking is widely used in compressed image formats such as JPEG and is effective against lossy compression and minor manipulations.

4.2.2 Discrete Fourier Transform (DFT)

The DFT represents an image in terms of its global frequency characteristics. Watermarking with DFT typically involves modifying the magnitude or phase components of the transform domain. It offers strong resilience against geometric attacks like rotation, scaling, and translation, as such transformations affect the spatial domain more than the frequency magnitude [24]. Though DFT is computationally intensive, its robustness makes it suitable for high-security applications, including document authentication and copyright protection [25].

4.2.3 Discrete Wavelet Transform (DWT)

The DWT provides a multi-resolution representation of an image, dividing it into various sub-bands (LL, LH, HL, HH) corresponding to different frequency ranges [26]. Watermarks are often embedded into the higher-frequency sub-bands to maintain imperceptibility, or in lower-frequency bands for improved robustness. DWT is particularly useful in medical imaging applications due to its ability to preserve critical diagnostic information while ensuring secure watermark embedding [27]. Its layered decomposition also makes it highly adaptable for hierarchical and scalable watermarking.

4.2.4 Fast Fourier Transform (FFT)

The FFT is a computationally efficient algorithm for performing the DFT. It retains the core benefits of DFTs robustness to geometric and signal-based attacks, while significantly reducing processing time. FFT is suitable for real-time watermarking and high-resolution image scenarios where performance and scalability are essential [28]. Like DFT, FFT-based watermarking embeds data in the frequency domain, making it harder for attackers to detect or tamper with the watermark without altering the image noticeably [29].

4.3 Watermarking Based on Human Perception

Digital watermarking techniques that leverage human perception are broadly classified into two categories: visible and invisible watermarking. These classifications are based on the perceptibility of the watermark to the Human Visual System (HVS).

4.3.1 Visible Watermarking

Visible watermarking refers to the deliberate embedding of logos, text, or patterns onto the visible part of an image. These watermarks are clearly perceptible to human viewers and are typically placed in a prominent location within the image, such as a corner or center, to declare ownership or assert copyright. Commonly used in digital photography, broadcasting, and online image sharing, visible watermarks serve as a deterrent against unauthorized use or reproduction. Although they are easily noticed, visible watermarks must still be carefully designed to avoid obstructing critical content in the image, especially in sensitive domains like medical imaging. The challenge lies in achieving an optimal balance between visibility, aesthetic quality, and tamper resistance.

4.3.2 Invisible Watermarking

Invisible watermarking involves embedding watermark data into the image in a manner that is imperceptible to the human eye but can be detected or extracted through computational methods. These watermarks are typically used for copyright protection, authentication, and data integrity verification. Invisible watermarking techniques take advantage of the HVS by embedding data in areas where visual sensitivity is low, such as high-frequency regions or textured areas of the image. Advanced algorithms also incorporate perceptual models that consider luminance masking, contrast sensitivity, and texture masking to maintain the image's visual fidelity. Invisible watermarking is widely applied in scenarios where preserving the image quality is critical, such as in medical imaging, legal evidence, or confidential document exchange, while still maintaining a hidden layer of security.

Both visible and invisible watermarking methods play crucial roles in digital rights management and secure multimedia distribution. While visible watermarking emphasizes public attribution and deterrence, invisible watermarking focuses on covert protection and forensic tracking without altering the visual experience. The choice between the two depends on the application context and the required trade-off between perceptibility, robustness, and security [30].

4.4 Watermarking Based on the Method of Detection

Digital watermarking techniques can also be classified based on the method used to detect or extract the watermark from the watermarked image. This classification affects the system's complexity, security, and practicality in real-world applications. The three main categories under this approach are: Blind, Semi-Blind, and Non-Blind watermarking.

4.4.1 Blind Watermarking (Oblivious Detection)

Blind watermarking refers to techniques in which the watermark can be detected or extracted without requiring access to the original (unwatermarked) image. This method is highly practical, especially in real-time or large-scale applications, since storing or accessing the original image during detection is not necessary [31]. Blind detection is ideal for applications like copyright enforcement, content tracking, and authentication in decentralized systems. However, designing blind watermarking schemes that are both robust (resistant to attacks) and imperceptible (not visible) is more challenging, as the extraction must rely solely on the information present in the watermarked image.

4.4.2 Semi-Blind Watermarking

Semi-blind watermarking requires partial information about the original content for watermark detection. This may include a secret key, watermark sequence, or some feature of the original image, but not the complete image itself [32]. It offers a compromise between robustness and practicality, less complex than non-blind methods and more accurate than blind methods. Semi-blind detection methods are useful in authentication systems where the watermark needs to be validated using reference data (like a hash or template) but storing the entire original image is impractical due to memory or bandwidth limitations.

4.4.3 Non-Blind Watermarking (Informed Detection)

Non-blind watermarking, also known as informed detection, requires full access to the original image during the watermark extraction process. This approach allows for more accurate and reliable watermark detection, especially in the presence of distortions, as the detector can directly compare the watermarked image with the original [33]. Non-blind watermarking is commonly used in controlled environments such as medical imaging, secure digital archiving, and legal evidence management, where the original data is available and verification accuracy is critical. However, its dependence on the original image makes it less suitable for scenarios involving large-scale distribution or remote verification.

4.5 Watermarking Based on the Type of Document

Digital watermarking techniques are tailored according to the nature of the content being protected. The type of media, whether it is an image, video, audio, or text—significantly influences the choice of embedding strategy, robustness requirements, and perceptual constraints. The following are the common classifications based on the type of document:

4.5.1 Image Watermarking

Image watermarking involves embedding watermark data into still images. This is one of the most researched areas in digital watermarking due to the widespread use of digital images across the internet, especially in medical imaging, digital photography, and media [34]. Watermarks can be embedded in the spatial domain (e.g., LSB, correlation-based) or frequency domain (e.g., DCT, DWT, DFT). Image watermarking must ensure high imperceptibility and robustness against operations like compression, cropping, resizing, and filtering. Applications include copyright protection, medical image security, and image authentication.

4.5.2 Video Watermarking

Video watermarking extends image watermarking techniques to temporal data. A video is essentially a sequence of image frames, often accompanied by audio [35]. Watermarking in video can be done frame-by-frame or by using temporal characteristics like motion vectors or scene changes. Frequency-domain techniques (like DWT-DCT hybrids) are frequently used for robustness. Video watermarking must meet stricter requirements for real-time processing, synchronization, and resilience to compression (e.g., MPEG), frame dropping, temporal scaling, and re-encoding. It is commonly applied in broadcast monitoring, digital cinema, surveillance, and streaming media protection.

4.5.3 Audio Watermarking

Audio watermarking focuses on embedding data into digital audio signals such as speech, music, or sound recordings. The watermark must be inaudible to human listeners while remaining robust against common audio transformations like compression (e.g., MP3), filtering, and noise addition. Techniques typically use time domain (e.g., echo hiding, phase coding) or frequency domain (e.g., FFT, DCT, wavelet transforms) [36]. Psychoacoustic models are often employed to exploit the limitations of the Human Auditory System (HAS) for perceptual transparency. Applications include music rights management, audio fingerprinting, and broadcast tracking.

4.5.4 Text Watermarking

Text watermarking is more challenging due to the discrete and limited redundancy in text documents. Unlike images or audio, where small changes can be imperceptible, even minor alterations in text can be easily noticeable or disrupt semantics. Text watermarking techniques include formatting-based methods (e.g., altering spacing, font, or punctuation), syntactic methods (rephrasing sentences), and semantic methods (replacing synonyms without changing meaning) [37]. The goal is to embed information without affecting readability or content integrity. Applications include document authentication, plagiarism detection, and copyright protection of digital manuscripts or e-books.

Each type of document presents unique challenges for watermarking, and the techniques must be adapted accordingly to ensure imperceptibility, robustness, security, and efficiency. The choice of approach is highly dependent on the media's perceptual characteristics and the intended application domain.

5. Digital Image Watermarking System Requirements

For particular objectives, like in medical applications, few other characteristics like imperceptibility and reversibility should be included and it is completely explained in medical segment.

Fidelity: This metric decides similarity amongst the watermarked and non-watermarked image. Otherwise said, fidelity refers to the degree of invisibility of the watermark present in the watermarked image.

Robustness: In contrary to fragile watermarking, robustness indicates the resilience against different nondeliberate and unauthorized attacks. Cropping, resizing, and compression are instances of unintentional attacks, which may occur generally during the processing of a digital image. Noise inclusion and geometrical distortion constitute the two examples of intrusive attacks, which may be utilized by attackers for removing the watermark.

Data Payload (Capacity): it his aspect depicts maximum amount of data, which can be inserted into an image with no significant reduction in the image quality. The effect of capacity on robustness and perceptibility of watermarked image is very important; for example, when the data payload is increased, the robustness will reduce and the perceptibility will improve. The dimensions of the host image must also take into consideration, due to the fact that the more the image resolution, the higher the degree of watermark is suitable in terms of bits [38].

Security: This metric is associated with the usage of various types of keys, like public or private, such that unauthenticated individuals cannot compromise the watermark.

Computational Complexity (Speed): This measure is associated with the computation time taken to embed and extract the watermark, which directly decides the computational complexity. For instance, real-time application needs rapid techniques. But, for higher-security applications, time consumption of embedding as well as extracting techniques are generally high.

Perceptibility: This metric is associated with the degree of distortion appearing on watermarked image once a watermark is inserted. In the case of imperceptible watermarks, this metric must be a minimal value.

6. Applications of Digital Watermarking System

Watermarking approaches are application based. Various techniques show diverse constraints and criteria. Below is a list of a few uses:

Copyright Protection: This application claims that the digital image clearly incorporates the owner's copyright information, and it may be extracted to demonstrate ownership in the event of an infringement. To do this, the watermark has to be resistant to both approved and illegal assaults. It is not appropriate to apply this kind of watermark to prevent users from duplicating the digital image.

Fingerprinting: The creator of this program should add various watermarks according to each user's identification. It implies that the data, which are utilized in the form of a watermark, will be selected as per the information of the client. This method makes it easier for the proprietor to identify the origin of illicit copies and quickly apprehend users who break licensing agreements. Additionally, this watermark ought to be trustworthy and undetectable.

Authentication as well as Integrity Verification:

This application's goal is to determine whether or not the digital picture has been altered, and if so, to identify the location of the alteration. Fragile or semi-fragile watermarking methods, which are unreliable against content changes, must be utilized in this application. Digital picture watermarking may also be used for clandestine communication, content description, even broadcast monitoring.

7. Issues In Encryption, and Digital Watermarking of Medical Images

All the existing image encryption techniques do not ensure complete robustness towards digital watermarks in encryption domains. In case of few of these image encryption approaches, the extraction of watermarks could be carried out after embedding the watermarks. However, owing to the presence of numerous interferences like Gaussian noise, median filtering, rotations, etc., the quality of the watermarks become poorer, therefore the robustness of the watermarks could not be assured [39, 40]. Considering plaintext domains, even though numerous effective digital image watermarking approaches were formulated, owing to the restrictions in the encryption techniques, transplanting these effective digital image watermarking approaches directly to the encryption domains become little tedious task especially when processing medical images as these medical image security applications need specific requirements. Imperceptibility is considered as one of the major concerns while processing medical images using digital image watermarking techniques. In many applications, altering the medical images after embedding watermarks is not permitted. Imperceptibility could be attained by picking the Region of non-interest (RNOI) watermarking, where the watermarks are inserted in the medical images' RNOI region. Moreover, imperceptibility could be attained with the help of reversible watermarking approaches that assist in recovering the original medical images by performing the reverse operation of watermark embedding mechanism at receiver end. At receiver end, it must be able to easily extract the original medical images as well as embedded watermarks. This property which is commonly referred as reversibility of medical image watermarking has to be seriously encountered. Moreover, for enabling e-treatment, most of the medical images were transmitted via internet so as to accomplish remote diagnosis. In these cases, transmission speed has a serious impact, therefore the chosen algorithm must be of reduced complexity for minimizing the execution time.

8. Recent Notable Works

E-healthcare applications are increasingly vulnerable to various cyberattacks, which may lead to severe consequences including unauthorized data access, manipulation, or loss of sensitive medical information. These threats undermine the security, confidentiality, and integrity of electronic health records and transmitted medical images.

Hosny et al. (2024) presented an in-depth survey on digital image watermarking using deep learning techniques, outlining recent advancements and applications in securing visual data [41]. The study categorized various deep learning-based watermarking approaches into supervised, unsupervised, and generative models, highlighting their effectiveness in terms of robustness, imperceptibility, and capacity. The authors noted that deep neural networks (DNNs), especially convolutional neural networks (CNNs) and autoencoders**,** have shown promising results in embedding and extracting watermarks under a variety of attacks. Their work emphasized the growing potential of AI-powered watermarking in adapting to increasingly complex threats in multimedia security.

Sharma et al. (2024) conducted a comprehensive review on the use of image watermarking for identity protection and verification**,** particularly in the context of biometric and personal data [42]. Their study focused on how watermarking techniques are integrated into identity authentication systems to prevent spoofing, tampering, and identity theft. The paper examined domain-specific methods such as DWT-SVD and hybrid transform-based watermarking, and assessed their performance in terms of fidelity, security, and real-time processing capabilities. This work reinforces the critical role of watermarking in safeguarding identity within secure access systems and digital identification platforms.

Yang et al. (2025) explored a novel frontier in watermarking its application in large language models (LLMs)**.** Their survey discussed the design and implementation of watermarking strategies for protecting and tracing outputs generated by LLMs, such as GPT-style models [43]. Key methods reviewed include prompt-level watermarking, output perturbation, and probabilistic watermarking for text generation. The study highlighted the importance of such techniques in intellectual property protection, content authenticity, and misinformation control, especially in an era where AI-generated content is widely disseminated.

Ye et al. (2025) proposed a periodic watermarking scheme for copyright protection of LLMs within cloud computing environments [44]. Their approach embeds periodic watermarks directly into the output patterns of language models, allowing for efficient tracking of model usage and protection against unauthorized distribution. The study also introduced a detection framework that uses periodic signature analysis for watermark verification, even under adversarial transformations. This method enhances cloud security by enabling copyright holders to prove ownership and monitor model misuse without compromising performance.

Ye et al. (2025) also introduced a hybrid security framework for social image protection**,** combining encryption and watermarking across multiple domains [45]. Their method employs multi-domain watermarking**,** embedding data in both spatial and transform domains while concurrently encrypting the image to ensure end-to-end confidentiality. This dual-layer approach enhances protection against unauthorized sharing, tampering, and reverse engineering in social media contexts. Their research demonstrates how combining cryptographic encryption with robust watermarking significantly strengthens data security in publicly shared digital content.

Wandile et al. (2025) developed a compact and secure image encryption model tailored for IoT-based medical systems**,** combining Elliptic Curve Cryptography (ECC) with Advanced Encryption Standard (AES) [46]. Their hybrid cryptographic approach ensures a strong balance between lightweight processing and robust encryption, which is critical for resource-constrained environments like IoT healthcare devices. The proposed scheme showed notable improvements in execution speed and energy efficiency while maintaining high levels of image confidentiality and integrity. The model is particularly useful in e-health applications where real-time encryption of sensitive medical images is required.

Pandey and Sharma (2025) introduced a novel encryption-validation mechanism based on ECC for medical images, enhanced with genetic algorithms for embedding watermark data in the low-frequency region of the image spectrum [47]. This method not only secures the image through strong encryption but also integrates a validation process to verify authenticity. By targeting low-frequency regions, the embedded watermark remains resilient against common image processing operations such as compression and filtering. Their approach provides a dual-layer defense system that ensures both security and **v**alidation of transmitted medical content.

El-Rahman et al. (2025) proposed C-HIDE, a steganographic and encryption framework that introduces a coverless hybrid image encryption scheme using ECC and AES to ensure enhanced data hiding and confidentiality [48]. Unlike conventional watermarking, C-HIDE focuses on robust steganography**,** eliminating the need for a visible or detectable cover medium. The system supports high payload capacity and security through an advanced hybrid cryptographic model, making it ideal for embedding sensitive patient information within medical images in telemedicine and cloud-based healthcare systems.

Chaouch et al. (2025) addressed image security in cloud computing environments by developing a hybrid encryption technique that combines ECC with spatiotemporal cryptography [49]. Their model introduces dynamic temporal encryption parameters, increasing resistance to known-plaintext and chosen-ciphertext attacks. The approach enhances data protection during storage and transmission of medical images in distributed cloud networks. The use of ECC ensures computational efficiency, while spatiotemporal scrambling adds an additional layer of unpredictability and resilience, making this method highly applicable to modern e-health infrastructures.

9. Performance Metrics Analysis

Peak Signal to Noise Ratio (PSNR): It is the highest power to noise distortion image representation ratio, or peak signal to noise ratio (PSNR). Typically, PSNR is presented using a decibel scale. A common metric for assessing image quality is PSNR. The original data in this case is the signal, while the error is the noise. Higher PSNR displays higher image quality. PSNR is most easily defined via the mean squared error is provided in equation (1).

$$MSE = \frac{1}{mn}\sum_{i=0}^{m-1}\sum_{j=0}^{n-1}\left[I(i,j)-K(i,j)\right]^2 \tag{1}$$

The PSNR (in dB) shall be defined using equation (2).

$$PSNR = 10\log_{10}\frac{(255)^2}{MSE} \tag{2}$$

The original, watermarked images are I and K respectively.

Compression Ratio (CR): The compression ratio refers to the proportion between the size of the original image and the size of the compressed image. It indicates how effectively an image compression algorithm reduces data. A higher compression ratio means more data reduction, resulting in smaller file sizes, which is especially important for storing and transmitting large medical images. However, care must be taken to maintain image quality, especially in medical applications where diagnostic accuracy is critical.

CR= Original Image in bytes/ Compressed Image in bytes (3)

Normalized Correlation (NC): is a metric used to evaluate the similarity between the extracted watermark from a compromised or distorted image and the original watermark. It measures how closely the retrieved watermark matches the original, with values typically ranging from 0 to 1. A value closer to 1 indicates high similarity, implying that the watermarking technique is robust against attacks or distortions. This makes NC a crucial parameter in assessing the reliability and effectiveness of digital watermarking systems.

$$NC = \frac{\sum_{i=1}^{m}\sum_{j=1}^{n}\left(I(i,j)*K(i,j)\right)}{\sum_{i=1}^{m}\sum_{j=1}^{n}I(i,j)^2} \tag{4}$$

Embedding Capacity (EC): Embedding Capacity refers to the amount of data that can be embedded within an image without significantly degrading its quality. It is commonly measured in bits per pixel (bpp)**,** indicating how many bits of watermark or hidden data are stored in each pixel of the host image. A higher embedding capacity allows for more information to be embedded, but it must be balanced with imperceptibility and robustness to ensure that the watermark remains invisible and resistant to attacks.

$$Capacity = \frac{|m|}{|A|} \tag{5}$$

Where, m is the message that is embedded in cover image.

Structural Similarity Index Measure (SSIM): The calculation of the structural similarity index tests the similarity to structures and compares normal luminance and contrast patterns in local pixel intensities. The concept behind this quality assessment is that the visual system is good for the collection of structural details. Structural awareness is the concept of strong interdependence in the pixels, particularly when near the space. These dependencies provide valuable information on the organization of the visual scene components. Several windows of an image are used to compute the structural similarity (SSIM) measure. The range of its value is [0, 1]. Equation (6) is used to represent the measure across two windows of common size N×N.

$$SSIM(x,y) = \frac{(2*\mu_x*\mu_y + C_1)(2*\sigma_{xy} + C_2)}{(\mu_x^2 + \mu_y^2 + C_1)(\sigma_x^2 + \sigma_y^2 + C_2)} \quad (6)$$

where, μ_x - An average of x, μ_y - An average of y , σ_x^2 - A variance of x, σ_y^2 - A variance of y and

σ_{xy} - A covariance of x as well as y. $C_1 = (k_1 L)^2, C_2 = (k_2 L)^2$ represents the two variables that maintain the weak denominator division. L is the pixel-values' dynamic range and K_1 =0.010 and k_2 =0.030, the standard value.

10. Conclusion

With the increasing use of digital communication in healthcare, especially through telemedicine, teleradiology, remote diagnosis, and virtual consultations, ensuring the security, authenticity, and integrity of medical images has become more important than ever. To meet these growing demands, researchers have proposed various medical image watermarking techniques, each offering certain advantages while also facing specific limitations. In this study, we presented a detailed overview of medical image watermarking methods, emphasizing their fundamental concepts, practical challenges, and real-world applications. We discussed the basic structure of watermarking systems, explained where digital watermarks are typically embedded within medical images, and outlined key requirements such as robustness, invisibility, and embedding capacity. Additionally, we explored common threats and evaluated how different techniques can protect against them. This review aims to guide future research and development in building secure and reliable systems for medical image protection in modern healthcare environments.

References

1. Li, Xiang, Yuchen Jiang, Juan J. Rodriguez-Andina, Hao Luo, Shen Yin, and Okyay Kaynak. "When medical images meet generative adversarial network: recent development and research opportunities." *Discover Artificial Intelligence* 1 (2021): 1-20.
2. Chen, Yung-Yao, Yu-Chen Hu, Hsiang-Yun Kao, and Yu-Hsiu Lin. "Security for eHealth system: data hiding in AMBTC compressed images via gradient-based coding." *Complex & Intelligent Systems* 9, no. 3 (2023): 2699-2711.
3. Kruse, Clemens Scott, Brenna Smith, Hannah Vanderlinden, and Alexandra Nealand. "Security techniques for the electronic health records." *Journal of medical systems* 41 (2017): 1-9.
4. Masood, Fawad, Maha Driss, Wadii Boulila, Jawad Ahmad, Sadaqat Ur Rehman, Sana Ullah Jan, Abdullah Qayyum, and William J. Buchanan. "A lightweight chaos-based medical image encryption scheme using random shuffling and XOR operations." *Wireless personal communications* 127, no. 2 (2022): 1405-1432.
5. Elamir, Mona M., Walid I. Al-atabany, and Mai S. Mabrouk. "Hybrid image encryption scheme for secure E-health systems." *Network Modeling Analysis in Health Informatics and Bioinformatics* 10, no. 1 (2021): 35.
6. Gao, Hang, and Tiegang Gao. "A secure lossless recovery for medical images based on image encoding and data self-embedding." *Cluster Computing* 25, no. 1 (2022): 707-725.

7. Ogundokun, Roseline Oluwaseun, and Oluwakemi Christiana Abikoye. "A safe and secured medical textual information using an improved LSB image steganography." *International Journal of Digital Multimedia Broadcasting* 2021, no. 1 (2021): 8827055.
8. Thanki, Rohit, and Ashish Kothari. "Multi-level security of medical images based on encryption and watermarking for telemedicine applications." *Multimedia tools and applications* 80, no. 3 (2021): 4307-4325.
9. Priya, S., and B. Santhi. "A novel visual medical image encryption for secure transmission of authenticated watermarked medical images." *Mobile networks and applications* 26, no. 6 (2021): 2501-2508.
10. Kumar, Manish, and Prateek Gupta. "A new medical image encryption algorithm based on the 1D logistic map associated with pseudo-random numbers." *Multimedia Tools and Applications* 80, no. 12 (2021): 18941-18967.
11. Li, Jian, Zelin Zhang, Shengyu Li, Ryan Benton, Yulong Huang, Mohan Vamsi Kasukurthi, Dongqi Li et al. "A partial encryption algorithm for medical images based on quick response code and reversible data hiding technology." *BMC Medical Informatics and Decision Making* 20 (2020): 1-16.
12. Vaidya, S. Prasanth, and V. Ravi Kishore. "Adaptive medical image watermarking system for e-health care applications." *SN Computer Science* 3, no. 2 (2022): 107.
13. Zermi, Narima, Amine Khaldi, Med Redouane Kafi, Fares Kahlessenane, and Salah Euschi. "A lossless DWT-SVD domain watermarking for medical information security." *Multimedia Tools and Applications* 80 (2021): 24823-24841.
14. Soualmi, Abdallah, Adel Alti, and Lamri Laouamer. "A new blind medical image watermarking based on weber descriptors and Arnold chaotic map." *Arabian Journal for Science and Engineering* 43, no. 12 (2018): 7893-7905.
15. Wee, Tan Chi, Mohd Shafry Mohd Rahim, Gloria Jennis Tan, Ghazali Sulong, and Chaw Jun Kit. "High imperceptibility medical image watermarking scheme based on Slantlet transform by using dynamic visibility threshold." In *2020 6th International Conference on Interactive Digital Media (ICIDM)*, pp. 1-5. IEEE, 2020.
16. Bansal, Kriti, Aman Agrawal, and Nency Bansal. "A survey on steganography using least significant bit (lsb) embedding approach." In *2020 4th International Conference on Trends in Electronics and Informatics (ICOEI)(48184)*, pp. 64-69. IEEE, 2020.
17. Tseng, Hsien-Wen, and Hui-Shih Leng. "A reversible modified least significant bit (LSB) matching revisited method." *Signal Processing: Image Communication* 101 (2022): 116556.
18. Ahmed, Farid, and Ira S. Moskowitz. "Correlation-based watermarking method for image authentication applications." *Optical Engineering* 43, no. 8 (2004): 1833-1838.
19. Ejima, Masataka, and Akio Miyazaki. "An analysis of correlation-based watermarking systems." *Electronics and Communications in Japan (Part III: Fundamental Electronic Science)* 86, no. 11 (2003): 1-12.
20. Xiang, Yong, Iynkaran Natgunanathan, Yue Rong, and Song Guo. "Spread spectrum-based high embedding capacity watermarking method for audio signals." *IEEE/ACM transactions on audio, speech, and language processing* 23, no. 12 (2015): 2228-2237.
21. Maity, Santi P., and Malay K. Kundu. "Performance improvement in spread spectrum image watermarking using wavelets." *International Journal of Wavelets, Multiresolution and Information Processing* 9, no. 01 (2011): 1-33.
22. Alotaibi, Reem A., and Lamiaa A. Elrefaei. "Text-image watermarking based on integer wavelet transform (IWT) and discrete cosine transform (DCT)." *Applied Computing and Informatics* 15, no. 2 (2019): 191-202.
23. Alomoush, Waleed, Osama A. Khashan, Ayat Alrosan, Hani H. Attar, Ammar Almomani, Fuad Alhosban, and Sharif Naser Makhadmeh. "Digital image watermarking using discrete cosine transformation based linear modulation." *Journal of Cloud Computing* 12, no. 1 (2023): 96.
24. Zhang, Xueting, Qingtang Su, Zihan Yuan, and Decheng Liu. "An efficient blind color image watermarking algorithm in spatial domain combining discrete Fourier transform." *Optik* 219 (2020): 165272.
25. Solikhin, Mukhammad, Yohanssen Pratama, Purnama Pasaribu, Josua Rumahorbo, and Bona Simanullang. "Analisis Watermarking Menggunakan Metode Discrete Cosine Transform (DCT) dan Discrete Fourier Transform (DFT)." *Jurnal Sistem Cerdas* 5, no. 3 (2022): 155-170.

26. Kashyap, Nikita, and G. R. Sinha. "Image watermarking using 3-level discrete wavelet transform (DWT)." *International Journal of Modern Education and Computer Science* 4, no. 3 (2012): 50.
27. Barnouti, Nawaf Hazim, Zaid Saeb Sabri, and Khaldoun L. Hameed. "Digital watermarking based on DWT (discrete wavelet transform) and DCT (discrete cosine transform)." *International Journal of Engineering & Technology* 7, no. 4 (2018): 4825-4829.
28. Dhar, Pranab Kumar, and Jong-Myon Kim. "Digital watermarking scheme based on fast Fourier transformation for audio copyright protection." *International Journal of Security and Its Applications* 5, no. 2 (2011): 33-48.
29. Pourhashemi, Seyed Mostafa, Mohammad Mosleh, and Yousof Erfani. "Audio watermarking based on synergy between Lucas regular sequence and Fast Fourier Transform." *Multimedia Tools and Applications* 78, no. 16 (2019): 22883-22908.
30. Wang, Qingzhu, Xiaoming Chen, Mengying Wei, and Zhuang Miao. "Simultaneous encryption and compression of medical images based on optimized tensor compressed sensing with 3D Lorenz." *Biomedical engineering online* 15 (2016): 1-20.
31. Eggers, Joachim J., and Bernd Girod. "Blind watermarking applied to image authentication." In *2001 IEEE International Conference on Acoustics, Speech, and Signal Processing. Proceedings (Cat. No. 01CH37221)*, vol. 3, pp. 1977-1980. IEEE, 2001.
32. PVSSR, Chandra Mouli. "A robust semi-blind watermarking for color images based on multiple decompositions." *Multimedia Tools and Applications* 76, no. 24 (2017): 25623-25656.
33. Houmansadr, Amir, Negar Kiyavash, and Nikita Borisov. "Non-blind watermarking of network flows." *IEEE/ACM Transactions on Networking* 22, no. 4 (2013): 1232-1244.
34. Begum, Mahbuba, and Mohammad Shorif Uddin. "Digital image watermarking techniques: a review." *Information* 11, no. 2 (2020): 110.
35. Asikuzzaman, Md, and Mark R. Pickering. "An overview of digital video watermarking." *IEEE Transactions on Circuits and Systems for Video Technology* 28, no. 9 (2017): 2131-2153.
36. Hua, Guang, Jiwu Huang, Yun Q. Shi, Jonathan Goh, and Vrizlynn LL Thing. "Twenty years of digital audio watermarking—a comprehensive review." *Signal processing* 128 (2016): 222-242.
37. Kamaruddin, Nurul Shamimi, Amirrudin Kamsin, Lip Yee Por, and Hameedur Rahman. "A review of text watermarking: theory, methods, and applications." *IEEE Access* 6 (2018): 8011-8028.
38. Jabade, Vaishali S., and Sachin R. Gengaje. "Literature review of wavelet based digital image watermarking techniques." *International Journal of Computer Applications* 31, no. 7 (2011): 28-35.
39. Bhardwaj, Rupali, and Ashutosh Aggarwal. "Hiding clinical information in medical images: an enhanced encrypted reversible data hiding algorithm grounded on hierarchical absolute moment block truncation coding." *Multidimensional Systems and Signal Processing* 31, no. 3 (2020): 1051-1074.
40. Ahmed, Saja Theab, Dalal Abdulmohsin Hammood, Raad Farhood Chisab, Ali Al-Naji, and Javaan Chahl. "Medical image encryption: a comprehensive review." *Computers* 12, no. 8 (2023): 160.
41. Hosny, Khalid M., Amal Magdi, Osama ElKomy, and Hanaa M. Hamza. "Digital image watermarking using deep learning: A survey." *Computer Science Review* 53 (2024): 100662.
42. Sharma, Sunpreet, Ju Jia Zou, Gu Fang, Pancham Shukla, and Weidong Cai. "A review of image watermarking for identity protection and verification." *Multimedia Tools and Applications* 83, no. 11 (2024): 31829-31891.
43. Yang, Zhiguang, Gejian Zhao, and Hanzhou Wu. "Watermarking for large language models: A survey." *Mathematics* 13, no. 9 (2025): 1420.
44. Ye, Pei-Gen, Zhengdao Li, Zuopeng Yang, Pengyu Chen, Zhenxin Zhang, Ning Li, and Jun Zheng. "Periodic watermarking for copyright protection of large language models in cloud computing security." *Computer Standards & Interfaces* 94 (2025): 103983.
45. Ye, Conghuan, Shenglong Tan, Jun Wang, Li Shi, Qiankun Zuo, and Wei Feng. "Social image security with encryption and watermarking in hybrid domains." *Entropy* 27, no. 3 (2025): 276.
46. Wandile, Piyush S., Bhupendra Singh Kirar, Saurabh Jain, and Yatendra Sahu. "Compact and Secure Image Encryption for IoT Systems Employing ECC and AES Hybrid Cryptography." In *2025 IEEE International Students' Conference on Electrical, Electronics and Computer Science (SCEECS)*, pp. 1-6. IEEE, 2025.
47. Pandey, Kartikey, and Deepmala Sharma. "Digital image encryption with validation by ECC and embedding at low frequency region using the genetic approach." *International Journal of Electronics and Telecommunications* (2025): 87-93.

48. El-Rahman, Sahar A., Ahmed E. Mansour, Leila Jamel, Manal Abdullah Alohali, Mohamed Seifeldin, and Yasmin Alkady. "C-HIDE: A Steganographic Framework for Robust Data Hiding and Advanced Security Using Coverless Hybrid Image Encryption With AES and ECC." *IEEE Access* 13 (2025): 41367-41381.
49. Chaouch, Ismehene, Anis Naanaa, and Sadok El Asmi. "Enhanced Image Security in Cloud Computing Using Hybrid Encryption with ECC and Spatiotemporal Cryptography." In *International Conference on Advanced Information Networking and Applications*, pp. 175-187. Cham: Springer Nature Switzerland, 2025.

International Journal of Intelligent Communication and Computer Science
Vol. 3, No. 1, 2025, Pages 87-114.

Advanced Manufacturing Techniques for Aerospace Antennas

S. Khalid[1]

IBMM Research, Sudan

Email: skhalid@Ibmmacl.org

Review Paper

Received: 17 Jun 2025, Revised: 21 Aug. 2025 Accepted: 10S ep 2025

Abstract:
The aerospace industry continually demands antennas that meet increasingly stringent requirements for performance, reliability, weight, and environmental resilience. This review paper comprehensively surveys the state-of-the-art advanced manufacturing techniques employed in aerospace antenna fabrication, focusing on their applicability, advantages, and limitations in addressing the unique challenges of the sector. It covers a broad spectrum of methods, including additive manufacturing, precision machining, composite material fabrication, and advanced integration and assembly techniques. Special attention is given to recent advancements such as hybrid manufacturing processes that combine multiple fabrication approaches, the use of smart and multifunctional materials, and the integration of nanotechnology to enhance antenna performance and durability. The paper also discusses emerging trends in the field, particularly the application of artificial intelligence and machine learning to optimize design, fabrication, and quality control processes. Through a critical analysis of recent research findings, case studies, and industrial applications, this review provides valuable insights into current capabilities and future directions. It aims to serve as a comprehensive reference for researchers, engineers, and industry professionals involved in aerospace antenna development, enabling them to harness advanced manufacturing technologies to meet the evolving demands of aerospace communication systems.

Keywords: Aerospace antennas, advanced manufacturing, additive manufacturing, precision machining, composite materials.

1. Introduction

The aerospace industry has long been recognized as a pioneer in adopting and driving cutting-edge technologies, propelled by the constant quest for improved performance, reliability, and operational efficiency [1]. This drive is particularly crucial given the challenging and often extreme environments in which aerospace systems operate—ranging from the vacuum and radiation of space to the turbulent and variable conditions of Earth's atmosphere. Within this high-stakes context, antennas play a pivotal role as essential components that enable communication, navigation, and sensing capabilities across a broad spectrum of aerospace applications, including satellite communications, radar systems, unmanned aerial vehicles (UAVs), and deep-space exploration missions [2].

Antennas are fundamental to the successful operation of aerospace platforms because they directly impact the quality and reliability of data transmission and reception. As aerospace missions become more complex and multifaceted—requiring higher data rates, greater bandwidth, miniaturization, and multifunctionality—the design and manufacturing of antennas have correspondingly become more sophisticated. The antennas must not only achieve exceptional electromagnetic performance but also withstand stringent mechanical, thermal, and environmental stresses while maintaining minimal weight and volume.

Traditional manufacturing methods for aerospace antennas, such as subtractive machining and manual assembly, are increasingly challenged by the need for precision, repeatability, and integration of novel materials and structures. These demands have catalyzed the development and adoption of advanced manufacturing techniques, including additive manufacturing (3D printing), precision micro-machining, and composite fabrication processes. Such methods enable the production of highly complex geometries, integration of multifunctional materials, and customization at reduced lead times and cost [2].

Moreover, the emergence of new materials, such as lightweight composites and smart materials with tunable electromagnetic properties, alongside technological innovations like nanotechnology and embedded sensors, requires novel fabrication approaches that can reliably integrate these elements into antenna structures. Additionally, the integration of digital technologies, such as computer-aided design (CAD), artificial intelligence (AI), and machine learning, is revolutionizing the antenna manufacturing landscape by enabling predictive quality control, adaptive process optimization, and enhanced system integration [3].

This review paper aims to provide a comprehensive examination of these advanced manufacturing techniques as applied to aerospace antennas. By surveying the latest research, case studies, and industrial practices, the paper seeks to highlight the capabilities, challenges, and future prospects of modern fabrication methods in meeting the demanding performance criteria of aerospace systems. Ultimately, it serves as a valuable resource for researchers, engineers, and industry professionals striving to push the boundaries of antenna technology within the aerospace sector.

2. Background

Antennas designed for aerospace applications encounter a distinctive set of challenges that differentiate them markedly from those used in terrestrial or commercial environments. These antennas must deliver consistent, reliable performance while enduring some of the harshest operational conditions imaginable. For instance, aerospace antennas are exposed to extreme temperature variations that can range from the intense cold of outer space to the high thermal loads encountered during atmospheric re-entry or prolonged sunlight exposure. In addition to temperature extremes, these antennas must withstand significant changes in atmospheric pressure as vehicles ascend to high altitudes, where reduced pressure can impact material properties and structural integrity.

Another critical factor is the exposure to intense mechanical stresses, including high-frequency vibrations and shocks experienced during rocket launches, flight manoeuvres, and landing operations. Such dynamic loads demand antennas that possess not only robust mechanical durability but also electromagnetic stability, ensuring uninterrupted signal transmission and reception under all conditions. Furthermore, aerospace platforms impose strict constraints on size, weight, and power consumption. The aerospace industry's ongoing pursuit of lighter, more fuel-efficient vehicles places immense pressure on antenna designers to develop solutions that are compact and lightweight without compromising on performance or reliability [4].

Historically, aerospace antennas have been fabricated using well-established conventional manufacturing processes such as precision machining, chemical etching, and manual assembly. These methods have provided reliable and repeatable results for many decades, enabling the production of antennas with relatively simple geometries and proven performance. However, as aerospace communication and sensing systems grow in complexity—demanding higher data rates, multi-band operation, conformal designs, and integration with advanced materials—traditional fabrication techniques increasingly struggle to keep pace.

Conventional processes often lack the flexibility to realize complex antenna architectures, such as 3D structures or embedded multifunctional components, and may involve time-consuming steps that limit rapid prototyping and customization. Additionally, limitations in precision and repeatability can hinder the ability to meet tight tolerances necessary for high-frequency and millimeter-wave antennas. These challenges underscore the need for adopting advanced manufacturing technologies that can deliver superior precision, scalability, and integration capabilities, thereby meeting the evolving demands of aerospace applications.

In this context, recent advancements in additive manufacturing, composite fabrication, and hybrid processes offer promising alternatives. These emerging techniques provide enhanced design freedom, enabling the realization of intricate antenna geometries with embedded features and novel materials that are difficult or impossible to achieve through traditional methods. Alongside these manufacturing innovations, the integration of smart materials and the application of artificial intelligence for process control are poised to transform the landscape of aerospace antenna production, ensuring that future antennas are not only more capable but also more adaptable to the stringent requirements of aerospace environments.

The limitations of traditional manufacturing methods include:

1. Geometric constraints that restrict the design of complex antenna structures
2. Material waste and high production costs, especially for low-volume production
3. Limited ability to integrate antennas seamlessly into aerospace structures
4. Challenges in achieving the necessary precision for high-frequency applications

These limitations have spurred the development and adoption of advanced manufacturing techniques specifically tailored to address the unique needs of aerospace antenna production [5].

2.1 Objectives of the Review

This comprehensive review aims to provide a thorough examination of the state-of-the-art in advanced manufacturing techniques for aerospace antennas. The primary objectives of this chapter are:

1. To elucidate the fundamental requirements and challenges specific to aerospace antenna manufacturing
2. To explore and analyse various advanced manufacturing techniques currently employed in the production of aerospace antennas
3. To assess the advantages, limitations, and potential applications of each manufacturing technique
4. To highlight recent research findings and case studies that demonstrate the efficacy of these advanced techniques
5. To identify emerging trends and future directions in aerospace antenna manufacturing

By addressing these objectives, this review seeks to offer valuable insights to researchers, engineers, and industry professionals involved in the design and production of aerospace antennas.

2.2 Scope of the Review

The scope of this review encompasses a wide range of advanced manufacturing techniques applicable to aerospace antenna production. These include, but are not limited to:

1. Various 3D printing technologies such as stereolithography (SLA), fused deposition modelling (FDM), and selective laser sintering (SLS) are examined for their potential in creating complex antenna geometries with high precision [6].
2. Advanced machining techniques, including computer numerical control (CNC) milling, laser cutting, and microfabrication, are explored for their role in achieving the tight tolerances required for high-frequency antennas [7].
3. The use of advanced composites, such as carbon fiber-reinforced polymers (CFRP) and ceramic matrix composites, is investigated for their potential to create lightweight, durable antennas with excellent thermal and mechanical properties [8].
4. Methods for seamlessly integrating antennas into aerospace structures, including conformal and embedded antenna designs, are discussed [9].
5. The review also touches upon cutting-edge developments such as the use of smart materials, hybrid manufacturing processes, and nanotechnology in antenna fabrication [10].

2.3 Significance of Advanced Manufacturing in Aerospace Antenna Development

The adoption of advanced manufacturing techniques in aerospace antenna production has far-reaching implications for the industry. These techniques offer several significant advantages:

1. Advanced manufacturing methods, particularly additive manufacturing, allow for the creation of complex geometries that were previously impossible or impractical to produce. This expanded design space enables engineers to optimize antenna performance without being constrained by traditional manufacturing limitations.
2. The ability to fabricate intricate structures with high precision translates to antennas with superior electromagnetic performance, including enhanced gain, bandwidth, and efficiency.

3. Advanced techniques facilitate the production of lightweight antennas through the use of novel materials and optimized structures, contributing to the overall goal of reducing aircraft weight and improving fuel efficiency.
4. While initial investment in advanced manufacturing equipment may be high, these techniques often lead to reduced material waste, faster production times, and lower costs for low-volume or customized production runs.
5. Many advanced manufacturing techniques, especially 3D printing, allow for quick prototyping and testing of new antenna designs, accelerating the development cycle and fostering innovation.
6. Advanced manufacturing enables the seamless integration of antennas into aerospace structures, potentially improving aerodynamics and structural integrity while maintaining optimal antenna performance.

2.4 Challenges and Considerations

Despite the numerous advantages, the adoption of advanced manufacturing techniques for aerospace antennas is not without challenges. Some key considerations include:

1. Ensuring that materials used in advanced manufacturing processes possess the necessary electromagnetic, thermal, and mechanical properties for aerospace applications.
2. Developing robust quality control processes to ensure consistency and reliability in antenna production, especially for safety-critical applications.
3. Navigating the complex landscape of aerospace certification requirements and establishing industry standards for advanced manufacturing processes.
4. Addressing the challenges of scaling advanced manufacturing techniques from prototyping to large-scale production.
5. Training and developing a workforce skilled in both antenna design and advanced manufacturing techniques.

By addressing these challenges and leveraging the potential of advanced manufacturing techniques, the aerospace industry can continue to push the boundaries of antenna performance and integration, leading to more capable and efficient aerospace systems.

This paper aims to provide a comprehensive understanding of these advanced manufacturing techniques, their applications, and their potential impact on the future of aerospace antenna development. Through a detailed examination of current practices, research findings, and emerging trends, this chapter serves as a valuable resource for those seeking to navigate the rapidly evolving landscape of aerospace antenna manufacturing.

3. Fundamental Requirements for Aerospace Antennas

Aerospace antennas must meet stringent requirements to function effectively in the harsh environments encountered during flight and space operations. This section outlines the key requirements for aerospace antennas, focusing on mechanical robustness, thermal stability, and electromagnetic performance.

3.1 Mechanical Robustness

Aerospace antennas are subjected to extreme mechanical stresses throughout their operational lifecycle, particularly during launch, atmospheric flight, and in-orbit manoeuvres. To ensure long-term functionality and signal integrity, these antennas must be designed to meet stringent mechanical robustness criteria. The primary mechanical requirements include:

3.1.1 Vibration Resistance

During launch and flight, aerospace structures experience high-frequency and high-amplitude vibrations generated by engines, aerodynamic forces, and structural resonances. Antennas must be able to maintain both their structural integrity and electromagnetic performance under these conditions. Improper vibration handling can lead to material fatigue, misalignment, or even structural failure. Materials and joint designs are often tested using random and sinusoidal vibration profiles to simulate real-world launch environments [2].

3.1.2 Shock Resistance

Launch vehicles and satellite deployment mechanisms can subject antennas to sudden and intense mechanical shocks. These shocks may occur due to stage separation, pyrotechnic events, or unanticipated impacts. Shock resistance ensures the antenna can endure these abrupt accelerations and decelerations without experiencing mechanical damage or loss in performance [4].

3.1.3 Structural Integrity

Antennas must retain their structural geometry and alignment under various loading conditions, including aerodynamic forces, g-loads during manoeuvres, and thermally induced stresses. Structural deformations can affect antenna beam patterns, gain, and polarization characteristics. Therefore, maintaining structural integrity is essential for ensuring consistent communication performance and pointing accuracy [5]. The mechanical requirements for aerospace antenna is given in Table 1.

Table 1. Mechanical Requirements for Aerospace Antennas

Requirement	Typical Value	Description
Vibration	20-2000 Hz	Random vibration profile
Shock	100-10,000 g	Pyrotechnic shock
Load	Up to 20 g	Sustained acceleration

Note: Values may vary depending on specific mission requirements.

3.2 Thermal Stability

Aerospace antennas are routinely exposed to extreme and rapidly changing temperatures, both in the atmosphere and in space. These variations can significantly affect the physical and electrical properties of antenna materials, potentially degrading performance. To ensure reliability and accuracy, aerospace antennas must meet stringent thermal stability requirements. These include:

3.2.1 Temperature Range

Antennas must remain operational and maintain performance across a wide temperature spectrum. In aerospace applications, this range typically spans from −65°C to +150°C, depending on mission parameters and altitude. Materials used in antenna structures and components must retain their electrical and mechanical properties across this entire range. Extreme cold can make materials brittle, while high heat may cause warping or melting if not properly managed [7].

3.2.2 Thermal Cycling Resistance

Spacecraft and high-altitude vehicles often experience repeated cycles of heating and cooling—such as during orbital day/night transitions or re-entry phases. Antennas must endure thermal cycling without experiencing material fatigue, delamination, or loss of adhesion. These cycles can induce microcracks or degrade material interfaces, ultimately impacting antenna alignment and RF performance [8].

3.2.3 Thermal Expansion Control

Changes in temperature lead to expansion and contraction of materials. In high-precision antenna systems, even slight dimensional changes can distort the antenna's geometry, causing misalignment of beams or degradation in radiation patterns. Antennas must therefore be designed with low coefficients of thermal expansion (CTE) or incorporate composite materials that compensate for differential expansion [9]. Table 2 outlines the typical thermal requirements for aerospace antennas:

Table 2. Thermal Requirements for Aerospace Antennas

Requirement	Typical Value	Description
Temperature Range	-65°C to +150°C	Operational temperature
Thermal Cycling	>1000 cycles	-55°C to +125°C
Coefficient of Thermal Expansion	<5 ppm/°C	For dimensional stability

3.3 Electromagnetic Performance

The core function of aerospace antennas is the reliable transmission and reception of electromagnetic signals. In space and aerospace environments, where communication links must span vast distances and endure harsh conditions, antennas must demonstrate exceptional electromagnetic performance. This ensures not only signal clarity and reliability but also efficient use of limited onboard power resources. Key performance parameters include:

3.3.1 Frequency Range

Aerospace antennas must operate within specific frequency bands tailored to their mission objectives, such as S-band, X-band, Ku-band, or Ka-band. Many modern systems also require multiband or wideband operation to support various communication, telemetry, and navigation functions simultaneously. Precise frequency control is critical to avoid interference and meet regulatory standards [10].

3.3.2 Gain and Directivity

High gain antennas concentrate energy in a specific direction, which is vital for long-range space communication, such as satellite-to-ground or inter-satellite links. Directivity ensures that energy is radiated or received primarily in the desired direction, minimizing losses and improving signal strength. Parabolic reflectors, phased arrays, and high-gain horn antennas are commonly used to achieve these characteristics [6].

3.3.3 Polarization

To ensure efficient signal transmission and reception, antennas must maintain proper polarization—typically linear, circular, or dual-polarized—depending on the application. Matching the polarization between the transmitting and receiving antennas reduces signal loss due to polarization mismatch and improves link quality, especially in multipath or rotating platforms [11].

3.3.4 Efficiency

Antenna efficiency measures how effectively input power is converted into radiated energy. High efficiency is particularly important in aerospace systems, where available power is limited. Losses due to dielectric materials, impedance mismatches, or surface roughness must be minimized to ensure that most of the transmitted power reaches its destination. Table 3 presents typical electromagnetic performance requirements for aerospace antennas:

Table 3. Electromagnetic Performance Requirements for Aerospace Antennas

Requirement	Typical Value	Description
Frequency Range	1-40 GHz	Varies by application
Gain	>10 dBi	For directional antennas
Polarization	Circular or Linear	Mission-dependent
Efficiency	>80%	At operating frequency

3.3.5 Radiation pattern

The radiation pattern of an aerospace antenna must be carefully controlled to ensure optimal coverage and minimize interference. Depending on the application, antennas may require highly directional patterns for point-to-point communications or more omnidirectional patterns for broader coverage [2].

3.3.6 Bandwidth

Aerospace antennas often need to operate over wide frequency ranges to support multiple communication systems or to provide flexibility in operational frequencies. Wideband or multi-band performance is crucial for many aerospace applications [4].

3.3.7 Phase stability

For applications such as phased array antennas or interferometric systems, maintaining phase stability across temperature variations and mechanical stresses is critical [7]. Table 4 presents additional electromagnetic performance requirements for aerospace antennas:

Table 4. Additional Electromagnetic Performance Requirements for Aerospace Antennas

Requirement	Typical Value	Description
Radiation Pattern	Mission-specific	Directional or omnidirectional
Bandwidth	10-30%	Percentage of center frequency
Phase Stability	< 5° variation	Over operational temperature range

3.4 Environmental Resistance

In addition to mechanical and thermal challenges, aerospace antennas are exposed to a variety of environmental hazards that can compromise their performance and reliability. Whether operating in the upper atmosphere or in the harsh conditions of space, antennas must be engineered to resist degradation caused by radiation, vacuum exposure, and corrosive environments. Ensuring environmental resistance is essential for long-term mission success and minimizing maintenance or replacement needs.

3.4.1 Radiation Hardness

Antennas deployed in space are exposed to ionizing radiation from cosmic rays, solar flares, and trapped particle belts. This radiation can deteriorate dielectric materials, reduce conductivity in metallic elements, and damage embedded electronics. Radiation-hardened materials and coatings are therefore used to ensure long-term functionality, particularly in geostationary or deep-space missions [5].

3.4.2 Vacuum Compatibility

In the vacuum of space, materials must not outgas volatile substances, which can condense on sensitive components and impair performance. Additionally, the absence of atmospheric pressure and the presence of extreme temperature differentials can cause material embrittlement or delamination. Antennas must be manufactured using vacuum-rated adhesives, composites, and structural materials that remain stable and non-reactive under such conditions [8].

3.4.3 Corrosion Resistance

For aerospace antennas operating within Earth's atmosphere—particularly on aircraft—corrosion resistance is critical. Exposure to moisture, salt-laden air, UV radiation, and pollutants can lead to oxidation, pitting, or structural weakening. Protective surface treatments, such as anodizing, plating, or the use of corrosion-resistant alloys, help extend the service life of these systems [9]. Table 5 presents additional electromagnetic resistance requirements for aerospace antennas:

Table 5. Environmental Resistance Requirements for Aerospace Antennas

Requirement	Typical Value	Description
Radiation Tolerance	Up to 100 krad	Total Ionizing Dose (TID)
Outgassing	<1% TML, <0.1% CVCM	As per ASTM E595
Corrosion Resistance	1000+ hours salt spray	As per ASTM B117

Note: TML = Total Mass Loss, CVCM = Collected Volatile Condensable Material

3.5 Size and Weight Constraints

In aerospace systems, antenna size and weight are critical design parameters that influence overall vehicle performance, structural design, fuel efficiency, and payload capacity. Because launch and flight systems operate under strict mass and volume limitations, antenna technologies must evolve to meet these constraints without sacrificing electromagnetic performance. Key considerations include:

3.5.1 Miniaturization

There is an ongoing push toward the miniaturization of antenna systems, especially in small satellites (CubeSats), UAVs, and compact spacecraft. Designers aim to reduce physical dimensions while maintaining acceptable gain, bandwidth, and efficiency. This often requires the use of novel antenna configurations (e.g., fractal, patch, and metamaterial-based designs) and high-permittivity substrates to compress the wavelength and reduce footprint [10].

3.5.2 Weight Reduction

Reducing the mass of antennas contributes significantly to fuel savings, improved manoeuvrability, and increased payload capacity**.** Weight reduction is especially crucial in launch vehicles and long-endurance aircraft. The use of lightweight composite materials**,** additive manufacturing (3D printing)**,** and thin-film technologies has enabled the production of high-performance antennas with minimal mass [6].

3.5.3 Integration with Structures

Modern aerospace systems increasingly rely on conformal and embedded antennas**,** which are integrated directly into the surface of airframes, fuselages, or satellite panels. This structural integration reduces aerodynamic drag, frees up internal volume, and enhances stealth in military applications. Materials such as flexible printed circuits and multifunctional composites enable these embedded solutions while preserving RF performance [11]. Table 6 outlines typical size and weight constraints for aerospace antennas:

Table 6. Size and Weight Constraints for Aerospace Antennas

Constraint	Typical Value	Description
Size	Application-specific	Often limited by available space
Weight	<1 kg/m^2	For planar array antennas
Integration	Conformal or embedded	Structural integration techniques

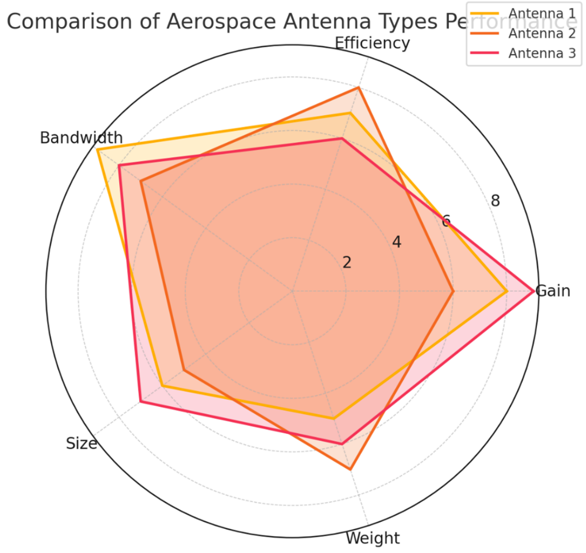

Figure 1. A spider chart comparing the performance characteristics (gain, efficiency, bandwidth, size, weight) of different aerospace antenna types.

A spider chart illustrating the comparative performance characteristics of various aerospace antenna types is presented in Figure 1. This visual representation highlights key parameters including gain, efficiency, bandwidth, size, and weight, enabling a clear assessment of trade-offs and strengths associated with each antenna type. By mapping these attributes on a unified scale, the chart facilitates a quick comparison of how different designs such as parabolic reflectors, patch antennas, helical antennas, and phased arrays perform relative to one another across critical performance metrics.

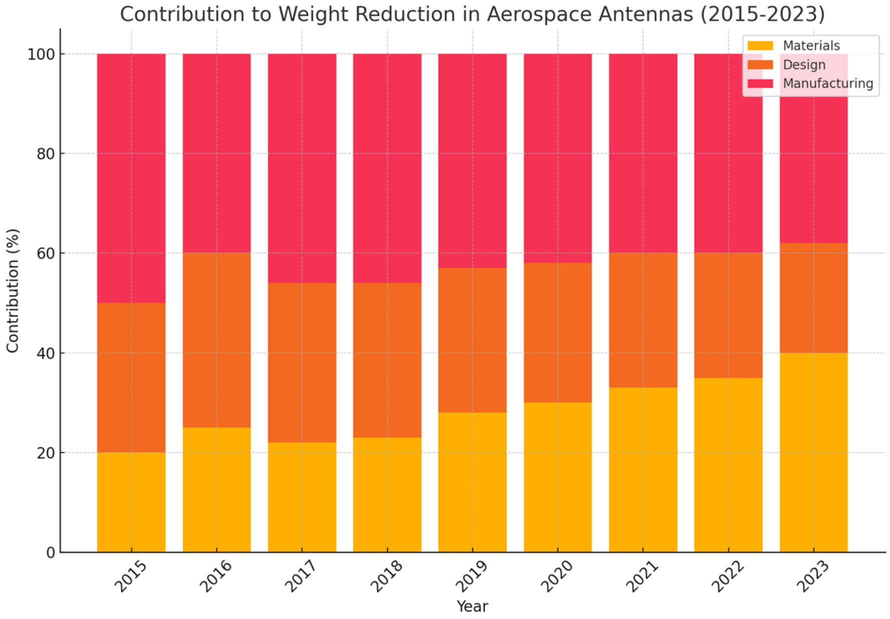

Figure 2. The contribution of various factors (materials, design, manufacturing technique) to the overall weight reduction in aerospace antennas over time

A stacked bar chart is presented in Figure 2 to illustrate the relative contributions of key factors—namely materials, design innovations, and manufacturing techniques—to the overall weight reduction of aerospace antennas over time. This visualization captures the evolving impact of each factor across different technological generations, highlighting how advancements such as lightweight composite materials, optimized structural designs, and additive manufacturing have collectively contributed to achieving significant mass savings in modern antenna systems.

In this section, we have provided a comprehensive overview of the fundamental requirements for aerospace antennas, covering mechanical robustness, thermal stability, electromagnetic performance, environmental resistance, and size and weight constraints. These requirements form the foundation for the advanced manufacturing techniques discussed in subsequent sections of this review.

3.6 Additive Manufacturing Techniques for Aerospace Antennas

Additive manufacturing (AM) has revolutionized the production of aerospace antennas, offering unprecedented design flexibility, material efficiency, and the ability to create complex geometries. This section explores the various AM techniques used in aerospace antenna fabrication, their advantages, and limitations.

3.6.1 Stereolithography (SLA)

Stereolithography (SLA) is one of the earliest and most established AM technologies, widely adopted in the aerospace industry for producing high-precision components—including parts for antenna systems. Its capability to fabricate complex geometries with fine detail makes it particularly advantageous for RF and antenna applications.

3.6.1.1 Process Overview

SLA operates by using an ultraviolet (UV) laser to selectively cure and solidify layers of liquid photopolymer resin, following the contours defined in a 3D CAD model. Each cured layer adheres to the previous one, gradually building up the final part with high resolution and surface quality. This layer-by-layer approach enables the creation of components with sub-millimeter features and smooth surfaces, which are essential in high-frequency antenna systems [7].

3.6.1.2 Applications in Aerospace Antennas

SLA is especially valuable for producing dielectric components of antennas, such as substrates, radomes, dielectric resonator elements, and supporting structures. The technique's high dimensional accuracy allows for the production of non-standard or miniaturized antenna geometries, including those used in conformal and embedded systems. These complex forms are often difficult or impractical to fabricate using conventional subtractive manufacturing methods. In addition, SLA supports rapid prototyping, accelerating the development cycle of aerospace antenna designs by enabling quick iteration and testing. Table 7 presents the Advantages and Limitations of SLA for Aerospace Antenna Fabrication.

Table 7. Advantages and Limitations of SLA for Aerospace Antenna Fabrication

Advantages	Limitations
High resolution (up to 25 microns)	Limited material options
Smooth surface finish	Post-curing required
Complex geometries possible	Relatively slow process
Good dimensional accuracy	Potential for warping during curing

3.6.2 Fused Deposition Modelling (FDM)

FDM is one of the most widely used and accessible AM techniques. Its affordability, material versatility, and ease of use have made it a popular choice for both prototyping and limited-scale production of aerospace components, including antenna systems.

3.6.2.1 Process Overview

FDM builds parts by extruding thermoplastic filaments through a heated nozzle, which deposits material layer by layer according to a digital model. As each layer is deposited, it cools and solidifies, gradually forming the complete structure. The process supports a wide range of materials, including standard thermoplastics (like ABS and PLA) and specialized filaments with properties such as electrical conductivity, thermal resistance, and mechanical strength [4].

3.6.2.2 Applications in Aerospace Antennas

FDM is widely used in the development of aerospace antennas for fabricating substrates, structural housings, and even radiating or ground plane elements when using conductive or metallized filaments. Although FDM generally offers lower resolution than techniques like SLA, its cost-effectiveness and material diversity make it ideal for rapid prototyping, functional testing, and low-volume production. Furthermore, its capability to print with composite materials (e.g., carbon-fiber reinforced polymers) can improve the mechanical and thermal properties of antenna components for aerospace use. A comparison of material used in aerospace antenna is provided in Table 8.

Table 8. Comparison of Materials Used in FDM for Aerospace Antennas

Material	Dielectric Constant	Loss Tangent	Thermal Stability
ABS	2.3-2.8	0.005-0.01	Moderate
PLA	3.0-3.5	0.01-0.02	Low
PEEK	3.2-3.4	0.002-0.004	High
Conductive PLA	Variable	Variable	Low

3.6.3 Selective Laser Sintering (SLS)

SLS is a powerful AM technique that offers significant advantages for the fabrication of aerospace antennas, particularly where complex geometries, structural strength, and material flexibility are critical. Unlike other AM methods, SLS enables the direct production of high-performance components with minimal post-processing.

3.6.3.1 Process Overview

SLS works by using a high-power laser to selectively sinter powdered materials—typically thermoplastics or metals—into solid layers based on a digital 3D model. The laser fuses the powder particles together, layer by layer, without the need for external support structures, as the surrounding unsintered powder acts as a natural support during the build process [5]. This allows for the creation of complex internal features, lightweight lattices, and topology-optimized designs that are difficult or impossible to manufacture with traditional methods.

3.6.3.2 Applications in Aerospace Antennas

In aerospace antenna development, SLS is particularly suited for producing structurally robust and lightweight components, such as antenna housings, substrates, and mounts. Its compatibility with nylon-based polymers (e.g., PA12) provides durability and thermal stability, while metal powder variants, such as aluminium or stainless steel, enable the direct fabrication of metallic antenna elements and RF structures. This reduces the need for complex assemblies, improves alignment accuracy, and enhances overall antenna performance. Additionally, the ability to manufacture integrated components helps reduce weight and volume—key factors in aerospace systems. The Key Parameters for SLS in Aerospace Antenna Fabrication are presented in Table 9.

Table 9. Key Parameters for SLS in Aerospace Antenna Fabrication

Parameter	Typical Range	Impact on Antenna Performance
Layer Thickness	0.06-0.15 mm	Affects surface roughness and dimensional accuracy
Laser Power	10-200 W	Influences material sintering and mechanical properties
Scan Speed	0.5-2.5 m/s	Affects build time and material properties
Powder Particle Size	20-100 μm	Impacts surface finish and minimum feature size

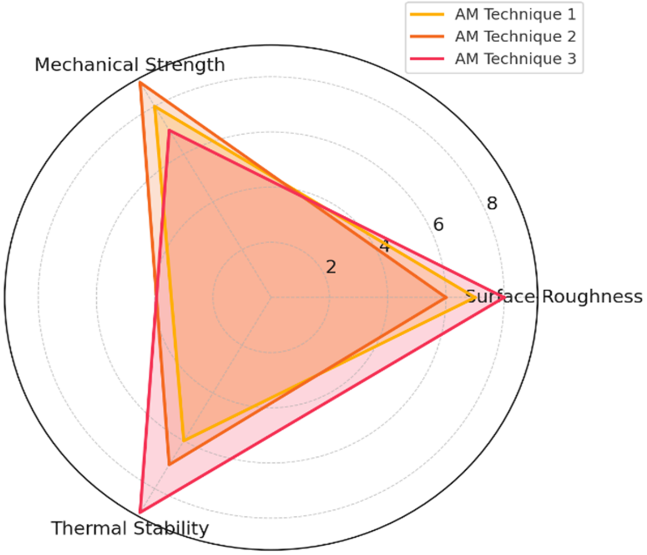

Figure 3. A radar chart comparing key performance metrics (surface roughness, mechanical strength, and thermal stability) of antennas produced by different additive manufacturing (AM) techniques

Figure 3 presents a radar chart comparing key performance metrics of antennas fabricated using different AM techniques, including SLA, FDM, and SLS. The chart evaluates and contrasts surface roughness, mechanical strength, and thermal stability, offering a visual representation of the trade-offs and strengths associated with each method. This comparison helps identify the most suitable AM approach based on specific performance requirements for aerospace antenna applications.

These AM techniques have significantly expanded the design possibilities for aerospace antennas, enabling the creation of lightweight, high-performance structures that were previously impossible or impractical to manufacture. As the technology continues to evolve, we can expect further improvements in material properties, printing resolution, and production speed, leading to even more innovative aerospace antenna designs.

3.7 Precision Machining Techniques for Aerospace Antennas

Precision machining techniques play a vital role in the fabrication of aerospace antennas, where high dimensional accuracy, fine surface finish, and geometric consistency are critical. These characteristics directly influence the electromagnetic performance, particularly in high-frequency and high-gain applications, where even slight deviations in geometry or surface quality can result in signal loss, reflection, or beam distortion. Precision machining supports the manufacturing of metallic and dielectric components that must adhere to strict aerospace specifications for reliability and performance. This section explores key precision machining methods used in aerospace antenna production, starting with CNC milling.

3.7.1 CNC Milling

Computer Numerical Control (CNC) milling is a widely used subtractive manufacturing process in aerospace antenna fabrication due to its versatility, precision, and repeatability.

3.7.1.1 Process Overview

CNC milling involves the use of computer-programmed cutting tools that move along multiple axes to remove material from a solid block (workpiece). The digital control system interprets 3D CAD models and executes complex tool paths with high speed and accuracy. This process enables the creation of precise, repeatable components with tight dimensional tolerances and smooth surface finishes [7].

3.7.1.2 Applications in Aerospace Antennas

In the aerospace sector, CNC milling is particularly effective for fabricating high-frequency antenna components such as,

- Feed horns
- Waveguides
- Slot antennas
- Mounting brackets
- Reflector elements

These components require precise internal and external geometries, often involving curved surfaces or critical alignment features. CNC milling can achieve tolerances on the order of microns, making it ideal for parts where even minimal dimensional error could degrade RF performance. Moreover, it supports the use of aerospace-grade materials like aluminium alloys, titanium, and copper, which offer excellent mechanical and electrical properties. The key parameters for CNC milling are summarize in Table 10.

Table 10. Key Parameters for CNC Milling in Aerospace Antenna Fabrication

Parameter	Typical Range	Impact on Antenna Performance
Spindle Speed	1,000-30,000 RPM	Affects surface finish and machining time
Feed Rate	0.1-1000 mm/min	Influences dimensional accuracy and tool wear
Cutting Depth	0.1-5 mm	Impacts surface quality and machining efficiency
Tool Diameter	0.1-25 mm	Determines minimum feature size and complexity

3.7.2 Laser Cutting

Laser cutting is a highly precise and versatile manufacturing process widely used in aerospace antenna fabrication, particularly for producing intricate features in sheet metal components. Its ability to deliver fine, accurate cuts with minimal thermal distortion makes it ideal for applications where precision and material integrity are paramount.

3.7.2.1 Process Overview

Laser cutting employs a focused, high-energy laser beam **to** melt, burn, or vaporize targeted areas of material. The process is typically guided by a computer numerical control (CNC) system, which interprets digital design files to execute exact cutting paths with high speed and repeatability. Because the laser can be finely tuned, laser cutting minimizes material waste and allows for extremely tight tolerances and sharp edge definitions, even on thin and delicate materials [6].

3.7.2.2 Applications in Aerospace Antennas

In the context of aerospace antennas, laser cutting is especially effective for fabricating:

- Radiating elements (e.g., dipoles, slots, spirals)
- Ground planes and backing plates
- Reflector panels for parabolic and planar antennas
- Mounting brackets and support frames

The process excels in producing complex geometries and fine features in thin metal sheets (such as aluminium, copper, or stainless steel), which are often required in high-frequency antenna designs. Additionally, laser cutting supports rapid prototyping and low- to mid-volume production, making it a practical choice for both development and deployment phases in aerospace applications. The pros and cons of the laser cutting is provided in Table 11.

Table 11. Advantages and Limitations of Laser Cutting for Aerospace Antennas

Advantages	Limitations
High precision (±0.1 mm)	Limited material thickness (typically <25 mm)
Minimal material distortion	Potential for heat-affected zones
Complex shape capabilities	Higher cost for thick materials
Fast processing speed	Limited to flat or slightly curved surfaces

3.7.3 Microfabrication

Microfabrication techniques are essential for producing miniaturized antenna components and high-frequency structures, enabling the realization of compact, lightweight, and highly efficient designs that are critical for aerospace applications. These methods allow engineers to translate complex antenna geometries into practical hardware with the precision required for operation in challenging environments.

3.7.3.1 Process Overview

Microfabrication encompasses a suite of advanced processes such as photolithography, etching, thin-film deposition, and surface micromachining. Photolithography provides the capability to define antenna patterns at the micro- and nanoscale with exceptional accuracy, while etching (both wet and dry) is used to selectively remove material to achieve desired geometrical features. Thin-film deposition techniques—including sputtering, evaporation, and chemical vapor deposition—enable the formation of conductive, dielectric, or magnetic layers that are fundamental for antenna performance. Together, these processes allow for the fabrication of extremely small and precise antenna structures that can operate efficiently at millimeter-wave and terahertz frequencies [12].

3.7.3.2 Applications in Aerospace Antennas

In aerospace systems, microfabrication is particularly valuable for designing and producing antennas where size, weight, and performance must be carefully optimized. This includes millimeter-wave and terahertz antennas used for high-data-rate satellite communications, radar imaging, and deep-space exploration. Furthermore, microfabrication plays a critical role in developing MEMS-based reconfigurable antennas, which can dynamically adjust their frequency, polarization, or radiation patterns in response to mission requirements. It also supports the integration of antenna arrays with other electronic subsystems, allowing for seamless packaging and enhanced performance in compact aerospace platforms. By leveraging microfabrication, aerospace engineers can create antenna systems that are not only efficient but also highly scalable and compatible with modern miniaturized electronics. Table 12 presents an overview of the key microfabrication techniques used in aerospace antennas, highlighting their processes, advantages, and application domains.

Table 12. Microfabrication Techniques for Aerospace Antennas

Technique	Resolution	Applications
Photolithography	Down to 0.5 μm	Planar antenna patterns, transmission lines
Reactive Ion Etching	10-100 nm	3D antenna structures, waveguides
E-beam Lithography	<10 nm	Nanoantenna structures, metamaterials
Thin-film Deposition	1-1000 nm	Conductive and dielectric layers

3.7.4 Challenges in Precision Machining

While precision machining provides distinct advantages in the fabrication of aerospace antennas—such as high dimensional accuracy and superior surface finish—it also introduces several challenges that must be carefully addressed to ensure reliable performance under demanding operational conditions. These challenges primarily arise from the interaction between advanced machining processes, the unique material requirements of aerospace systems, and the high-performance specifications of antenna structures.

3.7.4.1 Tool Wear and Thermal Effects

One of the most critical issues in precision machining is tool wear, which directly influences both dimensional accuracy and surface integrity. Excessive tool wear can lead to deviations in antenna geometry, negatively impacting resonance frequency, impedance matching, and radiation characteristics. Additionally, thermal effects generated during high-speed machining or prolonged tool–workpiece contact can cause localized heating. This thermal accumulation may induce distortions, residual stresses, or microstructural changes in the antenna substrate, potentially degrading its electrical and mechanical performance. To address these challenges, researchers and practitioners employ advanced tool materials such as polycrystalline diamond (PCD) or cubic boron nitride (CBN), along with optimized cutting parameters and high-efficiency cooling/lubrication strategies [13]. These approaches significantly reduce tool wear rates, improve heat dissipation, and enhance the consistency of machined features.

3.7.4.2 Material Considerations

Aerospace antennas often utilize specialized materials to meet requirements of lightweight design, high electrical conductivity, and resistance to harsh environments such as extreme temperatures, vibration, and radiation. Common materials include titanium alloys, aluminum composites, ceramic-based substrates, and advanced polymers. However, these materials frequently pose machinability challenges—titanium alloys exhibit low thermal conductivity and high hardness, while ceramics are brittle and prone to cracking under mechanical stress. Such difficulties necessitate tailored machining strategies, including the use of ultra-precision diamond turning, hybrid machining techniques (e.g., laser-assisted machining), and adaptive process control systems. These methods help maintain the balance between machinability, antenna performance, and long-term durability.

Table 13 summarizes the various strategies employed to overcome precision machining challenges in aerospace antenna fabrication, outlining their advantages and applicability across different material classes and machining scenarios.

Table 13. Strategies for Addressing Precision Machining Challenges

Challenge	Strategy	Benefit
Tool Wear	Use of advanced coatings (e.g., TiAlN)	Extended tool life, improved surface finish
Thermal Effects	Implementation of cryogenic cooling	Reduced thermal distortion, enhanced accuracy
Material Hardness	Ultrasonic-assisted machining	Improved machinability of hard materials
Surface Integrity	Optimized cutting parameters	Enhanced electromagnetic performance

Precision machining techniques continue to evolve, driven by the increasing demands of aerospace antenna applications. Future developments are likely to focus on enhancing precision, reducing manufacturing time, and expanding the range of machinable materials. Integration with other advanced manufacturing techniques, such as additive manufacturing, may lead to hybrid processes that combine the strengths of multiple fabrication methods.

3.8 Composite Material Fabrication for Aerospace Antennas

Composite materials have revolutionized the design and manufacturing of aerospace antennas by offering a unique combination of low weight, high mechanical strength, and customizable electromagnetic properties. Unlike traditional metallic structures, composites can be engineered at the material and structural levels to optimize both mechanical performance and radio-frequency (RF) characteristics. This flexibility makes them highly suitable for next-generation aerospace systems, where strict requirements for weight reduction, durability, and multifunctionality must be met simultaneously. This section discusses the use of advanced composites in antenna construction, their benefits, and fabrication strategies.

3.8.1 Advanced Composites in Antenna Construction

The adoption of advanced composites in aerospace antenna fabrication has accelerated due to their superior mechanical, thermal, and electrical properties compared to conventional materials such as aluminum or copper. Their lightweight nature directly contributes to reduced payload mass in satellites and aircraft, improving overall fuel efficiency and mission performance. Moreover, composite materials allow for integration of structural and electromagnetic functionality, enabling antennas to be embedded within load-bearing surfaces without compromising performance.

3.8.2 Carbon Fiber-Reinforced Polymers (CFRP)

Carbon Fiber-Reinforced Polymers (CFRPs) are among the most widely employed composites in aerospace antennas. CFRPs combine carbon fibers, known for their high tensile strength and low density, with polymer matrices that provide toughness and environmental resistance. Beyond their structural advantages, CFRPs offer tunable electromagnetic characteristics by adjusting fiber orientation, volume fraction, or resin composition. This makes them particularly valuable for lightweight reflector antennas, radomes, and conformal antenna arrays. Additionally, CFRPs are compatible with various fabrication methods such as filament winding, resin transfer molding, and automated fiber placement, supporting scalable production with high precision.

3.8.3 Ceramic Matrix Composites (CMC)

Ceramic Matrix Composites (CMCs) represent another important class of materials for aerospace antennas, particularly in high-temperature and high-frequency environments. CMCs are composed of ceramic fibers embedded within a ceramic matrix, offering exceptional thermal stability, low dielectric loss, and resistance to harsh operational conditions. These properties make them suitable for antennas used in supersonic aircraft, re-entry vehicles, and deep-space probes, where structural integrity must be maintained under extreme thermal loads. In addition, their electrical properties can be engineered to reduce RF losses, improving antenna efficiency at millimeter-wave and terahertz frequencies.

Table 14 presents the key properties of advanced composites used in aerospace antennas, highlighting their mechanical performance, electromagnetic characteristics, and application domains.

Table 14. Properties of Advanced Composites Used in Aerospace Antennas

Composite Material	Density (g/cm^3)	Tensile Strength (MPa)	Dielectric Constant	Loss Tangent
CFRP	1.5-1.6	600-3000	2.5-6.0	0.001-0.005
CMC	2.0-3.5	200-1000	5.0-10.0	0.0001-0.001
Glass Fiber	1.8-2.0	400-1800	4.0-5.0	0.001-0.01

3.9 Benefits of Composite Materials

Composite materials provide a number of distinct advantages over traditional metallic materials in aerospace antenna applications, making them a preferred choice in modern design and manufacturing. Their unique material properties not only enhance antenna performance but also contribute to overall system reliability and efficiency in demanding aerospace environments.

3.9.1 High Strength-to-Weight Ratio

One of the most significant benefits of composites is their exceptional strength-to-weight ratio. By combining lightweight matrices with high-strength reinforcements such as carbon fibers, composites enable the construction of antennas that are both structurally robust and considerably lighter than their metallic counterparts. This reduction in weight translates directly into improved fuel efficiency, increased payload capacity, and overall performance benefits for aircraft and spacecraft systems.

3.9.2 Corrosion Resistance

Unlike metals, composites exhibit excellent resistance to corrosion and degradation when exposed to harsh aerospace environments, including high humidity, salt-laden atmospheres, and varying radiation levels. This property enhances the operational lifespan of antennas, reducing maintenance costs and ensuring consistent performance throughout extended missions.

3.9.3 Thermal Stability

Advanced composites, particularly Ceramic Matrix Composites (CMCs), demonstrate outstanding thermal stability across a broad range of operating temperatures. This makes them particularly well-suited for antennas used in extreme environments such as high-speed aircraft, space vehicles, and re-entry systems, where components are subjected to rapid heating and cooling cycles. Their ability to retain structural and electromagnetic properties under these conditions ensures both durability and reliability of communication and sensing functions.

Table 15 presents the summarized advantages of composite materials in aerospace antenna applications, highlighting their role in achieving lightweight, durable, and thermally resilient designs.

Table 15. Advantages of Composite Materials in Aerospace Antenna Applications

Advantage	Description	Impact on Antenna Performance
Weight Reduction	Up to 50% lighter than metal equivalents	Improved fuel efficiency, increased payload capacity
Design Flexibility	Ability to create complex shapes	Enhanced antenna efficiency and directivity
Thermal Expansion Control	Low coefficient of thermal expansion	Improved dimensional stability in space environments
EMI Shielding	Tailorable electromagnetic properties	Better control of antenna radiation patterns

3.10 Fabrication Techniques

The fabrication of composite antennas for aerospace applications requires advanced manufacturing methods capable of producing lightweight, mechanically robust, and electromagnetically optimized structures. Several fabrication techniques have been developed to meet these requirements, each offering distinct advantages in terms of structural performance, design flexibility, and production scalability.

3.10.1 Autoclave Moulding

Autoclave moulding remains one of the most widely adopted techniques for producing high-performance composite antenna structures. In this process, prepreg (pre-impregnated) composite materials are placed into a mould and subjected to elevated temperature and pressure within an autoclave. The controlled curing environment ensures excellent consolidation, low void content, and high structural integrity, making this method particularly suitable for critical aerospace applications where reliability and performance are paramount.

3.10.2 Resin Transfer Moulding (RTM)

Resin Transfer Moulding is a versatile fabrication method that enables the production of complex antenna geometries with high dimensional accuracy. In RTM, dry fiber preforms are placed into a closed mould, and resin is injected under pressure to impregnate the fibers. This technique offers advantages such as high fiber volume fractions, consistent quality, and smooth surface finish, which are crucial for achieving the desired electromagnetic performance of antennas. RTM also facilitates higher production rates compared to autoclave moulding, making it attractive for applications requiring scalability.

3.10.3 Filament Winding

Filament winding is a highly specialized technique used primarily for fabricating cylindrical or conical antenna structures. Continuous fiber tows, pre-impregnated with resin, are wound under tension onto a rotating mandrel in predetermined patterns. This process allows for precise control over fiber orientation, which directly influences the mechanical strength and electromagnetic properties of the antenna. Filament winding is especially beneficial in applications requiring optimized load-bearing capacity and tailored anisotropy.

Table 16 presents the various composite fabrication techniques employed in aerospace antenna manufacturing, highlighting their advantages and application areas.

Table 16. Composite Fabrication Techniques for Aerospace Antennas

Technique	Advantages	Limitations	Typical Applications
Autoclave Moulding	High quality, low void content	High equipment cost	Reflector antennas, radomes
Resin Transfer Moulding	Complex shapes, good surface finish	Tooling complexity	Conformal antennas, antenna housings
Filament Winding	Precise fiber control, high strength	Limited to symmetrical shapes	Cylindrical array antennas, feed horns

3.11 Application Examples

Composite materials have become integral to modern aerospace antenna systems due to their unique combination of lightweight properties, structural strength, and tailored electromagnetic performance. Their adaptability allows engineers to design antennas that meet the stringent requirements of aerospace platforms, where weight, durability, and performance under extreme conditions are critical.

3.11.1 Reflector Antennas

One of the most prominent applications of composites is in large reflector antennas used for satellite communication and deep-space missions. Carbon Fiber-Reinforced Polymers (CFRPs) are particularly valuable in these structures because of their exceptional dimensional stability, low thermal expansion, and reduced mass compared to metallic alternatives. These properties ensure that reflector surfaces maintain their precise geometrical shape even under harsh thermal cycling in space, resulting in high gain and low signal distortion. By lowering antenna mass, CFRP reflectors also contribute to significant reductions in launch costs and improved payload efficiency.

3.11.2 Conformal Antennas

Composite materials also play a pivotal role in the development of conformal antennas, which are designed to integrate seamlessly with the curved surfaces of aircraft, spacecraft, or unmanned aerial vehicles (UAVs). The use of composites enables antennas to be embedded or mounted flush with the fuselage or wings, enhancing aerodynamics and stealth characteristics while maintaining robust communication capabilities. These antennas are particularly advantageous in military aerospace systems, where minimizing radar cross-section (RCS) without compromising signal quality is essential. Moreover, the electromagnetic tailoring of composites allows for frequency agility and wideband operation, broadening their range of applications.

Table 17 presents representative examples of composite antenna applications in aerospace systems, highlighting how materials such as CFRPs and ceramic matrix composites (CMCs) are leveraged to enhance performance across different antenna types.

Table 17. Examples of Composite Antennas in Aerospace Systems

Antenna Type	Composite Material	Key Performance Characteristics
Satellite Reflector	CFRP	High dimensional stability, low mass, wide temperature range operation
Aircraft Conformal Array	Glass Fiber Composite	Aerodynamic integration, wide bandwidth, low radar cross-section
Radome	Quartz Fiber Composite	Low signal attenuation, high impact resistance, thermal protection

3.11.3 Challenges and Future Directions

Although composite materials provide substantial benefits in aerospace antenna applications, several challenges must be addressed to fully exploit their potential.

3.11.3.1 Manufacturing Complexity

The fabrication of composite-based antennas often involves specialized mouldings, curing, and assembly processes that require high-precision equipment and skilled labour. Techniques such as autoclave mouldings or resin transfer mouldings (RTM) ensure structural integrity but also increase production costs and extend lead times. Furthermore, scaling these processes for large or intricate antenna geometries remains a technical challenge.

3.11.3.2 Electromagnetic Property Control

Another critical challenge lies in achieving consistent and predictable electromagnetic performance across large composite structures. Variations in fiber orientation, resin content, or curing conditions can alter dielectric properties, leading to deviations in antenna performance. Advanced material characterization and multi-physics simulations are therefore essential to accurately model and control these properties during the design and manufacturing phases.

3.11.3.3 Joining and Integration

The integration of composite antenna components with metallic structures, such as aircraft fuselages or satellite mounts, poses additional difficulties. Differences in thermal expansion coefficients, bonding reliability, and mechanical stress distribution must be carefully managed to prevent delamination or signal degradation. Hybrid joining techniques, including advanced adhesives and mechanical fasteners, are under active investigation to enhance structural and electromagnetic compatibility.

3.11.3.4 Future Directions

Ongoing research is exploring several promising avenues to overcome these challenges. Future developments in composite antenna fabrication are likely to focus on:

- **Advanced modelling techniques** that enable precise prediction of structural, thermal, and electromagnetic performance in composite antennas.
- **Novel composite materials**, such as nanocomposites or metamaterial-enhanced composites, designed to improve dielectric uniformity and electromagnetic tunability.
- **Improved manufacturing processes**, including additive manufacturing and out-of-autoclave curing methods, to reduce costs while maintaining high precision.

- **Integration of multifunctionality**, where composite antennas also serve as structural elements with embedded sensing, thermal management, or structural health monitoring capabilities.

As composite technologies advance, their role in next-generation aerospace antennas will expand significantly, enabling lighter, more efficient, and multifunctional systems. These innovations will be critical for supporting the increasing demands of satellite communications, deep-space exploration, and defense applications where performance and reliability are paramount.

3.12 Integration and Assembly Techniques for Aerospace Antennas

The integration and assembly of antennas within aerospace structures pose unique challenges but also offer opportunities to enhance overall system performance, reduce weight, and improve stealth and aerodynamic properties. This section examines advanced techniques for embedding antennas into aerospace platforms, with a particular emphasis on conformal antennas and their manufacturing considerations.

3.12.1 Conformal Antennas

Conformal antennas are engineered to follow the natural contours of aerospace vehicles, such as fuselages, wings, or satellite bodies. Unlike traditional protruding antennas, conformal designs minimize drag, improve stealth characteristics by reducing radar cross-section (RCS), and enable seamless integration with structural surfaces. Their ability to blend into the host platform makes them especially valuable in modern military and high-performance aerospace systems.

3.12.2 Manufacturing Methods for Curved Surfaces

Fabricating antennas that can accurately conform to curved or complex surfaces requires advanced manufacturing approaches. Flexible printed circuit board (PCB) fabrication is a common technique, allowing antenna elements to be deposited onto bendable substrates that adhere to the vehicle’s geometry. Composite layup techniques, where conductive materials are embedded within or on top of composite laminates, offer structural reinforcement along with electromagnetic functionality. Additionally, advanced additive manufacturing (3D printing) enables the creation of intricate curved antenna geometries with high precision and reduced material waste, supporting lightweight designs while maintaining electrical performance.

3.12.3 Integration with Aerospace Structures

The integration process must account for the host platform’s material composition, surface topology, and electromagnetic interactions. For instance, the dielectric properties of the underlying structure can significantly influence antenna performance, requiring co-design of both antenna and host materials. Mechanical considerations, such as bonding strength, thermal expansion compatibility, and vibration resistance, also play a critical role in ensuring durability under extreme flight conditions. Furthermore, integration strategies often involve hybrid techniques—such as embedding antenna traces within composite layers or co-curing conductive films with structural materials—to achieve seamless functionality.

Table 18 presents a comparative overview of the manufacturing methods commonly employed for conformal antennas, highlighting their suitability, advantages, and limitations in aerospace applications.

Table 18. Comparison of Manufacturing Methods for Conformal Antennas

Method	Advantages	Limitations	Typical Applications
Flexible PCB	Thin profile, lightweight	Limited to simple curvatures	Aircraft skin antennas
Shaped Composites	High strength, complex shapes	Higher cost, longer production time	Satellite antennas
3D Printing	Rapid prototyping, complex geometries	Material limitations	UAV antennas

3.13 Embedded Antennas

Embedded antennas are integrated directly into the load-bearing or protective structural components of aerospace platforms. This approach provides several advantages, including efficient use of limited space, reduced weight by eliminating the need for separate housings, and enhanced protection of the antenna from harsh environmental conditions such as mechanical stress, thermal fluctuations, and electromagnetic interference. By serving both structural and communication functions, embedded antennas contribute to the development of multifunctional aerospace systems.

3.13.1 Techniques for Incorporating Antennas into Structural Components

A variety of advanced techniques have been developed for embedding antennas into structural components. In-mould electronics (IME) involves embedding conductive traces and antenna elements within composite laminates during the mouldings process, enabling antennas to become integral parts of the structure. Structural electronics extend this concept by embedding entire electronic systems—beyond just antennas—within structural materials, thereby enhancing system compactness and functionality. Multi-material 3D printing represents another promising technique, as it allows for the precise co-fabrication of conductive and dielectric materials within a single manufacturing step, creating highly integrated and lightweight antenna structures. These methods enable aerospace engineers to design structures that simultaneously meet mechanical and electromagnetic performance requirements.

3.13.2 Challenges and Solutions

Despite their advantages, embedded antennas present several technical challenges. Maintaining consistent antenna performance can be difficult due to the influence of surrounding structural materials, which may alter electromagnetic properties such as dielectric constant and loss tangent. Ensuring structural integrity is equally critical, as embedding conductive elements should not weaken the host material or compromise load-bearing capacity. Additionally, thermal management becomes a concern, since embedded antennas may be subjected to heat generated during operation or by the host structure in extreme aerospace environments.

Solutions to these challenges include careful material selection**,** where composites and dielectric layers are tailored to minimize electromagnetic interference while preserving strength. Innovative design approaches**,** such as topology optimization and co-simulation of structural and electromagnetic properties, are increasingly used to balance antenna performance with mechanical requirements. Moreover, thermal management strategies**,** such as integrating heat-dissipating layers or employing materials with high thermal conductivity, help ensure long-term reliability.

Table 19 summarizes the key challenges and potential solutions associated with embedded antenna integration in aerospace systems.

Table 19. Challenges and Solutions in Embedded Antenna Integration

Challenge	Solution	Impact on Performance
Signal Attenuation	Use of low-loss materials	Improved antenna efficiency
Structural Integrity	Multi-physics simulation	Optimized structural-electromagnetic design
Thermal Management	Integration of cooling channels	Enhanced reliability in high-power applications

3.14 Impact on System Performance

The integration of antennas into aerospace structures has a profound influence on the overall performance of the platform, affecting not only communication and sensing capabilities but also aerodynamic efficiency, structural strength, and electromagnetic compatibility. Figure 4 illustrates the relationship between antenna integration level and aerodynamic efficiency, highlighting the performance benefits of advanced integration approaches compared to conventional protruding antennas.

3.14.1 Aerodynamic Considerations

Traditional protruding antennas disrupt the smooth airflow around an aerospace vehicle, increasing drag and reducing fuel efficiency. In contrast, conformal and embedded antennas are seamlessly integrated into the surface or structure, enabling streamlined aerodynamics. This results in lower drag coefficients, enhanced fuel economy, and improved manoeuvrability, particularly in high-speed aircraft and space vehicles where aerodynamic efficiency is critical. Additionally, reduced protrusions enhance stealth capabilities by minimizing radar cross-section (RCS).

3.14.2 Structural Integrity

When antennas are embedded within or conformally attached to aerospace structures, they can be designed to complement the host material's load-bearing function. Properly integrated antennas reduce the need for additional housings, brackets, or mounts, thereby lowering the platform's overall weight. In some cases, advanced composites allow antennas to function as multifunctional structural elements**,** simultaneously carrying loads and enabling communication. This dual functionality is especially beneficial for spacecraft and unmanned aerial vehicles (UAVs), where weight savings directly translate to extended mission durations and payload capacity.

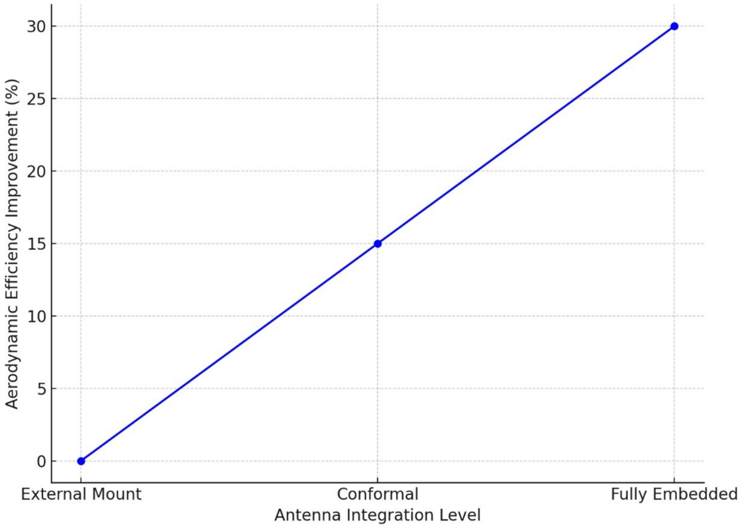

Figure 4. A line graph showing the relationship between antenna integration level and aerodynamic efficiency.

3.14.3 Electromagnetic Compatibility (EMC)

One of the main challenges of antenna integration is ensuring electromagnetic compatibility with other onboard systems. Proximity to avionics, sensors, and power systems can lead to interference that degrades performance. Integrated antennas require precise electromagnetic modelling and shielding techniques to minimize mutual coupling, interference, and signal distortion. Careful co-design of structural materials and antenna elements—such as controlling dielectric properties and grounding schemes—helps maintain reliable operation without compromising communication or sensing functions.

Overall, the integration of conformal and embedded antennas enhances aerospace platforms by improving aerodynamics, reducing weight, and maintaining structural integrity while ensuring electromagnetic reliability. These improvements contribute to next-generation aerospace systems that are lighter, more efficient, and capable of supporting increasingly complex mission requirements.

Table 20 shows the Impact of Antenna Integration on System Performance.

Table 20: Impact of Antenna Integration on System Performance

Performance Aspect	Conformal Antennas	Embedded Antennas
Aerodynamics	Significant drag reduction	Minimal impact on existing aerodynamics
Weight	Slight increase due to conforming materials	Potential weight reduction through multifunctionality
EMC	Improved due to reduced protrusions	Challenges due to proximity to other systems

3.15 Future Trends in Antenna Integration

Emerging trends in antenna integration for aerospace applications are increasingly focused on achieving multifunctionality, adaptability, and enhanced performance.

3.15.1 Smart Skins with Integrated Sensing and Communication

Smart skins represent a transformative approach to antenna integration, where antennas and sensors are directly embedded into the structural surfaces of aerospace vehicles. By combining communication and sensing functionalities within the skin of the aircraft or spacecraft, these systems eliminate protruding antenna structures, thereby reducing aerodynamic drag and improving stealth capabilities. Moreover, smart skins enable distributed communication networks and structural health monitoring, ensuring resilience and fault tolerance in critical aerospace missions. This multifunctional approach is particularly relevant for next-generation UAVs, stealth aircraft, and satellites where weight, efficiency, and survivability are crucial.

3.15.2 Metamaterial-Based Conformal Antennas

Metamaterial-based conformal antennas leverage engineered electromagnetic properties to achieve enhanced gain, bandwidth, and beam-steering capabilities in compact and low-profile designs. Unlike conventional antennas, these structures can manipulate electromagnetic waves in novel ways, enabling high-frequency operation, reduced radar cross-section, and reconfigurability. Their conformal nature allows seamless integration with curved aerospace surfaces, supporting applications in satellite communications, hypersonic vehicles, and advanced radar systems. By combining structural adaptability with superior electromagnetic performance, metamaterial antennas hold strong potential for improving both communication reliability and stealth characteristics in aerospace missions.

3.15.3 4D Printed Adaptive Antennas

4D printed antennas extend the concept of additive manufacturing by incorporating materials that respond dynamically to environmental stimuli such as temperature, pressure, or electromagnetic load. These antennas can adapt their geometry or electromagnetic properties in real time, allowing the system to optimize performance under varying flight conditions. For instance, an antenna may expand its aperture for long-range communication at high altitudes or reconfigure itself for short-range, high-capacity links in dense operational environments. This adaptability makes 4D printed antennas particularly suitable for flexible aerospace systems, including reusable spacecraft, UAV swarms, and next-generation satellites. By enabling real-time reconfiguration, 4D antennas push aerospace communication technology toward a new era of versatility and resilience.

3.16 Emerging Trends and Future Developments

As the field of aerospace antenna manufacturing continues to advance, several emerging trends and future developments show significant potential for enhancing antenna performance, functionality, and production efficiency. Innovations in smart materials**,** adaptive designs, and novel manufacturing methods are paving the way for next-generation aerospace antenna systems that are lighter, more efficient, and highly reconfigurable. This section highlights key advancements and their expected impact on the aerospace industry.

3.16.1 Smart Materials in Antenna Manufacturing

The integration of smart materials into antenna design and manufacturing has emerged as a promising research area. Smart materials enable the creation of antennas that are adaptive, reconfigurable, and capable of responding to changes in the surrounding environment. Such capabilities are particularly vital in aerospace applications, where conditions such as temperature, pressure, and electromagnetic interference can vary dramatically during operation.

3.16.2 Shape Memory Alloys (SMAs)

Shape Memory Alloys are metallic materials that can return to a pre-defined shape when subjected to specific stimuli, such as temperature changes. In antenna applications, SMAs can be used to dynamically alter the geometry of the antenna, enabling optimal performance across different flight regimes. For example, an SMA-based antenna can adjust its length or curvature to switch between frequency bands or improve gain under varying conditions. This adaptability reduces the need for multiple antenna systems, leading to weight savings and higher efficiency in aerospace platforms.

3.16.3 Piezoelectric Materials

Piezoelectric materials deform in response to applied electrical signals, offering unique opportunities for creating tunable and reconfigurable antenna elements. By incorporating piezoelectric actuators within antenna structures, it becomes possible to fine-tune resonance frequencies, adjust polarization states, or modify radiation patterns in real time. Such tunability is crucial in aerospace systems that require secure, interference-resistant communication and adaptive responses to mission-critical scenarios.

3.16.4 Applications of Smart Materials in Aerospace Antennas

The applications of smart materials such as SMAs and piezoelectric elements extend across a wide range of aerospace use cases. These include:

- Frequency-agile communication systems for aircraft and satellites
- Lightweight, reconfigurable antennas for UAVs and drones
- Adaptive beam steering for radar and surveillance systems
- Self-healing and damage-tolerant antenna structures for extended mission lifespans

Table 21 shows the Applications of Smart Materials in Aerospace Antennas, highlighting how these technologies are being leveraged to achieve greater adaptability, efficiency, and resilience.

Table 21. Applications of Smart Materials in Aerospace Antennas

Smart Material	Property	Potential Application
Shape Memory Alloys	Shape change with temperature	Reconfigurable antenna elements
Piezoelectric Materials	Deformation under electric field	Tunable antenna components
Magnetostrictive Materials	Shape change in magnetic fields	Adaptive antenna structures
Electroactive Polymers	Large deformation under electric field	Morphing antennas

3.17 Hybrid Manufacturing Processes

The adoption of hybrid manufacturing processes is gaining traction in aerospace antenna production, as it allows manufacturers to combine the strengths of different techniques for improved efficiency, precision, and performance. By integrating additive, subtractive, and adaptive methods into a single workflow, aerospace manufacturers can address the challenges of producing lightweight yet complex antenna structures while maintaining high reliability and quality standards.

3.17.1 Additive-Subtractive Hybrid Manufacturing

Additive-subtractive hybrid manufacturing merges the flexibility of additive manufacturing (AM), such as 3D printing, with the high-precision capabilities of subtractive processes like CNC machining. Additive manufacturing enables the creation of intricate and lightweight designs, including conformal antenna geometries and complex internal features that would be impossible to produce using traditional methods alone. Subtractive machining then refines these structures, achieving the required dimensional accuracy, smooth surfaces, and tight tolerances needed for aerospace applications. This dual approach ensures both innovation in design and consistency in performance.

3.17.2 In-Situ Monitoring and Adaptive Manufacturing

A critical advancement in hybrid processes is the integration of in-situ monitoring systems that continuously track and adjust the manufacturing process in real time. Equipped with advanced sensors and data analytics, these systems can detect deviations, optimize material deposition, and fine-tune process parameters during production. This adaptability not only improves overall quality and repeatability but also minimizes material waste, reduces production time, and enhances reliability of the final antenna product. For aerospace applications, where performance consistency is non-negotiable, adaptive manufacturing ensures antennas meet stringent safety and operational standards.

3.17.3 Advantages of Hybrid Manufacturing for Aerospace Antennas

By combining additive, subtractive, and adaptive techniques, hybrid manufacturing delivers several advantages for aerospace antenna production, including:

- Greater design flexibility for complex and lightweight structures
- Improved dimensional accuracy and surface quality
- Real-time quality assurance through in-situ monitoring
- Enhanced production efficiency and reduced material waste
- Customization and scalability for diverse aerospace platforms

The specific advantages of hybrid manufacturing processes in aerospace antennas are summarized in Table 22.

Table 22. Advantages of Hybrid Manufacturing for Aerospace Antennas

Hybrid Process	Advantages	Challenges
AM + CNC Machining	Improved surface finish, tighter tolerances	Process complexity, cost
AM + Electroforming	Enhanced conductivity, reduced weight	Material compatibility, process control
In-Situ Monitoring	Real-time quality control, reduced waste	Data management, sensor integration

3.18 Nanotechnology in Antenna Fabrication

The integration of nanotechnology into antenna fabrication is transforming aerospace systems by enabling unprecedented levels of miniaturization, efficiency, and multifunctionality. By leveraging nanomaterials and nanostructured designs, antennas can achieve superior electrical and electromagnetic properties compared to conventional counterparts, making them ideal for advanced aerospace applications where size, weight, and performance are critical.

3.18.1 Nanomaterials for Enhanced Performance

Nanomaterials such as carbon nanotubes (CNTs) and graphene have remarkable electrical, mechanical, and thermal properties that can significantly improve antenna performance.

- Graphene-based antennas offer ultra-high conductivity, excellent flexibility, and wide tunability, enabling compact, high-frequency designs.
- Carbon nanotube composites provide reduced resistive losses and improved radiation efficiency, especially valuable for lightweight aerospace platforms. By integrating these nanomaterials, antennas achieve improved bandwidth, signal strength, and energy efficiency while maintaining minimal mass and volume.

3.18.2 Nanostructured Surfaces

Nanostructured surfaces involve engineering materials at the nanoscale to precisely control electromagnetic interactions. By designing periodic nanostructures or surface patterns, it becomes possible to manipulate wave propagation, scattering, and absorption in highly controlled ways.

- Plasmonic nanostructures can enhance resonance effects, improving sensitivity and gain.
- Nano-patterned coatings reduce reflection losses and enable multi-band operation.
- Reconfigurable nanostructures allow antennas to adapt dynamically to different operating frequencies and environments.

These advancements open pathways for multifunctional aerospace antennas capable of combining communication, sensing, and stealth features within a single compact device. The specific roles of nanomaterials and nanostructures in aerospace antenna manufacturing are detailed in Table 23.

Table 23. Nanomaterials in Aerospace Antenna Manufacturing

Nanomaterial	Property	Potential Benefit
Carbon Nanotubes	High conductivity, low weight	Improved efficiency, reduced antenna size
Graphene	Extremely thin, flexible	Conformal antennas, wideband performance
Nano-engineered Metamaterials	Tailored electromagnetic properties	Enhanced gain, beam steering capabilities

3.19 Artificial Intelligence in Manufacturing

The integration of Artificial Intelligence (AI) and Machine Learning (ML) into aerospace antenna manufacturing is reshaping the way antennas are designed, fabricated, and validated. By leveraging intelligent algorithms and data-driven decision-making, the industry can achieve higher efficiency, improved precision, and reduced production costs. AI-driven manufacturing not only accelerates innovation but also ensures reliability in highly demanding aerospace environments.

3.19.1 Design Optimization

AI algorithms can evaluate vast design spaces far beyond traditional methods, rapidly identifying antenna geometries that maximize performance metrics such as gain, bandwidth, and efficiency. By incorporating manufacturing constraints directly into the optimization process, AI ensures that proposed designs are not only high-performing but also practical to fabricate. Techniques such as generative design and neural network-based modelling allow engineers to produce innovative antenna architectures tailored for aerospace applications.

3.19.2 Process Control and Quality Assurance

AI and ML play a pivotal role in real-time monitoring and adaptive process control during antenna production.

- Defect prediction and prevention: Machine learning models trained on historical manufacturing data can detect early signs of flaws, reducing rejection rates.
- Parameter optimization: AI systems continuously adjust variables such as temperature, deposition rates, or machining precision to ensure stable quality.
- Automated inspection: Computer vision and ML tools enable fast, accurate defect detection in finished antennas, guaranteeing compliance with aerospace standards.

These capabilities enhance overall production efficiency, minimize waste, and ensure consistent antenna performance. A list of applications of AI in aerospace antenna manufacturing is provided in Table 24.

Table 24. The applications of AI in Aerospace Antenna Manufacturing

AI Application	Function	Benefit
Design Optimization	Automated parameter tuning	Improved antenna performance
Process Control	Real-time adjustment of manufacturing parameters	Enhanced product consistency
Quality Inspection	Automated defect detection	Reduced errors, improved reliability
Predictive Maintenance	Anticipating equipment failures	Minimized downtime, increased efficiency

Figure 5 presents a bubble chart that illustrates the potential impact of emerging technologies on critical antenna performance metrics such as efficiency, bandwidth, adaptability, and reliability. The size of each bubble represents the relative significance of the technology, while its position reflects the degree of improvement expected in specific performance domains.

These emerging trends and future developments highlight the transformative direction of aerospace antenna manufacturing. As innovations such as smart materials, hybrid manufacturing, nanotechnology, and AI-driven design continue to mature, their integration will drive antennas toward unprecedented levels of performance, adaptability, and production efficiency**.** Collectively, these advancements will play a pivotal role in shaping next-generation aerospace systems, ensuring antennas remain highly reliable, multifunctional, and capable of meeting evolving mission demands.

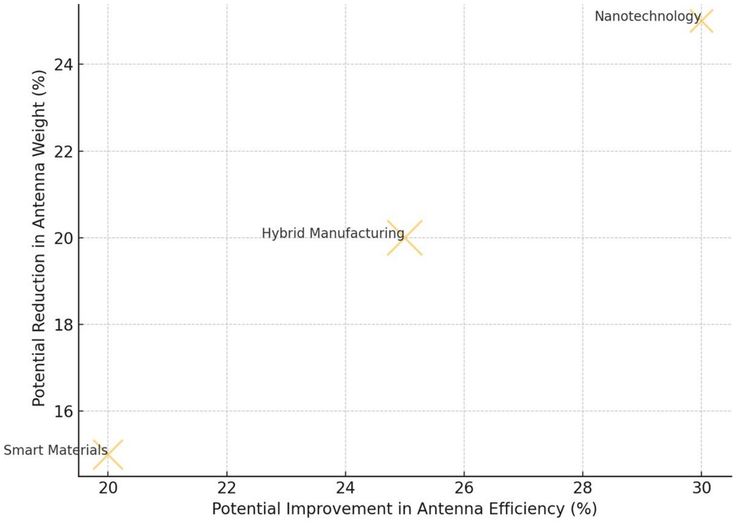

Figure 5. A bubble chart illustrating the potential impact of emerging technologies on key antenna performance metrics.

4. Conclusion and Future Directions

This comprehensive review has highlighted the transformative impact of advanced manufacturing techniques on the design and production of aerospace antennas. As the aerospace sector increasingly demands high-performance, lightweight, and durable components, these cutting-edge methods are proving essential in addressing such challenges. From additive manufacturing and precision machining to innovations in composite materials and structural integration, the manufacturing landscape is evolving rapidly to meet the complex needs of modern aerospace systems.

Key Takeaways

- **Additive Manufacturing** has opened new frontiers in antenna design with its unparalleled geometric freedom and material efficiency.
- **Precision Machining Techniques** are enabling the fabrication of antennas with superior accuracy and surface finish, critical for high-frequency applications.
- **Advanced Composites** are offering an ideal balance of strength, weight, and thermal stability, essential for demanding aerospace environments.
- **Integration and Assembly Innovations** such as conformal and embedded antennas are enhancing system-level performance while optimizing aerodynamics and structural integrity.

Future Outlook

The future of aerospace antenna manufacturing is poised for exciting developments driven by emerging technologies:

- **Smart Materials & Adaptive Antennas:** Materials that respond to environmental stimuli—such as shape memory alloys and piezoelectric elements—are expected to enable dynamically reconfigurable antennas for mission-adaptive performance.
- **Hybrid Manufacturing Approaches:** The fusion of additive and subtractive techniques will allow manufacturers to capitalize on the advantages of both, leading to more efficient and optimized antenna designs.
- **Nanotechnology Integration:** Nanomaterials and nanoscale fabrication methods will enhance conductivity, reduce signal losses, and allow further miniaturization without compromising performance.
- **AI-Driven Manufacturing:** Artificial intelligence and machine learning will increasingly support the optimization of design, quality control, and real-time process monitoring, driving significant gains in manufacturing speed, reliability, and cost-effectiveness.

Implications for the Aerospace Industry

The continued evolution of manufacturing techniques holds profound implications for the aerospace domain:

- Improved antenna performance will enable more reliable communication, navigation, and sensing systems across aviation and space platforms.
- Lighter and more efficient antennas will contribute to reduced fuel consumption and increased payload capacity.
- The ability to fabricate multifunctional, highly integrated antenna structures could pave the way for revolutionary aerospace designs.
- Streamlined and cost-effective manufacturing processes may accelerate innovation and reduce time-to-market for next-generation aerospace systems.

Final Thoughts

As these advanced manufacturing methods continue to mature and converge with emerging technologies, the aerospace industry stands on the cusp of a new era in antenna design and production. The antennas of the future will not only meet the ever-growing demands for performance and efficiency but will also redefine the possibilities of aerospace communication, navigation, and sensing systems.

References

1. Pop, Gheorghe Ioan, Aurel Mihail Titu, and Alina Bianca Pop. "Enhancing aerospace industry efficiency and sustainability: Process integration and quality management in the context of Industry 4.0." *Sustainability* 15, no. 23 (2023): 16206.
2. Balanis, Constantine A. *Antenna theory: analysis and design*. John wiley & sons, 2016.
3. Banerjee, Archita, Rajesh Singh, and Balasubramanian Kandasubramanian. "Additive Manufacturing in Antenna Design: Evaluating Mechanical Resilience and Electromagnetic Efficiency Across Diverse Material Compositions." *Journal of Advanced Manufacturing and Processing* 7, no. 4 (2025): e70036.
4. Zhang, Bing, Peter Linnér, Camilla Karnfelt, Pui Lam Tarn, Ulf Södervall, and Herbert Zirath. "Attempt of the metallic 3D printing technology for millimeter-wave antenna implementations." In *2015 Asia-Pacific Microwave Conference (APMC)*, vol. 2, pp. 1-3. IEEE, 2015.
5. Pizarro, Francisco, Rolando Salazar, Eva Rajo-Iglesias, Mauricio Rodriguez, Sebastian Fingerhuth, and Gabriel Hermosilla. "Parametric study of 3D additive printing parameters using conductive filaments on microwave topologies." *IEEE Access* 7 (2019): 106814-106823.
6. Zhang, Chengyan, Lixin Wang, Xiaoli Zu, and Wuzhou Meng. "Multi-objective optimization of experimental and analytical residual stresses in pre-stressed cutting of thin-walled ring using

glowworm swarm optimization algorithm." *The International Journal of Advanced Manufacturing Technology* 107, no. 9 (2020): 3897-3908.

7. Gu, Chao, Steven Gao, Vincent Fusco, Gregory Gibbons, Benito Sanz-Izquierdo, Alexander Standaert, Patrick Reynaert et al. "A D-band 3D-printed antenna." *IEEE Transactions on Terahertz Science and Technology* 10, no. 5 (2020): 433-442.
8. Radha, Sonapreetha Mohan, Geonyeong Shin, Pangun Park, and Ick-Jae Yoon. "Realization of electrically small, low-profile quasi-isotropic antenna using 3D printing technology." *IEEE Access* 8 (2020): 27067-27073.
9. Khan, Zahangir, Han He, Xiaochen Chen, and Johanna Virkki. "Dipole antennas 3D-printed from conductive thermoplastic filament." In *2020 IEEE 8th Electronics System-Integration Technology Conference (ESTC)*, pp. 1-4. IEEE, 2020.
10. Alkaraki, Shaker, Yue Gao, Max O. Munoz Torrico, Samuel Stremsdoerfer, Edouard Gayets, and Clive Parini. "Performance comparison of simple and low cost metallization techniques for 3D printed antennas at 10 GHz and 30 GHz." *IEEE Access* 6 (2018): 64261-64269.
11. Rojas-Nastrucci, Eduardo A. "Additively Manufactured Antennas for Aerospace Harsh Environments." In *Resilient Hybrid Electronics for Extreme/Harsh Environments*, pp. 31-45. CRC Press, 2024.
12. Apaydin, Elif. *Microfabrication techniques for printing on PDMS elastomers for antenna and biomedical applications*. The Ohio State University, 2009.
13. Gürgen, Selim, and Mehmet Alper Sofuoğlu. "Advancements in conventional machining: a case of vibration and heat-assisted machining of aerospace alloys." In *Advanced machining and finishing*, pp. 143-175. Elsevier, 2021.